12-2020

Robust Control of a Multi-phase Interleaved Boost Converter for Photovoltaic Application using μ-Synthesis Approach

Badur Mueedh Alharbi
University of Arkansas, Fayetteville

Robust Control of a Multi-phase Interleaved Boost Converter for

Photovoltaic Application using μ-Synthesis Approach

A dissertation submitted in partial fulfillment
of the requirements for the degree of
Doctor of Philosophy in Engineering with a concentration in Electrical Engineering

by

Badur Mueedh Alharbi
King Abdulaziz University
Bachelor of Science in Electrical Engineering, 1997
Cardiff University
Master of Science in Electrical Engineering, 1999
University of Arkansas
Master of Science in Electrical Engineering, 2020

December 2020
University of Arkansas

This dissertation is approved for recommendation to the Graduate Council

_____
Roy A. McCann, Ph.D.
Dissertation Director:

_____
Fung Luo, Ph.D
Committee Member

_____
Jingxian Wu, Ph.D
Committee Member

_____
Mark E. Arnold, Ph.D.
Committee Member

ABSTRACT

The high demand of energy efficiency has led to the development power converter topologies and control system designs within the field of power electronics. Recent advances of interleaved boost converters have showed improved features between the power conversion topologies in several aspects, including power quality, efficiency, sustainability and reliability.

Interleaved boost converter with multi-phase technique for PV system is an attractive area for distributed power generation. During load variation or power supply changes due to the weather changes the output voltage requires a robust control to maintain stable and perform robustness.

Connecting converters in series and parallel have the advantages of modularity, scalability, reliability, distributed location of capacitors which make it favorable in industrial applications. In this dissertation, a design of μ-synthesis controller is proposed to address the design specification of multi-phase interleaved boost converter at several power applications. This thesis contributes to the ongoing research on the IBC topology by proposing the modeling, applications uses and control techniques to the stability challenges. The research proposes a new strategy of robust control applied to a non-isolated DC/DC interleaved boost converter with a high step voltage ratio as multi-phase, multi-stage which is favorable for PV applications. The proposed controller is designed based on μ-synthesis technique to approach a high regulated output voltage, better efficiency, gain a fast regulation response against disturbance and load variation with a better dynamic performance and achieve robustness. The controller has been simulated using MATLAB/Simulink software and validated through experimental results which show the effectiveness and the robustness.

ACKNOWLEDGMENTS

I would like to express my deepest appreciation, leadership, understanding to my advisor, Prof. Roy McCann who guided me in the field of control systems of power electronics and enriched my knowledge during my Ph.D. research. I have learned a lot from his discussion. His guidance and generous support allowed me to complete the degree.

I would like to thank Dr. Simon Ang, Dr. Fung Luo and Dr. Mark Arnold for their support, academic guidance and for kindly agreeing to be on my committee. I am very indebted to my colleagues, Khalid Alharbi, Majid Alhomim, Obaid Aldosari and Waleed Alhosaini for sharing their ideas and research experiences.

I would like to dedicate my deepest gratitude to my mother, I am speechless to express my grateful of your support and being a way while you were sick. You are always the great supporter of me. For my brother Abdullah, thank you for the nice words of encouragement and support during my study years.

Lastly, without the support and the understanding of my wife and my kids this work would not have been done yet. I am grateful to have them on my life. For them I would say “thank you for your kindness and encouragement along my way”. My little kids, Rakan and Meshal have always put smiles back on my face during the hard days and for that I am grateful.

DEDICATION

To my mother.

TABLE OF CONTENTS

LIST OF FIGURES

LIST OF TABLES

CHAPTER 1

INTRODUCTION

1.1 Overview

The reduction of carbon dioxide emissions to provide the motivation toward renewable energy sources. Global warming is becoming an issue recent in years and the health issues increase gradually because of fusil fuel burning and emissions of greenhouses. Consequently, researchers are looking for alternative sources to supply electricity with less emission. One of these solutions is the solar energy system that provide electric energy by converting the sun light into electricity. Lower maintenance cost, no noise, no installation area limitation and unlimited source are the main features of solar energy system [1]. The main drawback of this system is the low output voltage. Power electronics devices have been always an important key in renewable energies and electric transportation to improve electric systems efficiency and reduce energy consumption.

DC/DC boost converter is one of the important power converters that used to boost the PV output voltage into higher voltage level, but it still is not able to reach the desired output voltage level. For that, improved efficiency and high voltage level step up dc–dc boost converters are demanded in many applications where the load voltage level is higher than the input voltage level. Interleaved boost voltage has the ability to boost the voltage into high voltage ratio with more advantages over the boost converter [2][3][4]. To handle the voltage and current stress in high power application, multi power devices is used to connect the devices in series and parallel. Due to the increase demand for energies as the individual converter is not enough to transfer the energy [5]. Thus, devices that work in cascade or in parallel are applied to meet the increasing energies demand [6].

The problem of stabilizing the uncertain linear dynamic systems for IBC has been discussed and analyzed for more than two decades as explained in [7]. The main issue with control systems are differences between the real system and its nominal model which is used in control system design.

Previous researches have approached robust stability for interleaved boost converter under nominal condition for all operating conditions but have not considered the model uncertainties. In this research, μ-synthesis which can utilizes the robust stability of LFT based on linear system with structed parametric uncertainties is applied to investigate the system robustness and performance. The main issue with DC/DC converter's control system is the differences between the actual or real operating system and the linearized nominal model that is used to build the controller. Perturbations such as external noises, parametric and dynamic uncertainties, unmodelled non-linearities should be considered by control designer.

1.2 Literature Review

The research on robust control design is said to be started between 1975 to 1985 with a breakthrough paper by Zames [8] which introduced theory which was quickly extended to more general problems.

High voltage gain converters play an important role in different power applications such as medical, aerospace, remote and dc distribution systems. Many high voltage gain topologies have been in discussed in [9-12] with normal high ratio. However, many of them are complex and costly. The IBC technique has gained interests in the field of power distribution systems as it provides solutions to maintain a high voltage gain, low devices stress, a high efficiency at normal duty ratio which make it more popular for many industrial applications.

The DC/DC interleaved boost converter is regulated by feedback control to maintain a constant output voltage. Many control techniques have been used to regulate the load voltage such as classical linear regulators (PID and PID)[9][10], and Linear Quadratic Regulator (LQR)[11] are based on averaged small-signal. They show fixed output voltage, but they show unsatisfactory performance in case of disturbance and load variation. The uncertainty presented by averaged small signal is large which make these regulators unsatisfied. Robust control techniques have been applied in many research to cope the uncertainty and to achieve a satisfactory performance [7][12][13][14]. This research proposes a robust controller using mu-synthesis approach to attain a fast-dynamic response, to maintain stability, robust performance, and sufficient disturbance rejection against the variation of input voltage, load, and reference voltage for different IBC applications. Many robust control techniques have been presented in [15][16][17][18] and [13]. The mentioned issue above has become the motivation for this research to design a robust controller for a DC-DC interleaved boost converter based on the μ-synthesis approach for several applications.

1.3 Research Objective

Due to the continuous emergence of interleaved boost converters and cascade converters, many questions about their modeling, control, advantages and disadvantages arise. Consequently, a significant effort has been devoted to developing the converter for medium voltage applications such as motor drives. Since the design of the cascade IBC requires a good conception of the operation principles of the converter, first the modeling approach should be chosen to provide an analysis of the converter's operation. Another issue to consider will be the design of the robust controller for the DC bus, which can be accomplished by applying mu-synthesis and H-infinity.

Some of the main drawbacks of the cascade IBC will be addressed in this research. One of these drawbacks is maximizing the reliability of the converter.

The main objective of this thesis is to introduce different IBC topologies for various power applications and to design a μ-controller to regulate the load voltage for different converter applications. By the theoretical studies, the applicability of the proposed topologies and the validation of the control strategy will be affirmed by simulation and experiment. Briefly, the dissertation's objectives are:

i) This study proposes the analysis and the robust control of multi-phase interleaved boost converter.

ii) A comprehensive model to describe the dynamics of the IBC

iii) Robust control based on μ-synthesis analysis for four-phase IBC is developed to achieve stability, high performance, and disturbance rejection ability against load changes, different reference voltages, and input supplies variation.

iv) Betterment in the response of load transient of average voltage-mode and current controlled interleaved boost converter is maintained.

v) To propose a novel DC/DC Multi-stage Multi-phase IBC for PV system, with less ripple current and devices stress.

vi) To propose closed-loop robust voltage and current controller of the IBC for cascade system and to achieve a high output voltage with reduced input current ripple and improved efficiency.

vii) To propose control strategies for the proposed topologies which regulate the DC-sides voltage and guarantee the robust performance for three-phase AC system.

viii) Improving the system reliability with less size and less cost.

1.4 Outline the thesis

The thesis is arranged as follows:

- Chapter 1, this chapter begins with an introduction followed by literature review. Thesis goals are mentioned in this chapter.
- Chapter 2 provides a comprehensive description on the design, modeling and analysis of multi-phase interleaved boost converter at different control strategies. Steady states are discussed, and comparison studies are presented. The transfer function of the output voltage to duty cycle is delivered.
- Chapter 3 discusses PV system, different PV applications interconnected with IBC are simulated and discussed in this chapter. A novel method to transfer high energy conversion is represented.
- Chapter 4 represents cascade converters and discusses the stability issue. Hamiltonian stability method and Middlebrook stability criterion are discussed to ensure stability and for different models of PV applications.
- Chapter 5 explains and introduces both the conventional and proposed the proposed control of μ-synthesis and the application of this technique on boost converter, four-phase IBC. The design of the prototype of the four-phase IBC is presented.
- Chapter 6, the simulation validation of the proposed control strategy is presented in this chapter for several power converter applications.
- Chapter 7 concludes the work undertaken in this research. Future work suggestions are mentioned.

CHAPTER 2

INTERLEAVED BOOST CONVERTER

This chapter deals with the principle of operation, design procedure, modeling analysis and simulation of Interleaved Boost Converter (IBC) for low and high-power application demands the use of DC/DC, AC/DC and DC/AC converters.

2.1 Boost converter

The boost converter or named a step-up converter is a device that used to boost or step up the input voltage level into higher voltage level and step-down the input current. It is a type of switch-mode power supply which includes a semiconductor transistor, *Q*, a power diode, *D*, an inductor, *L*, and a capacitor, *C*. Figure 2.1 depicts the circuit of boost converter. *Vi* is the supply voltage, and *R* is the resistive load.

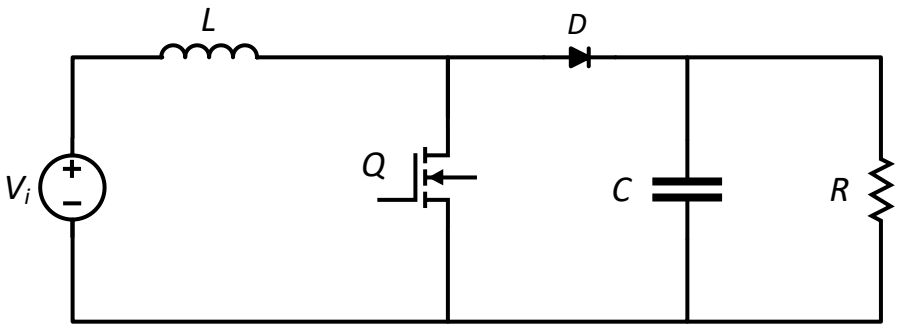

Figure 2.1 Boost Converter circuit.

The main drawbacks of boost converter are: 1) poor dynamic performance due to the right half plane zero. 2) hard to handle the high input current for high power application, 3) to obtain a high output voltage at low duty cycle ration, 4) unable to achieve a high voltage gain due to the parasitic resistance and inductance and 5) large input current and output voltage ripples that effect the stability and reduce the efficiency [19],[20].

2.2 Interleaved boost converter

IBC is used widely in some applications such as Photo Voltaic (PV), ultracapacitors, fuel cells, power factor correction, batteries, medical applications, hybrid electric vehicle and satellite applications where the input voltage is low, and the desired output voltage is much higher. IBC has many advantages compared to conventional boost converter such as [21][22][23][24][25][26][27]:

1) higher efficiency and improved reliability,
2) high voltage gain with moderate duty cycle,
3) improved steady-state and faster dynamic response,
4) high power density,
5) less input current and output voltage ripples because of the harmonic cancellation,
6) reduced electromagnetic emission EMI,
7) reduced components size and weight,
8) less voltage and current stress which result in better thermal performance.

Figure 2.2 shows the circuit diagram of IBC which contains of two boost or (multi boost converters) connected in parallel sharing input supply voltage, output capacitor and load. The inductor current frequency will be increased due to the interleaving technique that makes the it east to filter [28]. The semiconductor switches Q_1 and Q_2 are provided by the gate signal using different methods; same signal at the same time for all switches, positive signal for half period and the negative signal for the other half and phase shift delay of each switch that equal to ($360/n$) where n is the phase number.

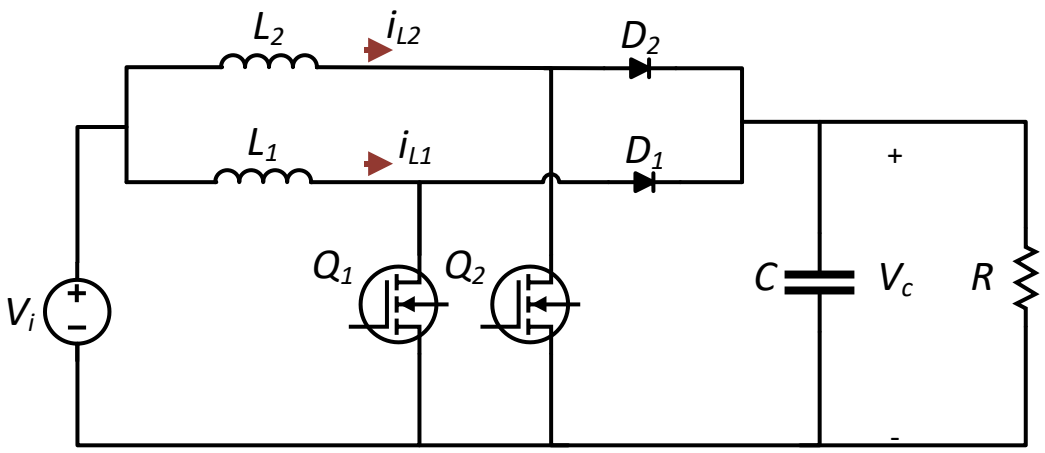

Figure 2.2 Interleaved boost converter (2-phase).

2.2.1 Modeling and Analysis of IBC:

The converter could work in Discontinuous Conduction Mode (DCM) or in Continuous Conduction Mode (CCM) but the performance with CCM has better operation of power devices, lower conduction losses and less input current ripple [21],[29]. Modes of operation can be analyzed based on the control signals applied for each switch. In CCM, stability problem is caused by right-plane zero in the transfer function [30],[31],[32]. The state-space averaging technique is applied to analysis the two-phase interleaved boost converter and to find its transfer function [33]. Mathematical model is obtained based on the state-space equations to linearize the system from the nonlinear time-varying model [34]. The capacitor voltage v_c and inductor currents i_L are the state variables. To illustrate the operation of IBC, the pulse signals of switches is shown in Figure 2.3 where the converter works on two modes with phase shift 360/2=180^o. There are two modes of operation:

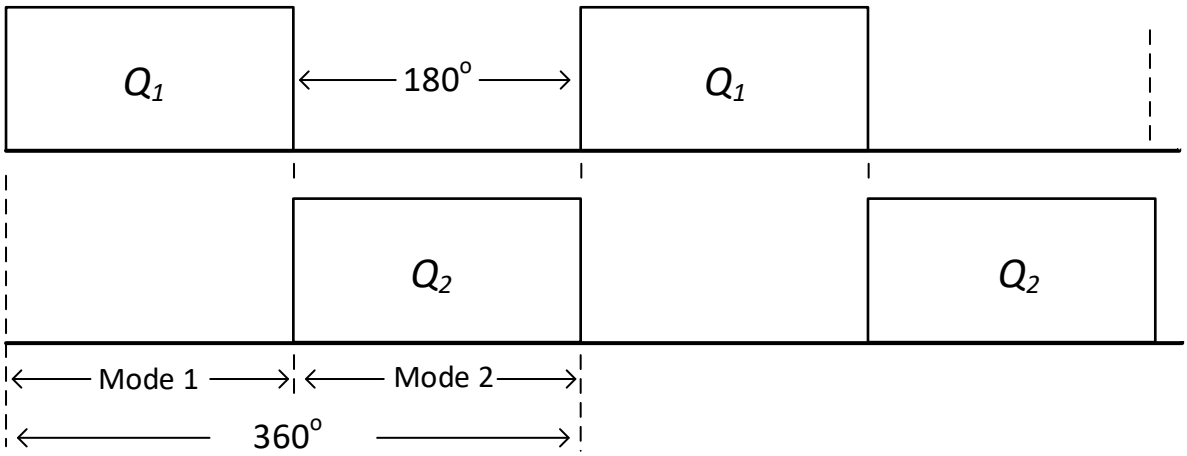

Figure 2.3 Control signal of Q_1 and Q_2.

1) Mode 1: Q_1 is ON and Q_2 is OFF. (Fig. 2.4)

The inductor current I_{L1} starts to raise and storing energy in L_1, while L_2 discharging energy into to the load side. Applying KVL and KCL of the circuit, the dynamic equations for this mode are derived as follows:Equation Section (Next)Equation Section (Next)

$$\frac{di_{L_1}}{dt} = \frac{V_i}{L_1} d \tag{2.1}$$

$$\frac{di_{L_2}}{dt} = \frac{V_i - v_c}{L_2} d \tag{2.2}$$

$$\frac{dv_c}{dt} = \frac{i_{L_2}}{C} - \frac{v_c}{RC} \tag{2.3}$$

$$A_1 = \begin{bmatrix} 0 & 0 & 0 \\ 0 & 0 & \frac{-d}{L_2} \\ 0 & \frac{1}{C} & \frac{-1}{RC} \end{bmatrix}, B_1 = \begin{bmatrix} \frac{d}{L_1} \\ \frac{d}{L_2} \\ 0 \end{bmatrix}. \tag{2.4}$$

2) Mode 2: Q_1 is OFF and Q_2 is ON. (Fig. 2.5)

The inductor current I_{L2} starts to raise and storing energy in L_2, while L_1 discharging energy into the load side. Applying KVL and KCL, the dynamic equations are written as:

$$\frac{di_{L_1}}{dt} = \frac{V_i - v_c}{L_1}(1-d) \tag{2.5}$$

$$\frac{di_{L_2}}{dt} = \frac{V_i}{L_2}(1-d) \tag{2.6}$$

$$\frac{dv_c}{dt} = \frac{i_{L_1}}{C} - \frac{v_c}{RC} \tag{2.7}$$

$$A_2 = \begin{bmatrix} 0 & 0 & \frac{-(1-d)}{L_1} \\ 0 & 0 & 0 \\ \frac{1}{C} & 0 & \frac{-1}{RC} \end{bmatrix}, B_2 = \begin{bmatrix} \frac{(1-d)}{L_1} \\ \frac{(1-d)}{L_2} \\ 0 \end{bmatrix}. \tag{2.8}$$

The linearized state-space averaged model of two-phase IBC is derived as:

$$\begin{aligned} \dot{X} &= AX + BU \\ Y &= CX + DU \end{aligned} \tag{2.9}$$

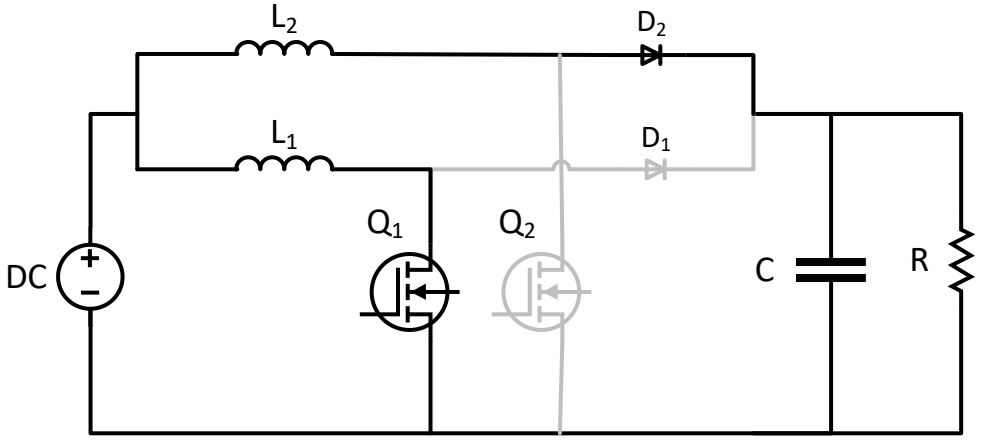

Figure 2.4 Equivalent circuit during mode 1.

Where $A = A_1 d_1 + A_2 d_2$, $B = B_1 d_1 + B_2 d_2$ and $d = d_1 + d_2$

$$\dot{X} = \begin{bmatrix} 0 & 0 & \frac{-(1-d)}{L_1} \\ 0 & 0 & \frac{-d}{L_2} \\ \frac{1}{C} & \frac{1}{C} & \frac{-1}{RC} \end{bmatrix} \begin{bmatrix} i_{L_1} \\ i_{L_2} \\ v_c \end{bmatrix} + \begin{bmatrix} \frac{1}{L_1} \\ \frac{1}{L_2} \\ 0 \end{bmatrix} u \tag{2.10}$$

$$Y = \begin{bmatrix} 0 & 0 & 1 \end{bmatrix} \begin{bmatrix} i_{L_1} \\ i_{L_2} \\ v_c \end{bmatrix}. \tag{2.11}$$

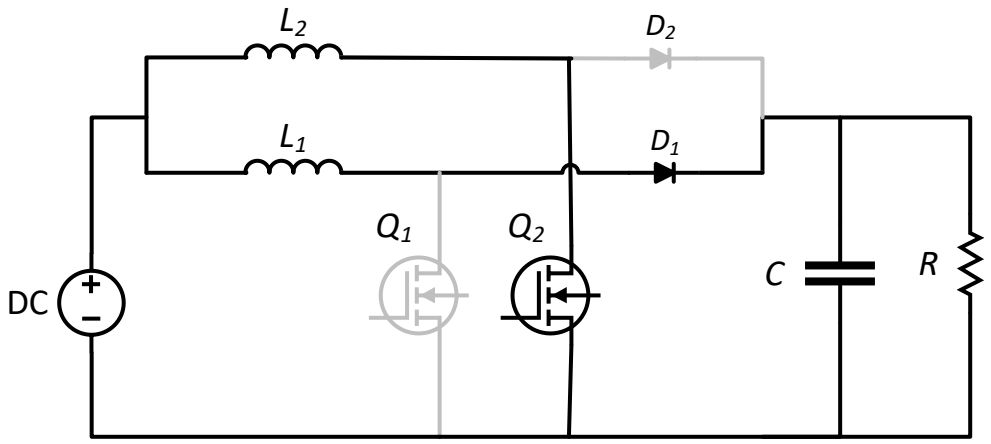

Figure 2.5 Equivalent circuit during mode 2.

The transfer functions of the two-phase IBC are determined as below [31],[35],[36]:

$$\frac{V_o(s)}{V_i(s)} = \frac{RCs+1}{(1-d)[\frac{LC}{(1-d)^2}s^2 + \frac{L}{R(1-d)^2}s+1]} \tag{2.12}$$

$$\frac{V_o(s)}{d(s)} = \frac{(-s+\frac{R(1-d)^2}{L})V_i}{RC(1-d)^2[s^2+\frac{1}{RC}s+\frac{(1-d)^2}{LC}]} \tag{2.13}$$

$$\frac{i_L(s)}{d(s)} = \frac{V_i}{L(1-d)} \frac{s + \frac{2}{RC}}{s^2 + \frac{s}{RC} + \frac{(1-d)^2}{LC}}. \quad (2.14)$$

2.2.2 Four-phase IBC

The four-phase interleaved boost converter consists of four boost converters connected in parallel as shown in Figure 2.6 [37]. The converter could operate in different cases as below:

- Case A: The switches of IBC have a phase shift delay of ($360^o/n$) or ($2\pi/n$) where n is the number of phases. In this case different operation settings are illustrated based on the value of the duty ratio are displayed in Figures 2.7 - 2.9.
- Case B: The switches of IBC have the same pulse signal for all switches as illustrated in Figure 2.10.
- Case C: The switches IBC have one signal for two-phases and the complementary signal for the next two-phases as illustrated in Figure 2.11 [38][39].

The Figures 2.7-2.11 display the inductor current and input current ripple for each case.

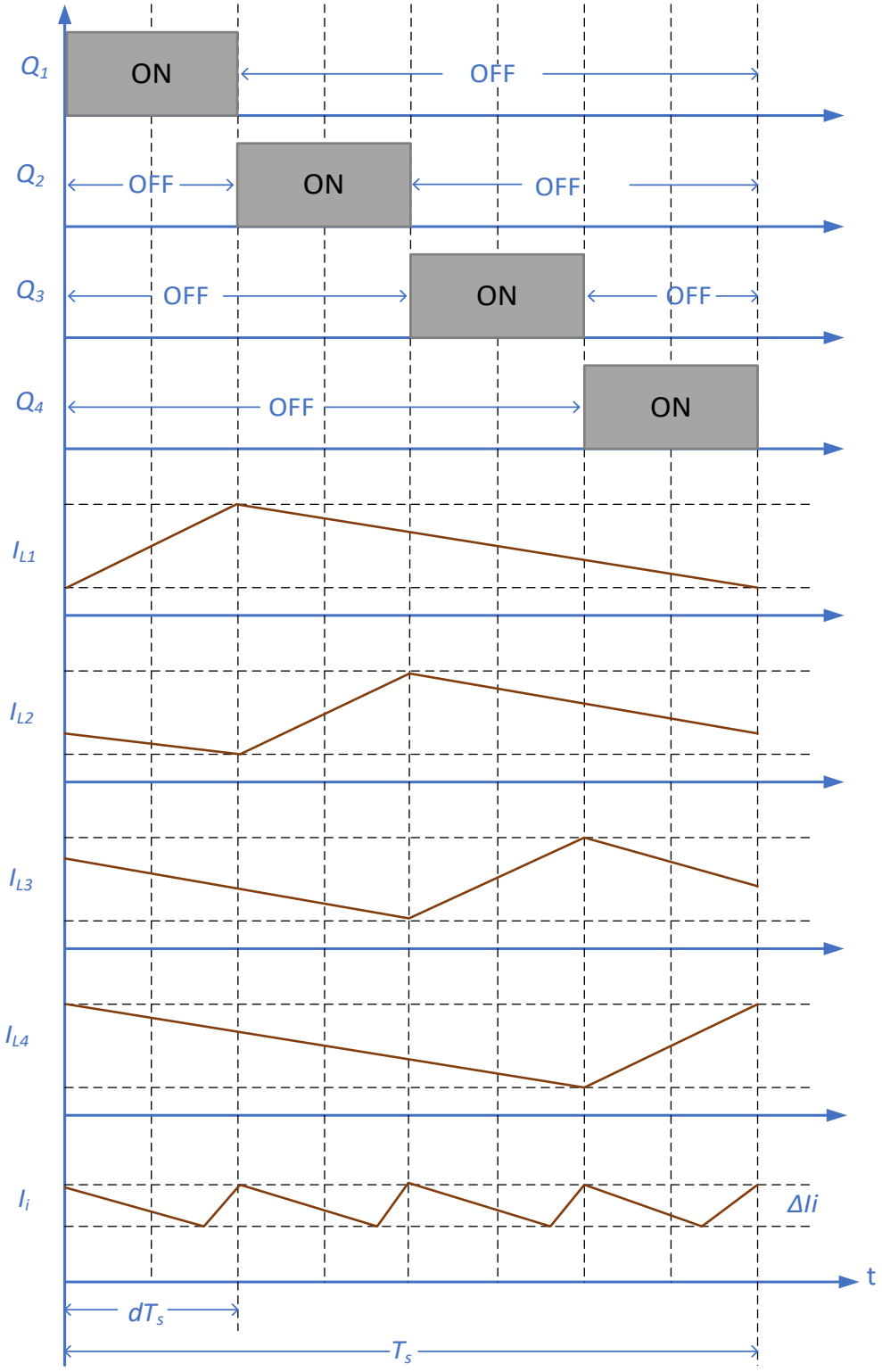

Figure 2.6 Switching type and inductor current waveforms (d = 0.25).

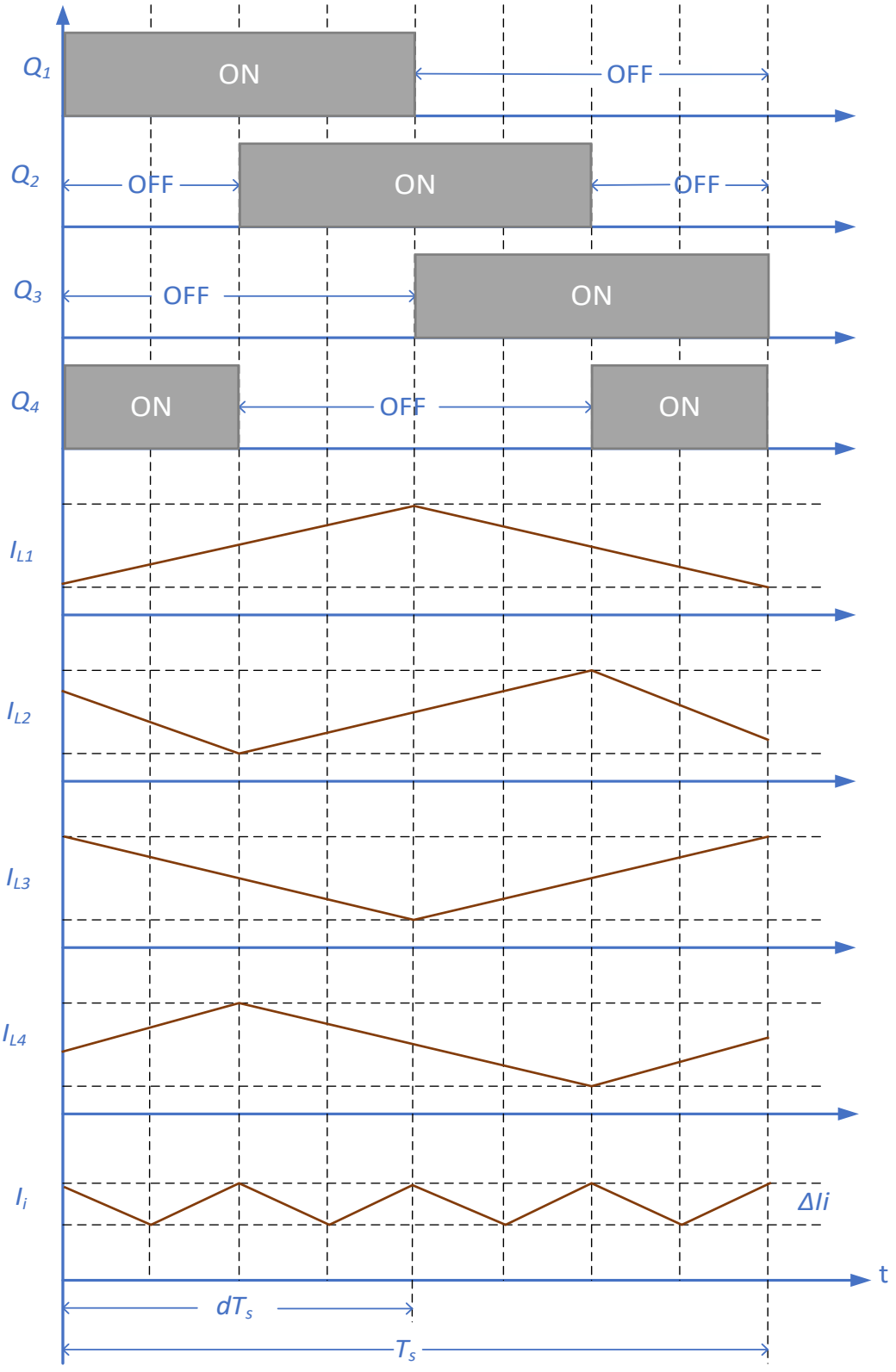

Figure 2.7 Switching type and inductor current waveforms (d = 0.5).

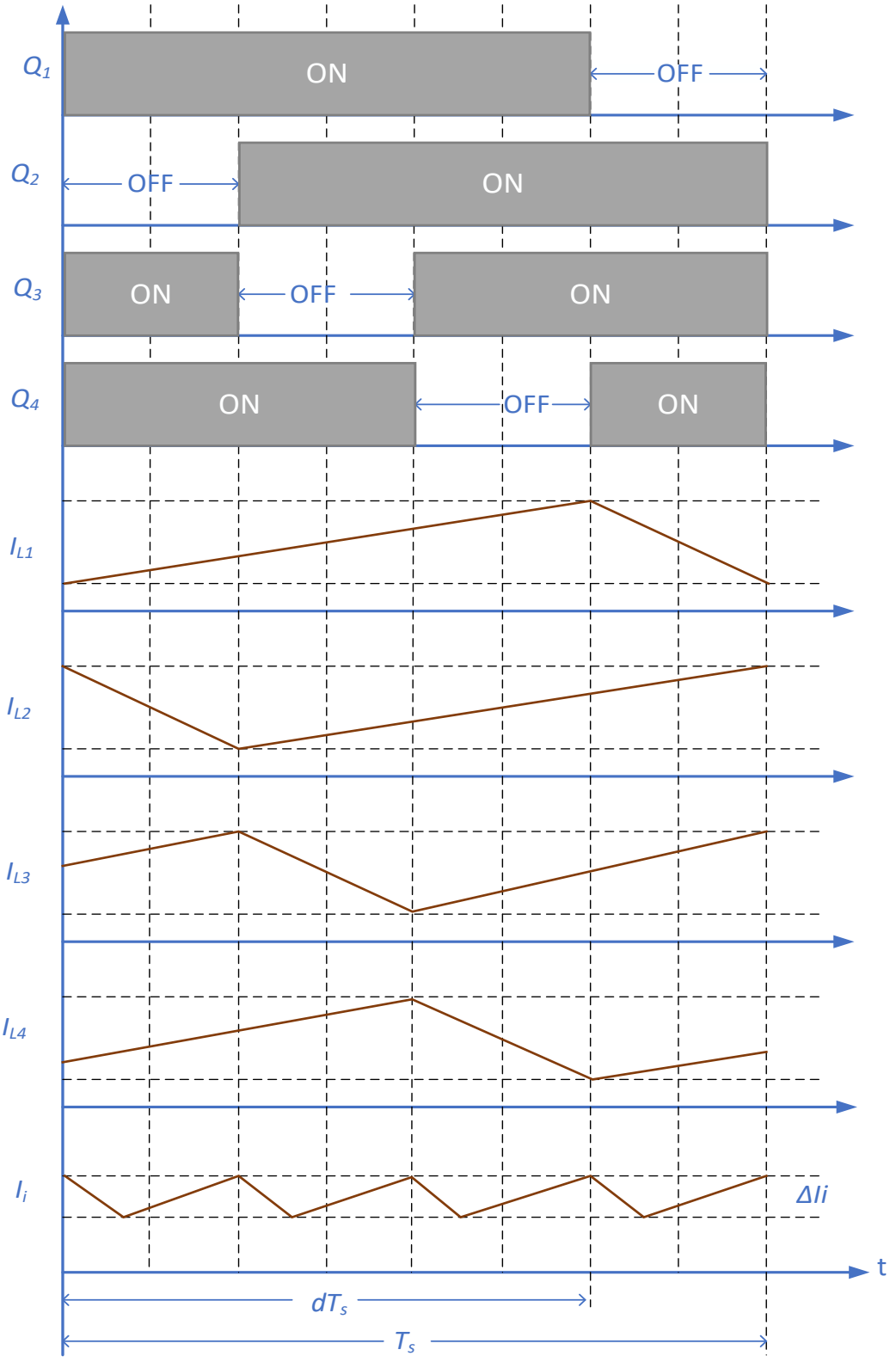

Figure 2.8 Switching type and inductor current waveforms (d = 0.75).

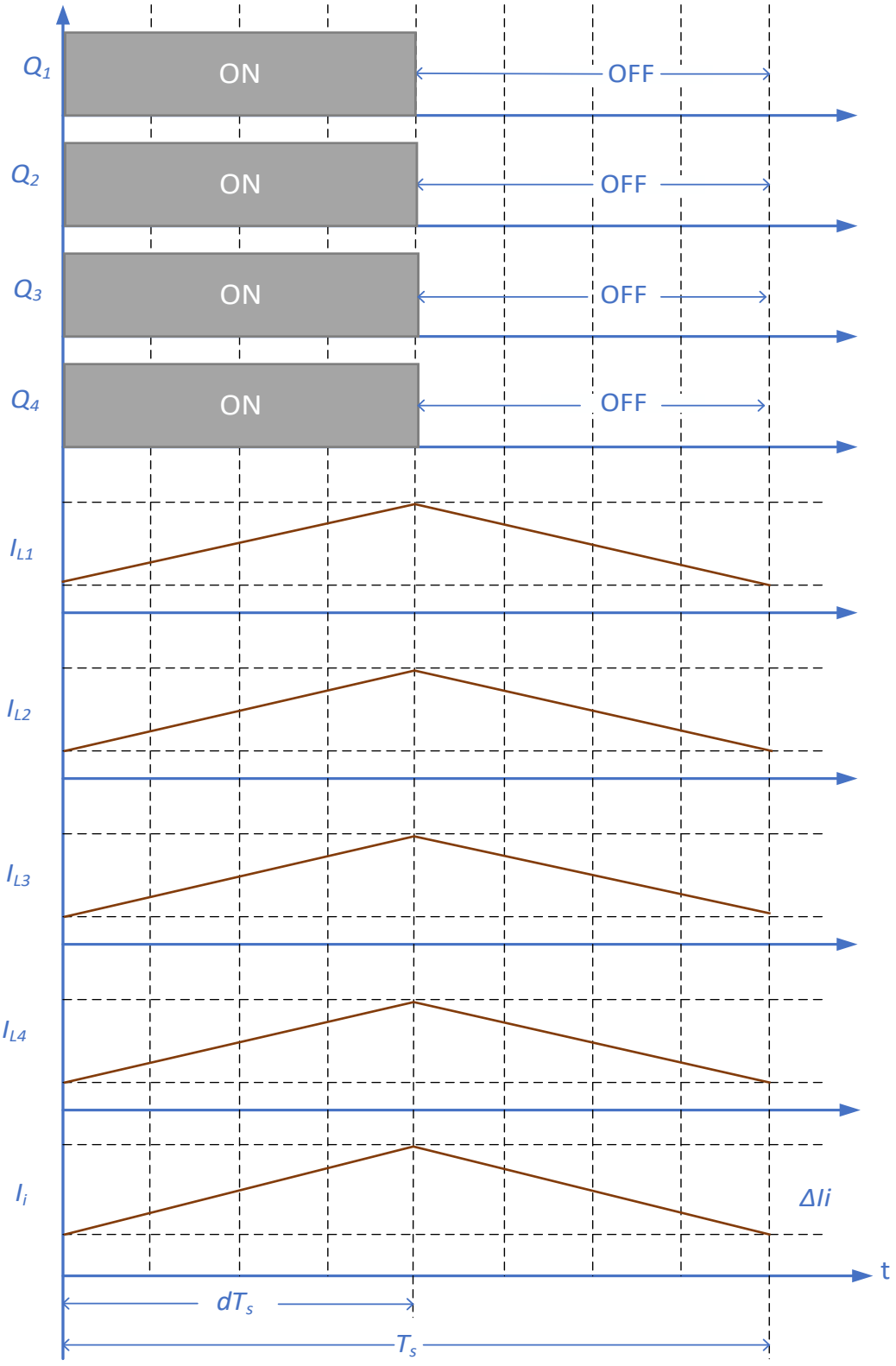

Figure 2.9 Switching type and inductor current waveforms (d = 0.5)

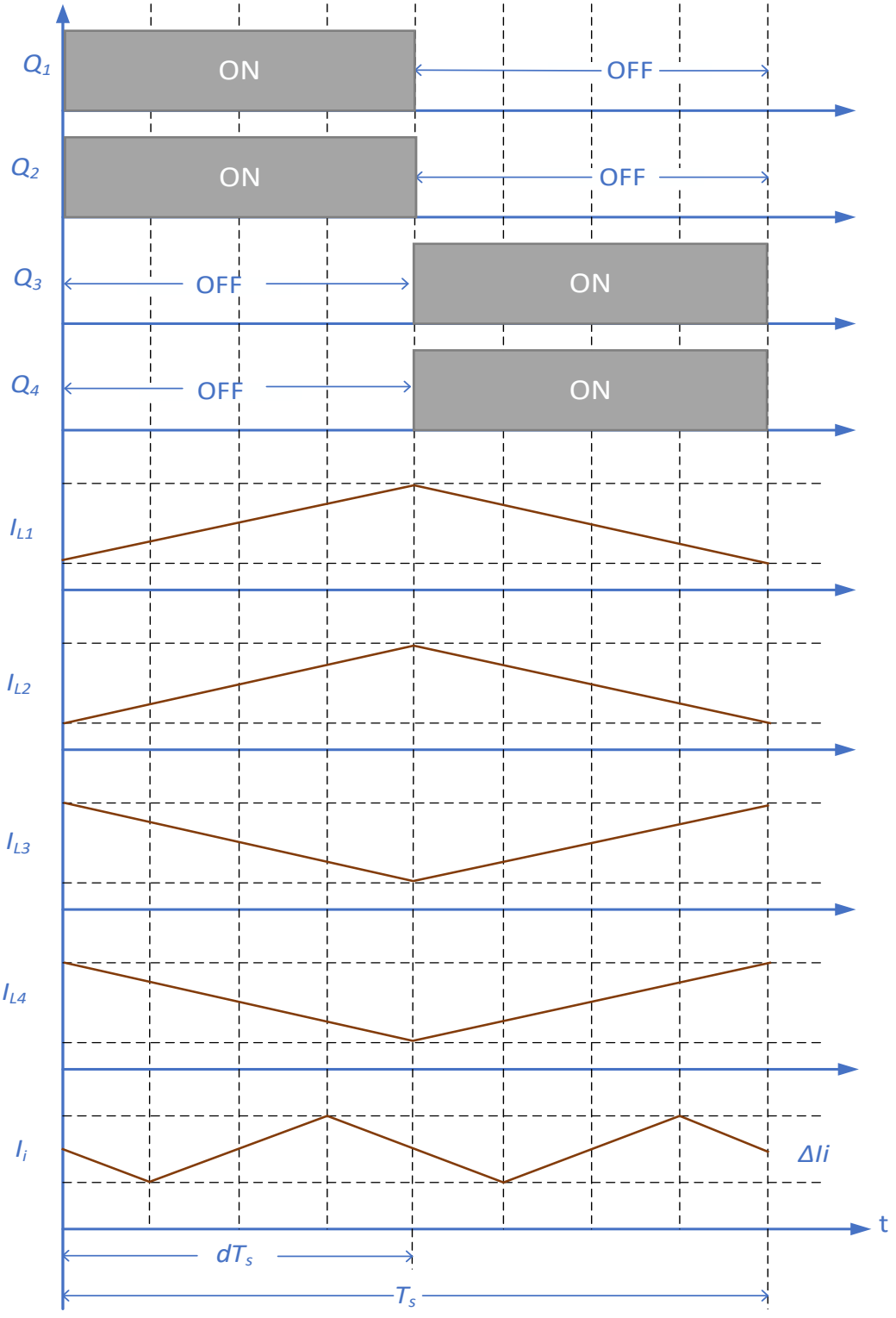

Figure 2.10 Switching type and inductor current waveforms (d = 0.5).

2.2.3 IBC design

Assume that V_i, P_o and R are known, the output voltage and current can be selected based on the following equation [40][41][42][43][6][44]:

$$P = \frac{V_o^2}{R} = V_o I_o . \tag{2.15}$$

1) Inductance, L

The minimum value of the inductance is calculated as [45]:

$$L_{\min} = \frac{d(1-d)^2 \cdot R}{2 f_s} . \tag{2.16}$$

In term of Δi_L which is chosen as follows:

$$\Delta i_L = \frac{V_s \cdot d}{f \cdot L} . \tag{2.17}$$

Then, the inductor value can be calculated as below:

$$L = \frac{V_s \cdot d}{\Delta i_L \cdot f_s} . \tag{2.18}$$

2) Capacitance, C

The capacitor value can be selected based on the following equation:

$$C_{\min} = \frac{V_o \cdot d}{R(\Delta V_o) f_s} . \tag{2.19}$$

3) Duty ratio, d

Duty cycle ratio is the same as for boost converter, which varies from 0 to 1.

$$d = 1 - \frac{V_i}{V_o}. \tag{2.20}$$

The converter operation conduction mode is approached based on these chosen parameters.

2.3 Simulink Model

Four-phase IBC is modeled using MATLAB/SIMULINK software and a comparison of different control signals is applied. Figure display the simulation model. The model parameters are listed in Table 1. The state-space equations of multi-phase IBC can be derived as a general form as fellow [46]:

$$L_n \frac{di_{L_n}}{dt} = V_i - (1 - d_n)V_o, \tag{2.21}$$

$$C \frac{dv_o}{dt} = \sum_{n=1}^{N} (1 - d_n) i_{L_n} - \frac{V_o}{R}. \tag{2.22}$$

where *n* is the number of phases.

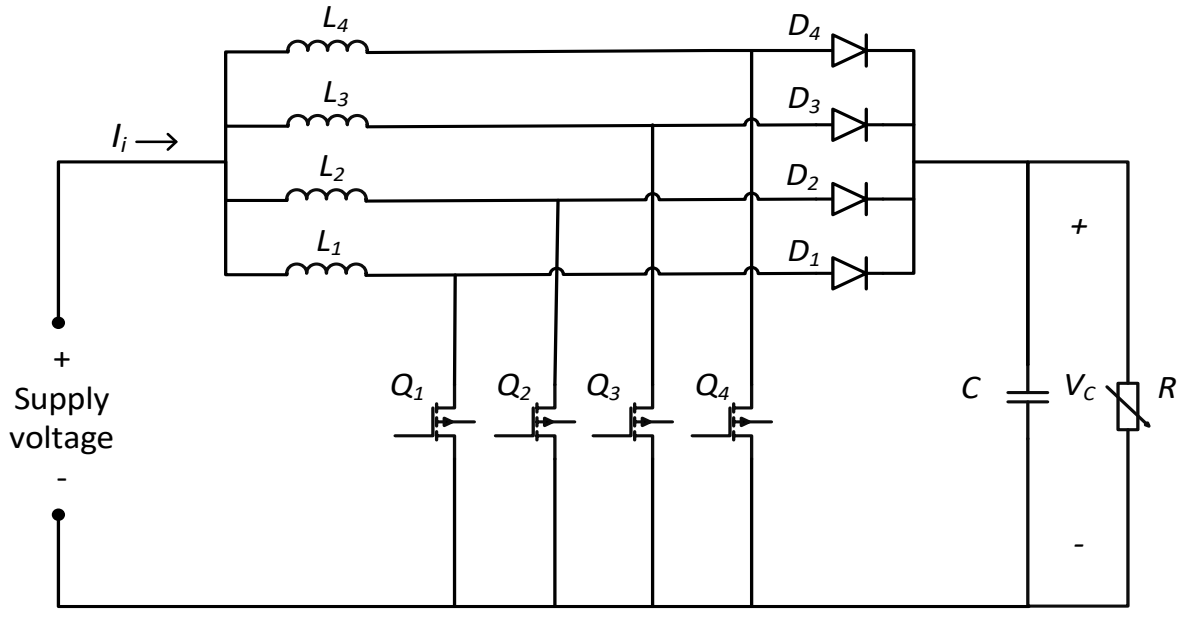

Figure 2.11 Simulation model of IBC.

Table 2.1 Model parameters.

Parameter	Value
Input voltage, V_i	15 V
Inductor, L_1=L_2=L_3=L_4	560×10^{-6} H
Capacitor, C	400×10^{-6} F
Resistor, R	250Ω to 125Ω
Switching frequency, f_s	10KHz
Output voltage, V_o	362 V

The simulation waveforms of the input current, output voltage, the inductor currents and PWM signals are shown in Figures 2.12-2.18.

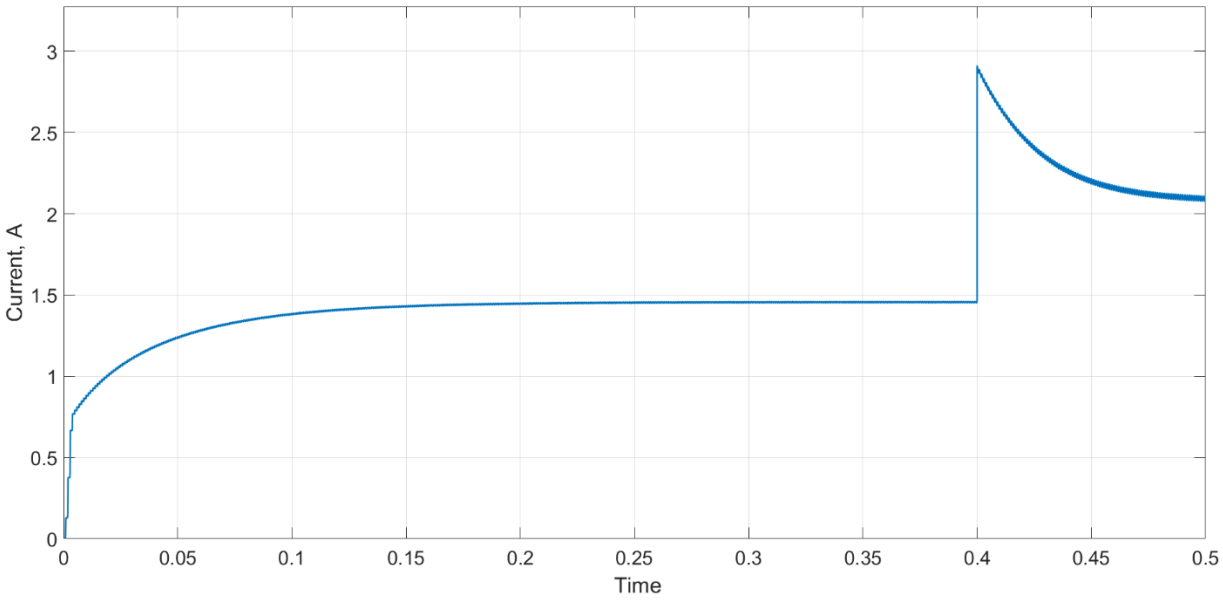

Figure 2.12 Output current

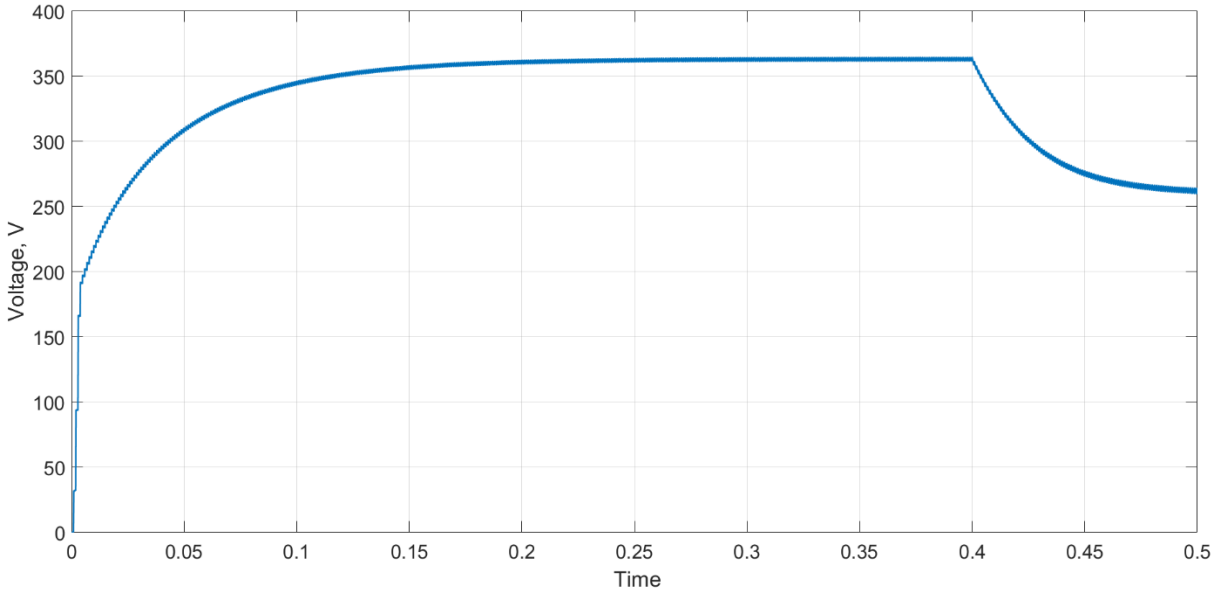

Figure 2.13 Output voltage

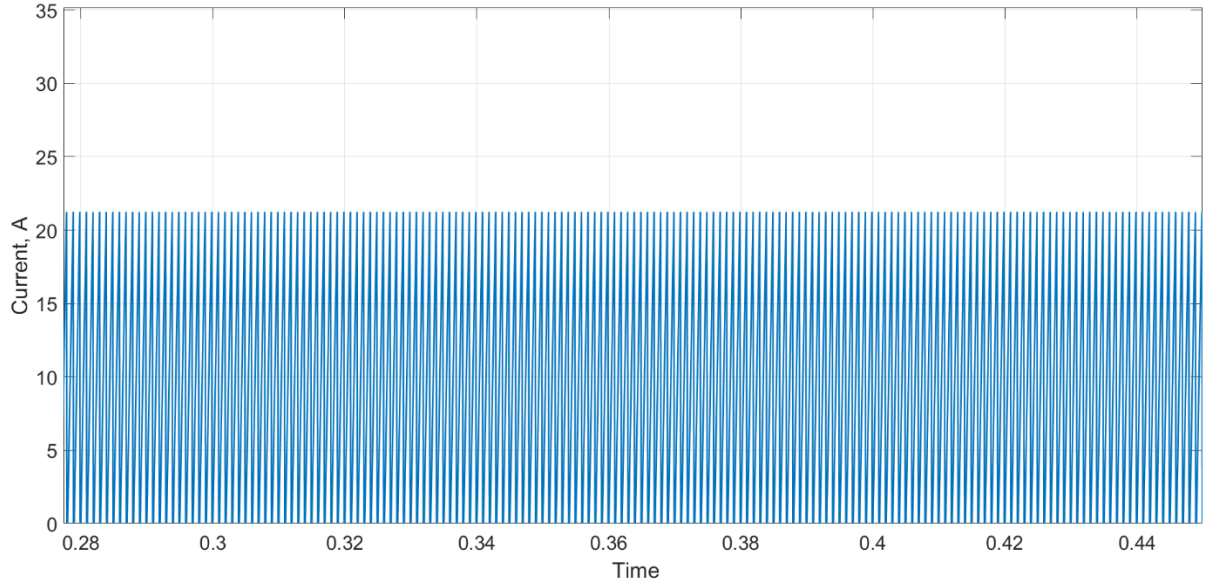

Figure 2.14 Inductor current

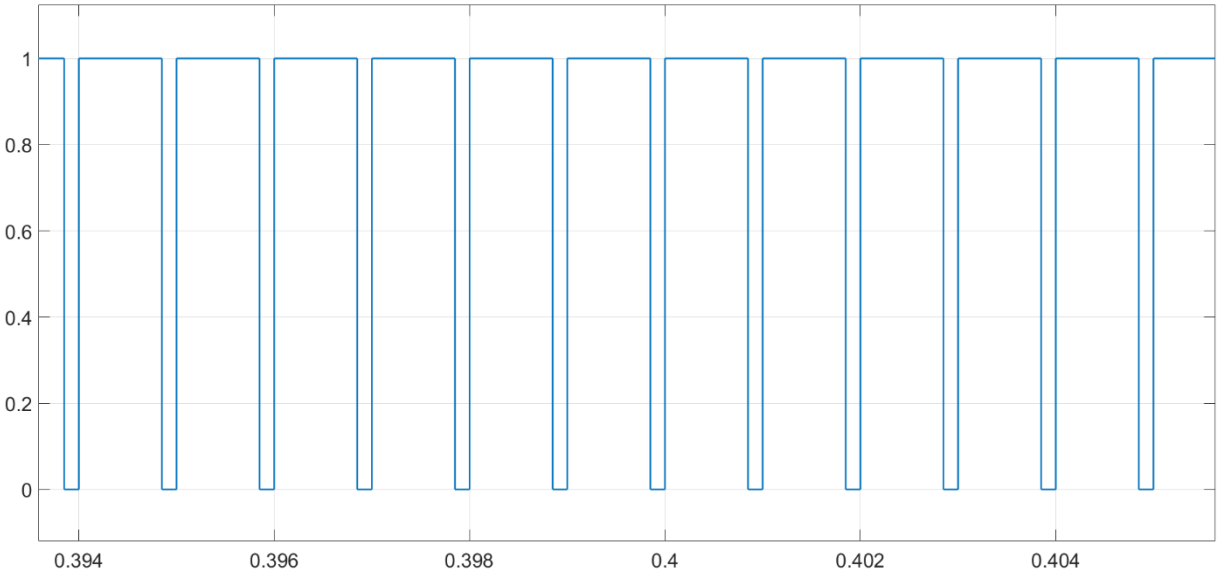

Figure 2.15 PWM waveform.

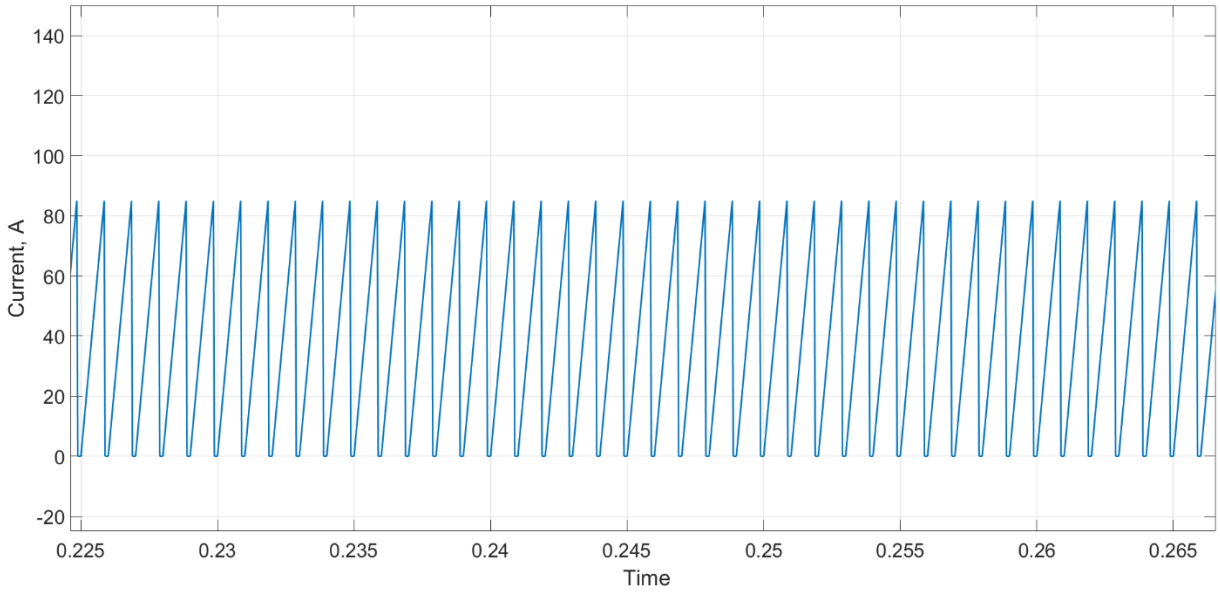

Figure 2.16 Input ripple current.

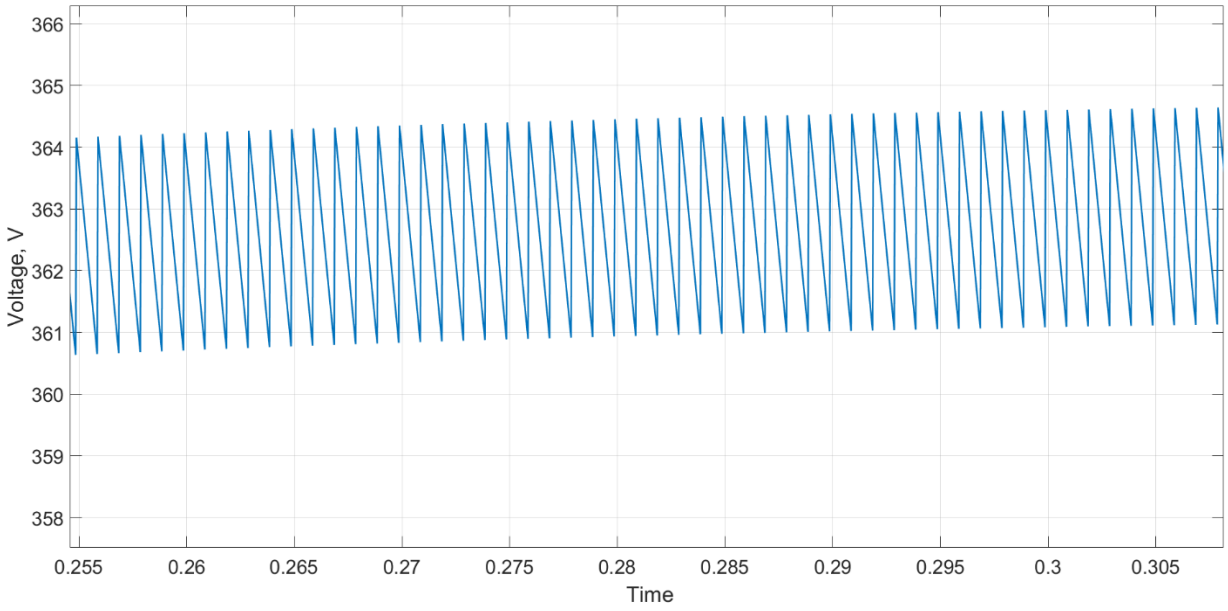

Figure 2.17 Output voltage ripple.

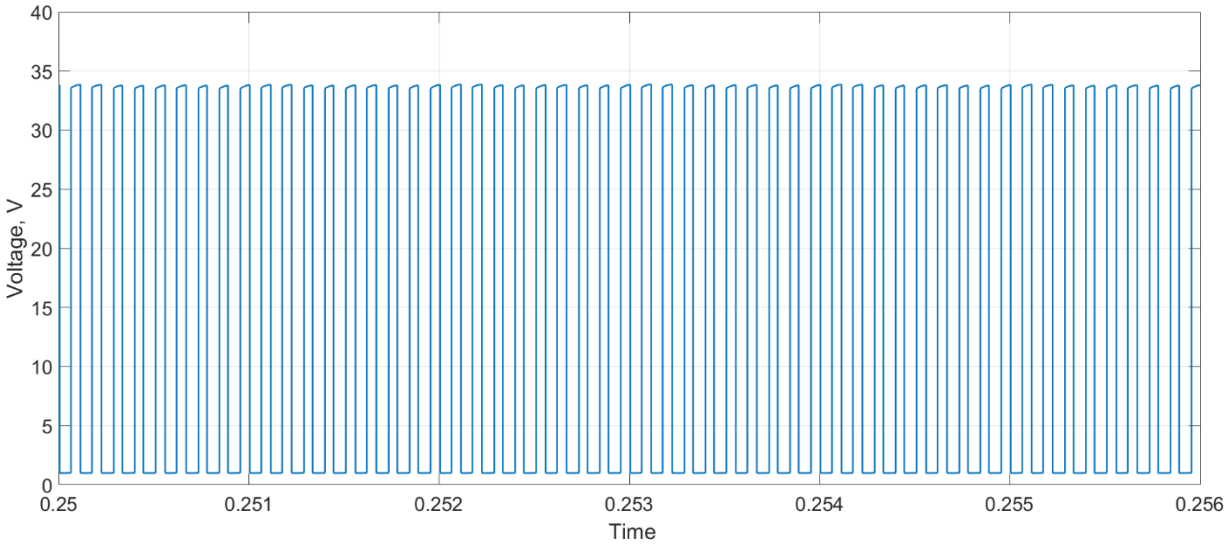

Figure 2.18 Voltage stress of switches.

2.4 AC/DC Interleaving Boost Converter

IBC has the features of reduced power factor and harmonic distortion to enhance the stability of AC/DC power system [47],[43]. That make it widely used in power factor corrections due to the high-power factor and reduced input current ripple [48]. The output filter capacitor causes a oscillating input current which affects the unity power factor and amount of harmonic distortion [49].

Fig. 2.19 depicts the block diagram of IBC for AC/DC power system (Power Factor Correction, PFC)

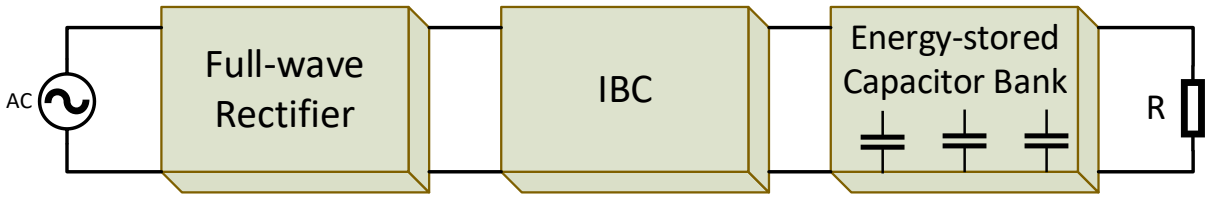

Figure 2.19 AC/DC power system.

2.5 DC/AC Interleaved Boost Convert

DC-AC power conversion with three phase inverter and boost converter is an advanced design to connect the PV source to the grid. IBC is used rather than the conventional boost converter, which provide high dc/ac voltage gain, to boost up the PV output voltage into desired grid voltage [50]. Using extremely efficient power converters such as IBC could help energy providers to save the energy and thus results in more economic benefits [51]. The DC distribution system when compared to AC distribution systems has the advantages of better efficiency and power quality beside the lower conversion units and improved performance than the AC

distribution systems [52]. The system consists of dc supply, four-phase IBC, the inverter, the filter, and the control system to improve the system performance as displayed in Fig. 2.20.

The desired ac grid voltage level from a low voltage dc source such as PV sources or batteries, is approached by using a transformer to step-up the inverter voltage. But this solution has many disadvantages such as loud noise, large size, lesser power/weight ratio, and costly. To overcome this issue, dc-dc IBC power electronic topologies can be used [50]. Many research are interested in producing a high voltage level (400 DCV) from a PV low voltage where the integration of the dc distribution request a high voltage gain converter [53]. The DC-link voltage suffer from the oscillation due to the fast dynamic of inter-area power transfer results in poor damping [47].

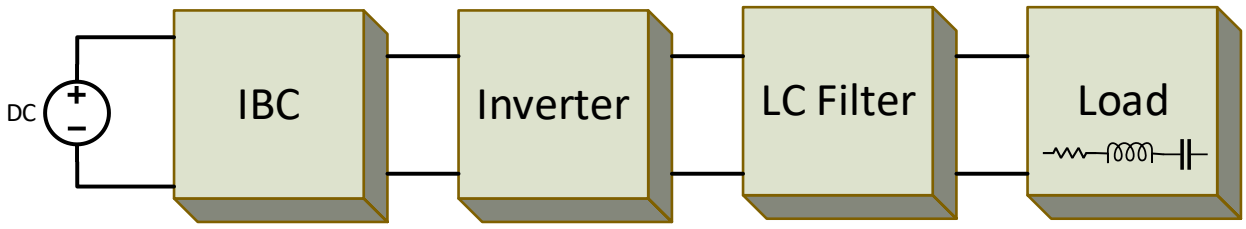

Figure 2.20 DC-grid configuration.

2.6 Conclusion

In this chapter, a multi-phase IBC is designed, analyzed and simulated at different cases. The IBC showed better performance with less input current ripple and size. Using of the technique of shift-delay has a significant effect on the input current and output voltage ripples. Based on the open loop simulation, the IBC shows higher voltage ratio and reduced input current and output voltage ripples.

CHAPTER 3

PHOTOVOLTAIC AND MPPT

3.1 Introduction

After the birth of transistor in late 1920s, scientists at Bell Telephone Laboratories have discovered the PV effect by noticing the electric current produced when the silicon exposed to the light by 1985 [54]. This discovery has made a large expanding for the use of PV energy. Solar PV generation raised by more than 30% in 2018 to 584.63 TWh/year and become the largest generation growth among all renewable sources for the first time. It is estimated to be the fastest growth of all renewable energy source in 2020. In term of generation, PV solar source is the fourth-largest renewable electricity technology with capacity of 97 GW. Figure 3.1 shows the increasing of global renewable energy generation and investment in solar renewable energy technology from 2000 to 2020 [55],[56],[57].

Generating power for electricity from green sources like PV source has more attention in the last decades and have been carried out by many researchers for different industrial application because of the negative impact of fuel generators on the environment. Solar PV converts the energy from the sun into electricity with less pollution, less maintenance, and less noise. Since the output voltage of the PV array is changeable due to the weather conditions, it is required to use power electronic for solar PV applications [58]. The output power fluctuates with the sun intensity and the temperature amount which make a power tracking system is needed to locate the highest power level and to maintain efficient operation for PV systems. Maximum Power Point Tracking MPPT is the technique that used to regulate the DC-DC converter to assure maximum power is harvested. This chapter scopes on modeling of solar PV and MPPT controller design for IBC and CIBC. The performance is analyzed and tested using MATLAB/Simulink software.

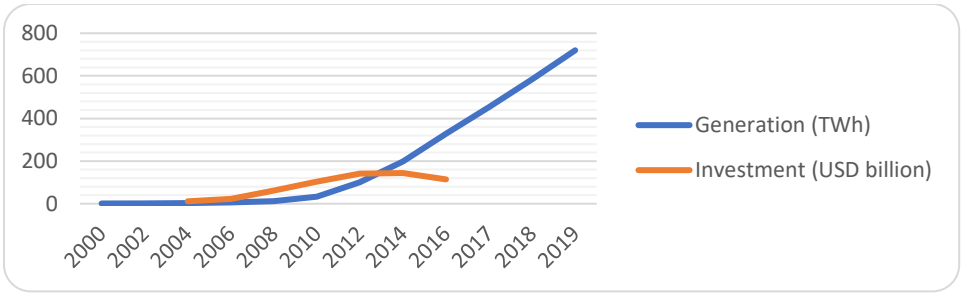

Figure 3.1 Generation power vs Investment of PV system

3.2 PV Characteristics

Solar cells are devices that use photovoltaic effect to transfer sun light into electricity. They are series and parallel connections to constitute the large PV array that meets the desired output voltage and current. PV cell circuit is equivalent to current supply circuit stimulated by the intensity of sun light or (irradiance) and temperature with parallel diode and resistance load, R_{sh} and another output resistance load, R_s in series as depicted in Figure 3.2. Equivalent circuit of PV array is depicted in Figure 3.3.

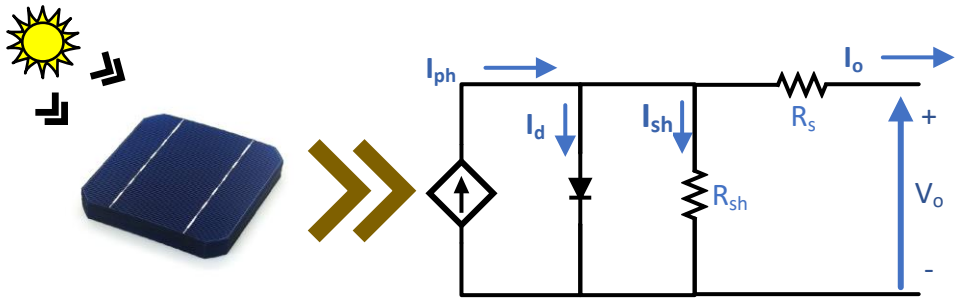

Figure 3.2 Equivalent circuit of single solar cell.

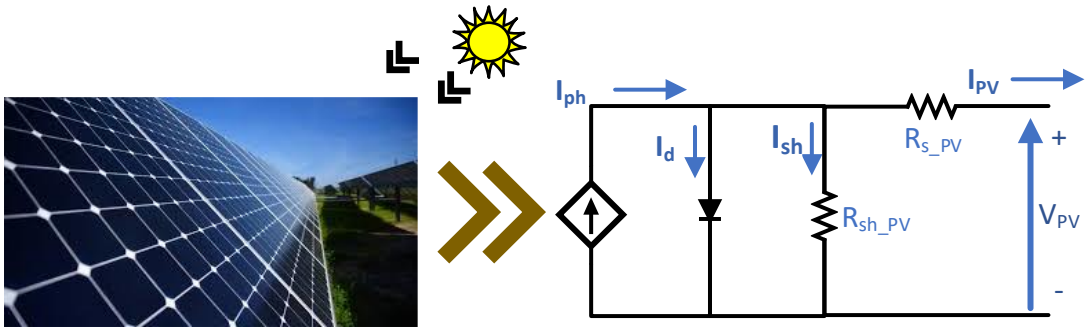

Figure 3.3 Equivalent circuit for complete PV array.

The light intensity (G) and temperature (T) have the influence on the solar panel to produce the amount of current. The output current is determined by [59]:

$$I_o = I_{ph} - I_d - I_{sh}, \tag{3.1}$$

where

$$\begin{aligned} I_{ph} &= [I_{sc} + K(T_o - T_{ref})]G \\ I_d &= I_s(e^{\frac{q(V_o + I_o R_s)}{pKT}} - 1) \\ I_{sh} &= \frac{V_o + I_o R_s}{R_{sh}} \end{aligned} \quad . \tag{3.2}$$

Here I_o is the output current, I_{ph} is the photocurrent, I_d is the saturation current of diode reverse, V_o is the PV output voltage, q is the electronic charge (1.6×10^{-19}C), K is Boltzmann constant (1.38×10^{-23}), p is the diode ideality constant, T is the outside temperature, G is the solar irradiance and I_{sc} is the short current of the cell. The output current of the PV system is given by the following equation [60]:

$$I_{PV} = n_p I_{ph} - n_p I_s(e^{\frac{q(V_{PV} + i_{PV} R_{s\_PV})}{n_s pKT}} - 1) - \frac{V_{PV} + I_{PV} R_{s\_PV}}{R_{sh\_PV}}, \tag{3.3}$$

where $R_{s\_PV} = \frac{n_s}{n_p} R_s$ and $R_{sh\_PV} = \frac{n_s}{n_p} R_{sh}$. n_p is the number of parallel cells and n_s is the number of series cells. The PV output voltage is increased by more series cells while parallel cells increases the output current.

The PV power is $P_o = V_{PV} \times I_o$ in watt. P-V characteristics curve based on the equation 3.3 is shown in Figure 3.4 which exhibits the changes of the maximum power amount with the changing effect of *G* and *T*.

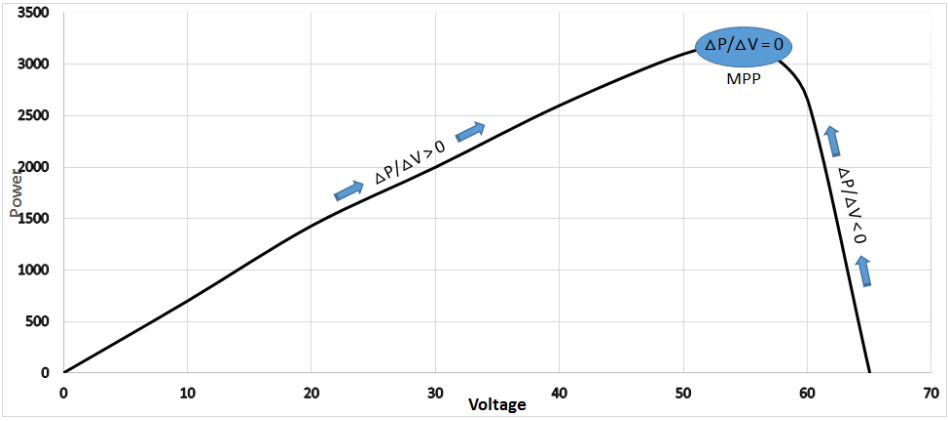

Figure 3.4 P-V characteristics.

The Fill Factor (FF) is to scale the junction quality and series resistance which is desired to unity can be determined as [61]:

$$FF = \frac{V_{mp} \times I_{mp}}{V_{oc} \times I_{sc}}. \tag{3.4}$$

The PV efficiency is defined as:

$$\eta = \frac{FF \times V_{oc} \times I_{oc}}{P_{in}}. \tag{3.5}$$

Here, P_{in} is the incident power.

3.3 MPPT Algorithms

MPPT algorithm is a technique used to generate the control signal of power switches for device connected between the PV panel and the load in order to achieve maximum efficiency. It plays an important role to stretch the efficiency of PV system because of the non-linear voltage-current (V-I) characteristics with a certain point to harvest the maximum power which depends on the weather changes the reflect on the temperature and the sun irradiance conditions. The algorithm is to track and locate the maximum power point under different weather conditions to provide the load with the available maximum power. The harvest power transferred by the solar PV system relys on PV voltage and the amount of load current in case of constant weather conditions. Many MPPT algorithms are discussed in [62][63][64][65].

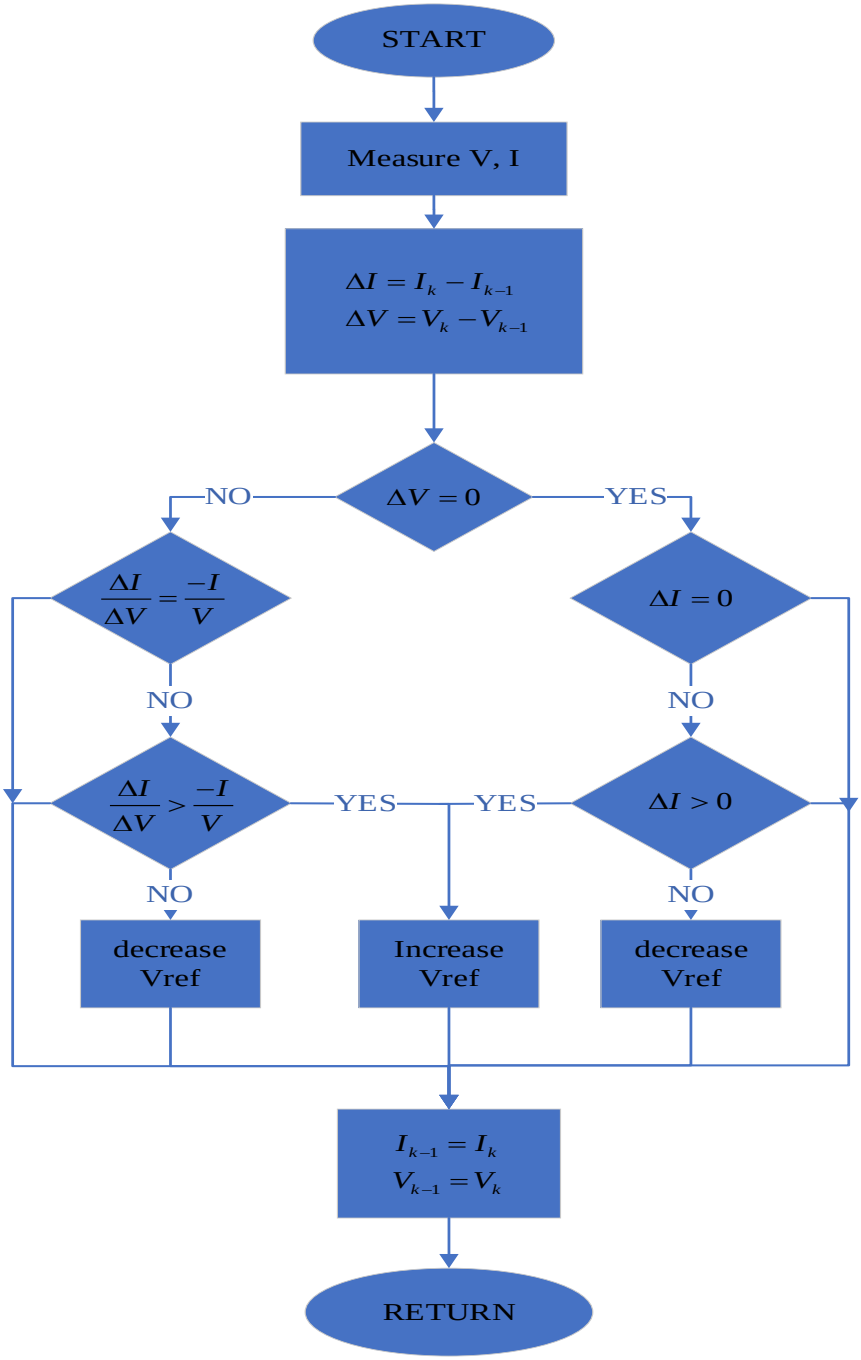

Figure 3.5 Flowchart of basic MPPT algorithm.

Types of MPPT Algorithms

MPPT algorithms are the techniques applied in controller designs for PV systems to ensure MPP are reached under variable irradiance and temperature. Several algorithms are described in the following.

1) Perturb and Observe P&O

The P&O method perturbs and operates the voltage regulation of the PV module in order to approach the maximum power's direction change that takes the same direction in case of the power increases, and reversed direction in case of the power decreases. The solar panel characteristics is not required as inputs for this technique which give it the advantage over the other methods. Beside the low-cost microcontroller, straight computation and the simple of implementation [66],[67]. Its method of operation is by perturbing the duty cycle regularly and comparing the PV output power with preceding measurement. Rapid weather changes may cause failure for this method.

2) Hill climbing algorithm

As displayed in the P-V characteristics (Figure 3.4), it is observed that when the system voltage is operating on the left of the MPP, incrementing the voltage raises the power and decrementing the voltage decreases the power while the opposite when operating on the right of the MPP. Therefore, the raise in power should the following perturbation the same to locate the MPP. The process will reach MPP when repeatedly. If oscillation occurs, then the perturbation step size should be reduced but this could the tracking of the MPP. Variable perturbation size is a solution of this issue which have been discussed in [68] and [67]. Rapidly weather changes might result in failure. Comparing the actual power point with another two proceeding points by using three-point weight comparison can solve this as proposed in [69].

3) Incremental conductance InC

The IC method is one of the efficient methods utilizes the PV array's incremental conductance *di/dv* by measuring the incremental conductance to the instantaneous conductance that applies the condition (*dp/dv=0*) to reach the highest power point which result in a high performance by increasing or decreasing the voltage under changing conditions while comparing these measurements [70],[71]. The MPP locates when the slope of PV equal zero, left when the slope is positive and right when the slope is negative as illustrated in Figure 3.4 [64]. In general, once the PV array is located at the MPP, the system will maintain at this point unless the weather conditions are changed, then the algorithm will decrement or increment to track the new MPP and to adjust the V_{MPP}.

4) Fuzzy logic control

This method became popular since the use of microcontrollers [64]. It has the advantages of working with different inputs, nonlinearity, and no need for perfect mathematical model[72][73].The technique depends of three steps: fuzzification, rule base table search, and defuzzification[64], [74]. The designer has the flexibility to choose the error which is the controller inputs.

5) DC-Link Capacitor Droop Control

The technique is designed for parallel connection PV array that fed an ac system which doesn't seek computation of the PV power. It is based on the relation of the grid output voltage and the PV voltage and the grid input current and stabilizing the power at each stage within the maximum power harvested from the PV array to keep the $V_{DC\text{-}link}$ constant [75].

The algorithms above are popular for MPPT but the differences between them in the implementation, tracking speed, number of steps, cost, and the efficiency [76]. For this work, a simple P&O and InC methods has been applied for the IBC.

3.3 DC-DC Interleaved Boost Converter for PV Application

DC-DC boost converter is used to raise the output voltage level of the PV array to desired grid voltage level to improve the efficiency of PV panel which can provide higher voltage gain with high current and voltage ripples which can be disadvantages [77]. Since the output voltage of PV system is low, a dc-dc boost converter is needed to step-up the PV output voltage into the load voltage. Boost converter can do the mission within limited input current. For high current, interleaved boost converter has the advantage to handle it with less ripple, less inductor size, improved reliability and better efficiency. IBC, as displayed in Figure 3.6, is multi boost converters connected in parallel and sharing the input voltage, output capacitor and load which leads to diminish current and voltage ripples, reduce harmonics and expedite efficiency [78],[79]. The phase shift of each switch is (*360/n*) where *n* is the number of phases. The dc-dc boost converter sourced by PV system is a third order nonlinear system with states of inductor current i_L, PV voltage V_{pv} and load voltage V_o. The state-space model is written as follows [59]:

$$\dot{i}_{L_1} = \frac{1}{L_1}(V_{PV} - V_o) + \frac{1}{L_1}V_o u \tag{3.6}$$

$$\dot{i}_{L_2} = \frac{1}{L_2}(V_{PV} - V_o) + \frac{1}{L_2}V_o u \tag{3.7}$$

$$\dot{i}_{L_3} = \frac{1}{L_3}(V_{PV} - V_o) + \frac{1}{L_3}V_o u \tag{3.8}$$

$$\dot{i}_{L_4} = \frac{1}{L_4}(V_{PV} - V_o) + \frac{1}{L_4}V_o u \tag{3.9}$$

$$\dot{v}_{PV} = \frac{1}{C_i}(i_{PV} - i_i) \tag{3.10}$$

$$\dot{v}_o = \frac{1}{C_o}(i_i - \frac{V_o}{R}) - \frac{1}{C_o} i_i u \,. \tag{3.11}$$

Where C_i is the input capacitor, C_o is the output capacitor, L is the inductor value, V_o is the desired output voltage, R is the load resistance and u is the converter switch signal which varies from 0 to 1.

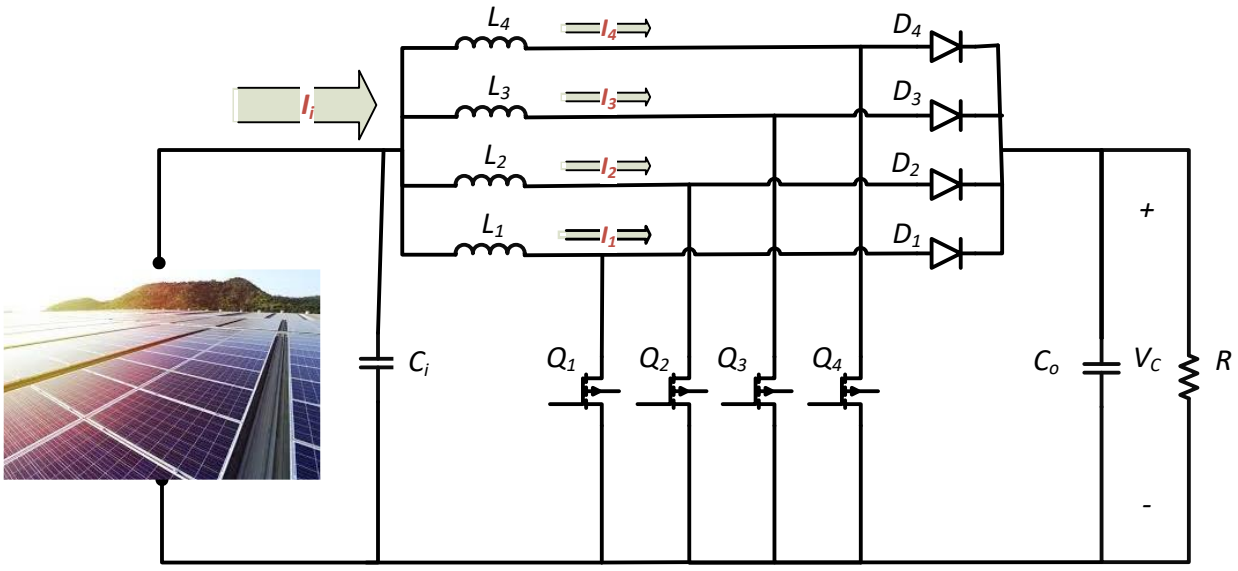

Figure 3.6 Four-phase interleaved boost converter for PV system.

A boost converter is compared with a two-phase interleaved boost converter for PV application.

The system specification is listed in Table 3.1. It is clear from Figure 3.7 which shows the inductor current for the boost and the two-phase IBC that the IBC has less inductor current and less ripple as well and it has higher output voltage as shown in Figure 3.8.

Table 3.1 PV-IBC specifications

Parameters	**Values**
Parallel cells, N_p	11 cells
Series cell, N_s	1 cell
Maximum power, P_m	305.226 W
Open circuit voltage, V_{oc}	64.2 V
Voltage at maximum power, V_{mp}	54.7 V
Short circuit current, I_{sc}	5.96 A
Current at maximum power, I_{mp}	5.58 A
Irradiance, I_r	800 W/m^2
Temperature, T	36 C^o
Inductor, L	560×10^{-6} H
Capacitor, C_i=C_o	100×10^{-6} F
Resistance load, R	200 Ω
Switching frequency, f_s	10 KHz

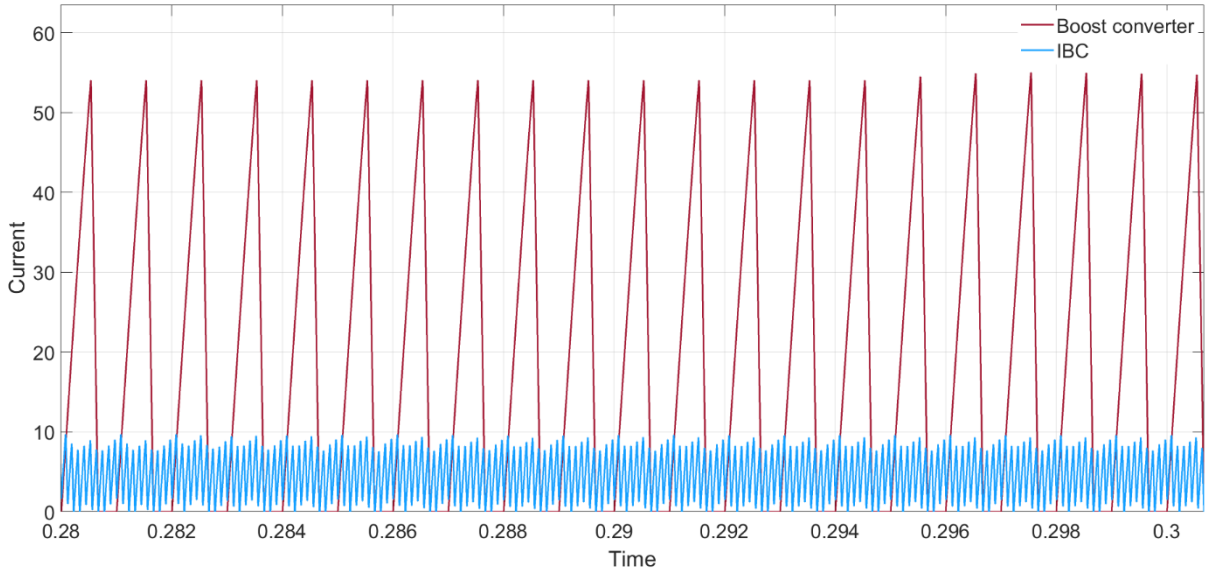

Figure 3.7 Inductor current.

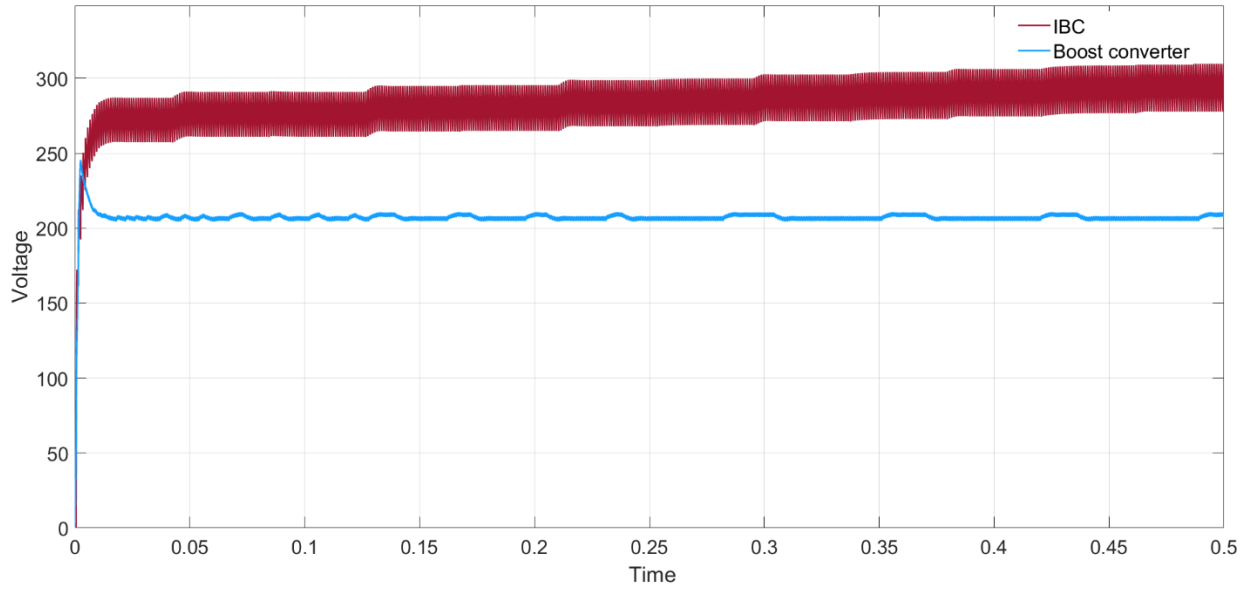

Figure 3.8 Output voltage.

3.4 Grid-connected PV system

PV solar system is used to deliver power into standalone applications and grid connected applications which has been introduced to enable the large amount of solar energy introduced from

distributed PV generation units [58], [80]. The IBC has the features of high reliability, reduced size and cost which make it favorable for PV-grid application.

The advantages of using IBC in PV-Grid application are:

- Improve the power conversion efficiency.
- Regulate the DC-bis voltage.
- Improve power factor.
- Reduce the total harmonic THD.

Simulation example:

A four-phase IBC is designed to interface PV grid with specifications listed in Table 3.2. The load is step changed at 0.4 sec which gives the output voltage in Figure 3.9 and output current in Figure 310.

Table 3.2 PV-grid specifications

Parameters	**Values**
Parallel cells, N_p	11 cells
Series cell, N_s	1 cell
Irradiance, I_r	800 W/m^2
Temperature, T	36 C^o
Maximum power, P_m	305.226 W
Open circuit voltage, V_{oc}	64.2 V
Voltage at maximum power, V_{mp}	54.7 V
Short circuit current, I_{sc}	5.96 A

Current at maximum power, I_{mp}	5.58 A
Inductor, L	560×10^{-6} H
Capacitor, C_i=C_o	100×10^{-6} F
Resistance load, R	100 Ω to 50 Ω
Switching frequency, f_s	10 KHz
AC frequency	50 Hz
DC-bus voltage	350 V
Grid peak voltage	400 V

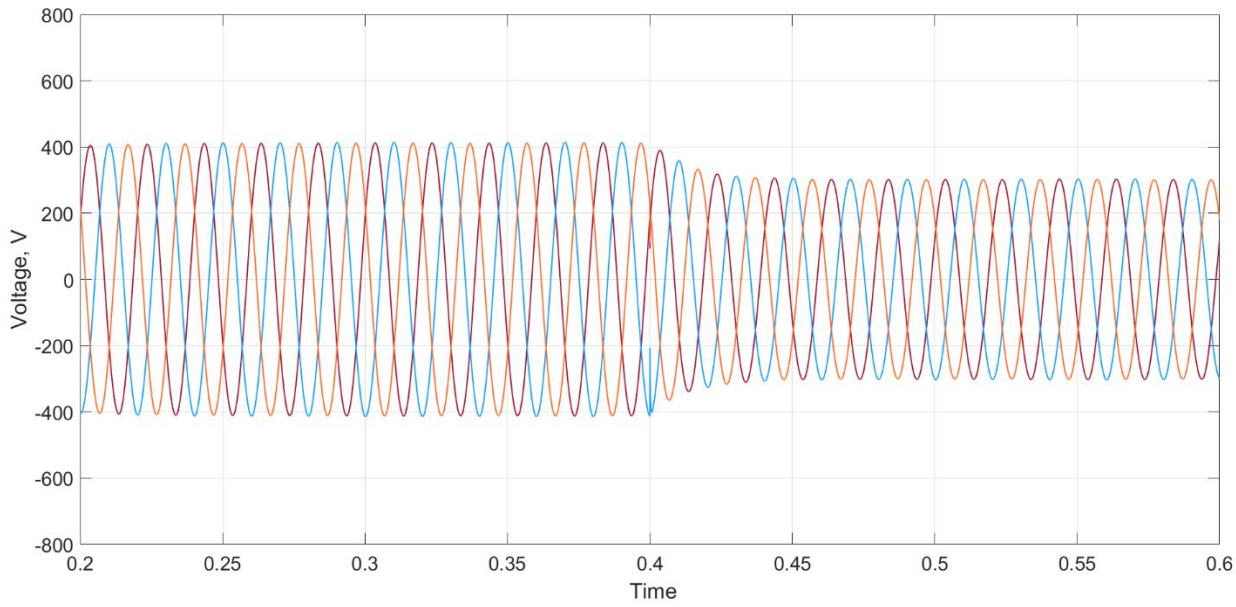

Figure 3.9 Grid output voltage.

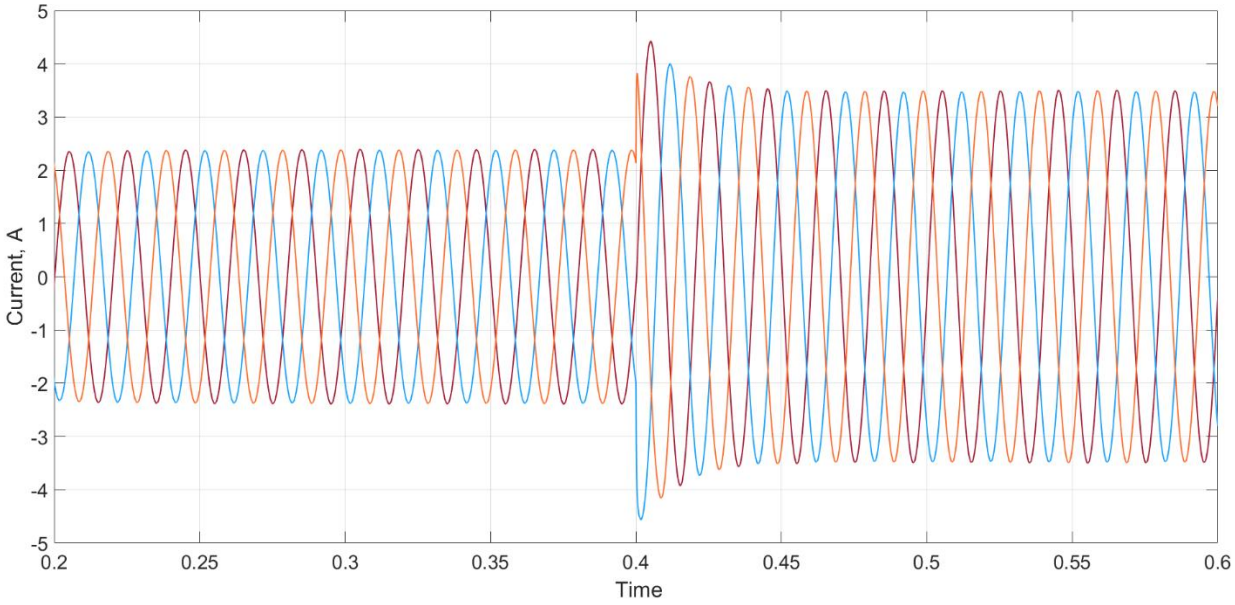

Figure 3.10 Grid output current.

3.5 Proposed control for cascade IBC for PV application.

The maximum power extraction of PV array is achieved by using Maximum Power Point Tracking (MPPT) technique to inject power to grid as a constant power load [81], as shown in Figure 3.11(a), but the system will suffer from the instability in case of load disturbance. Feedback voltage or current control technique, as shown in Figure 3.11(b), is applied to solve the stability issue but the maximum power extraction is not achieved. The use of Cascade Interleaved Boost Converter (CIBC) is a solution where the PV-converter is regulated by MPPT technique because its connected directly to the PV system and the load-converter is controlled by µ-controller to maintain the output voltage constant and stable as displayed in Figure 3.12. The objective of this is to design a robust control for CIBC to maintain constant output voltage and to ensure maximum power is transferred from the PV arrays to the system.

Figure 3.11 Control techniques: a) MPPT control, b) Feedback control.

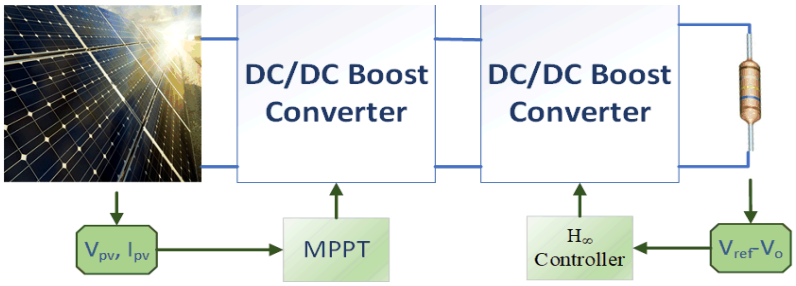

Figure 3.12 Proposed control system.

State-space Analysis

The state space analysis technique is applied to analysis the four-phase converter which will be controlled by MPPT controller. The four-phase IBC is working in different modes. In this study the four switches are phase-shifted by 90^{o} in four modes:

- Mode 1: Q_1, ON, while Q_2, Q_3 and Q_4 are OFF.

The supply current starts to storage energy in L_1, while L_2, L_3 and L_4 discharge energy into the load as displayed in Figure 3.13.

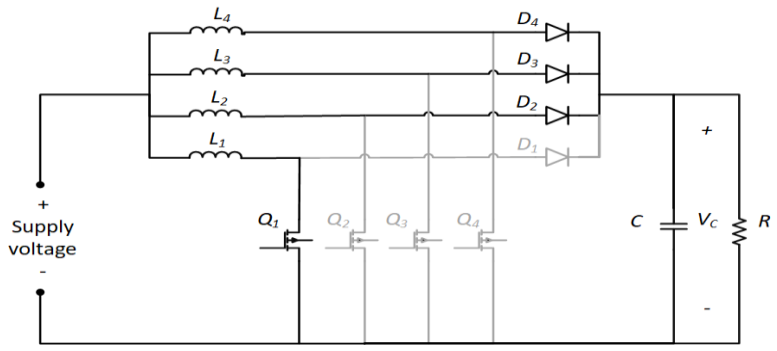

Figure 3.13 Equivalent circuit of Mode 1.

Applying Kirchhoff's laws to determine the state equations as follows:

$$\frac{di_{L_1}}{dt} = \frac{V_{PV}}{L_1} s_1 \tag{3.12}$$

$$\frac{di_{L_2}}{dt} = \frac{di_{L_3}}{dt} = \frac{di_{L_4}}{dt} = \frac{V_{PV} - v_c}{L_2}(1 - s_1) \tag{3.13}$$

$$\frac{dv_c}{dt} = \frac{i_{L_2}}{C} + \frac{i_{L_3}}{C} + \frac{i_{L_4}}{C} - \frac{v_c}{RC}. \tag{3.14}$$

- Mode 2: Q_2, ON, while Q_1, Q_3 and Q_4 are OFF.

The supply current starts to charge energy at L_2, while L_1, L_3 and L_4 discharge energy into the load as displayed in Figure 3.14.

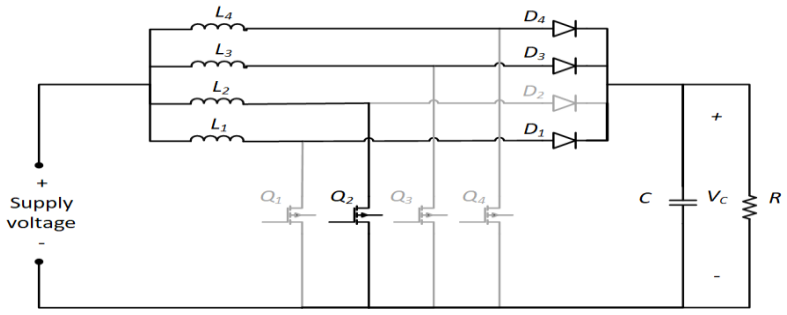

Figure 3.14 Equivalent circuit of Mode 2.

Kirchhoff's current and voltage laws can be written as:

$$\frac{di_{L_2}}{dt} = \frac{V_{PV}}{L_2} s_2 \tag{3.15}$$

$$\frac{di_{L_1}}{dt} = \frac{di_{L_3}}{dt} = \frac{di_{L_4}}{dt} = \frac{V_{PV} - v_c}{L_3}(1 - s_2) \tag{3.16}$$

$$\frac{dv_c}{dt} = \frac{i_{L_1}}{C} + \frac{i_{L_3}}{C} + \frac{i_{L_4}}{C} - \frac{v_c}{RC}. \tag{3.17}$$

- Mode 3: Q_3, ON, while Q_1, Q_2 and Q_4 are OFF.

The PV output current starts to charge energy at L_3, while L_1, L_2 and L_4 discharge energy into the load as displayed in Figure 3.15.

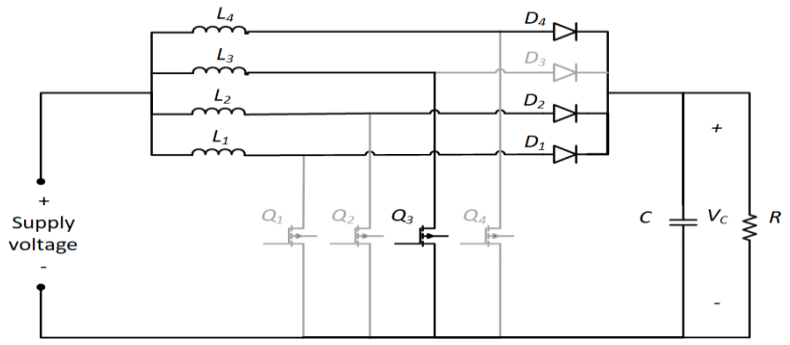

Figure 3. 15 Equivalent circuit of Mode 3.

Kirchhoff's current and voltage laws can be written as:

$$\frac{di_{L_3}}{dt} = \frac{V_{PV}}{L_3} s_3 \tag{3.18}$$

$$\frac{di_{L_1}}{dt} = \frac{di_{L_2}}{dt} = \frac{di_{L_4}}{dt} = \frac{V_{PV} - v_c}{L_1}(1 - s_3) \tag{3.19}$$

$$\frac{dv_c}{dt} = \frac{i_{L_1}}{C} + \frac{i_{L_2}}{C} + \frac{i_{L_4}}{C} - \frac{v_c}{RC}. \tag{3.20}$$

- Mode 4: Q_4, ON, while Q_1, Q_2 and Q_3 are OFF.

The PV output current starts to charge energy at L_4, while L_1, L_2 and L_3 discharge energy into the load as displayed in Figure 3.16.

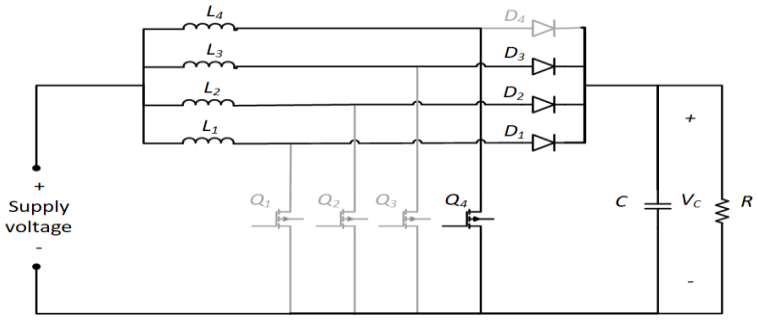

Figure 3.16 Equivalent circuit of Mode 4.

Kirchhoff's current and voltage laws can be written as:

$$\frac{di_{L_4}}{dt} = \frac{V_{PV}}{L_4} s_4 \tag{3.21}$$

$$\frac{di_{L_1}}{dt} = \frac{di_{L_2}}{dt} = \frac{di_{L_3}}{dt} = \frac{V_{PV} - v_c}{L_1}(1 - s_4) \tag{3.22}$$

$$\frac{dv_c}{dt} = \frac{i_{L_1}}{C} + \frac{i_{L_2}}{C} + \frac{i_{L_3}}{C} - \frac{v_c}{RC}. \tag{3.23}$$

CHAPTER 4

CONVERTERS CONNECTION

4.1 Introduction

Power converters could be connected in series (cascade) or parallel (multi-level) for high voltage or low current gain and high- power applications. They have been introduced and developed in 1960s and have applied to many industrial applications successfully and become a solution for different power distribution systems and renewable energy sources for medium and high voltage applications [82]. Nowadays, cascade converters for high-power applications are gaining more attention, and are becoming one of the choices for new topologies and control in many industry applications as it has many advantages such as (i) scalability to provide the required voltage level of the load , (ii) improved harmonic performance and efficiency, and (iii) increase the converter configuration. The industrial applications of power converters are such as Flexible AC Transmission System (FACTS), industrial drives and traction systems, distributed generation, military applications, submarine power systems, medical appliances, high voltage direct-current (HVDC) transmission, hybrid electric vehicles charge stations, clean energy such as PV and wind energy [83][84][85][86]. The design of cascade converters presents some challenges such as nonlinearity and stability issue due to the interaction between the converters.

The idea of multilevel topology was proposed by William McMurray in 1971 [87] for cascade H-bridge and Flying Capacitors by [88]. The diode-clamped converter was invented by Baker in 1980 [89] then followed by the three-level Neutral Point Clamped converter in 1981 [90] and become commercially available for medium voltage application in the 1990s.

In order to achieve high-voltage levels or high-power capability, a single converter would be insufficient. Therefore, to increase the voltage level and power capability, several converters

are connected in series to increase the voltage ratings, or in parallel to increase the current capability. Combination of both series and parallel converters is used in distributed power systems with high efficiency with high voltage rating and high current capability.

4.2 Cascade Converters

Series boost converters were introduced as a solution to exchange the conventional boost converter to boost the overall voltage gain and to enhance the system operation at low duty cycle by each converter where typical boost converter need extreme duty ratios to achieve the high-voltage step-up which result in more conduction losses and diode reverse recovery problem. When power boost converters are cascaded in series for high-voltage application, the steady-state and transient voltages will be divided equally among the individual series converters which is often challenging. The main drawbacks of cascade converters are the high number of semiconductors and switches which results in increased losses. Also, the oscillation produced on the first-stage could be enlarged within the next stages.

The power ratio of multi-stage boost converter is:

$$\frac{V_o}{V_i} = \left(\frac{1}{1-d}\right)^n . \tag{4.1}$$

The system efficiency for multi-stage boost converters is:

$$\eta_T = \eta_1 \eta_2 \cdots \eta_n , \tag{4.2}$$

where *n* is the number of cascaded converters as shown in Figure 4.1.

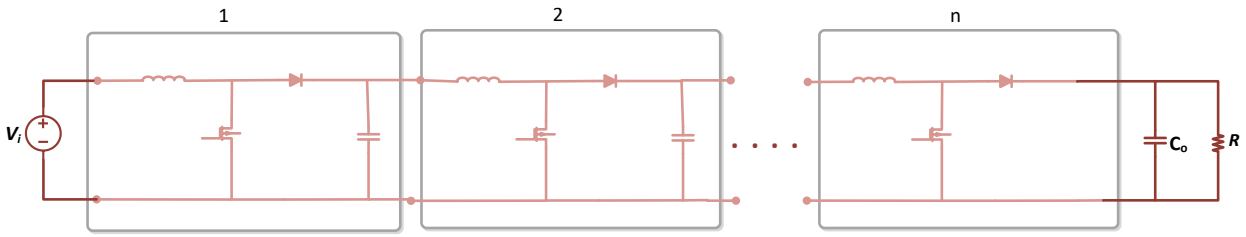

Figure 4.1 Cascade power boost converter.

4.3 Multi-level converters

Parallel or multilevel converters (Figure 4.2) are a good choice for supplying different applications and being used in the grid system, due to the features of good power quality, high efficiency, improved reliability, reduced harmonic, better electromagnetic compatibility (EMC), and long term maintainability [91]. By increasing the number of voltage levels within a converter, the harmonic content is decreased. This helps to avoid filtering, reduce electromagnetic interference, and reduce losses due to a lower switching frequency requirement. The main drawbacks are the high number of semiconductors and switches, and the high circulating current.

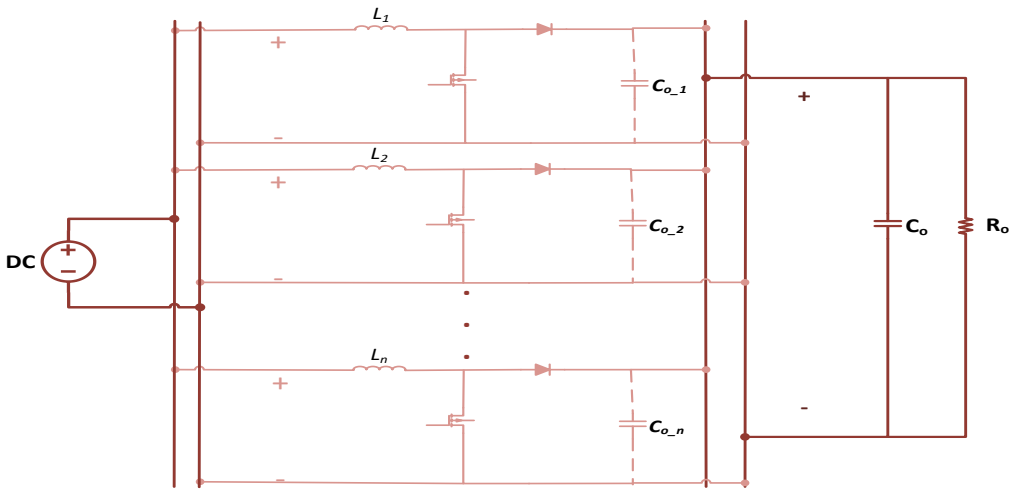

Figure 4.2 Multi-level boost power converters.

4.4 Cascade IBC

The features of IBC, mentioned in section 2.2, could be added into the cascading benefits to get more reliable system with better efficiency and to overcome the limitation of the voltage conversion of single converter. Two three-phase IBCs are connected in series and compared with two cascade boost converters. Figure 4.3 shows the inductor current comparison and Figure 4.4 shows the output voltage comparison. It is noticed that the CIBCs deliver higher output voltage level with less inductor current.

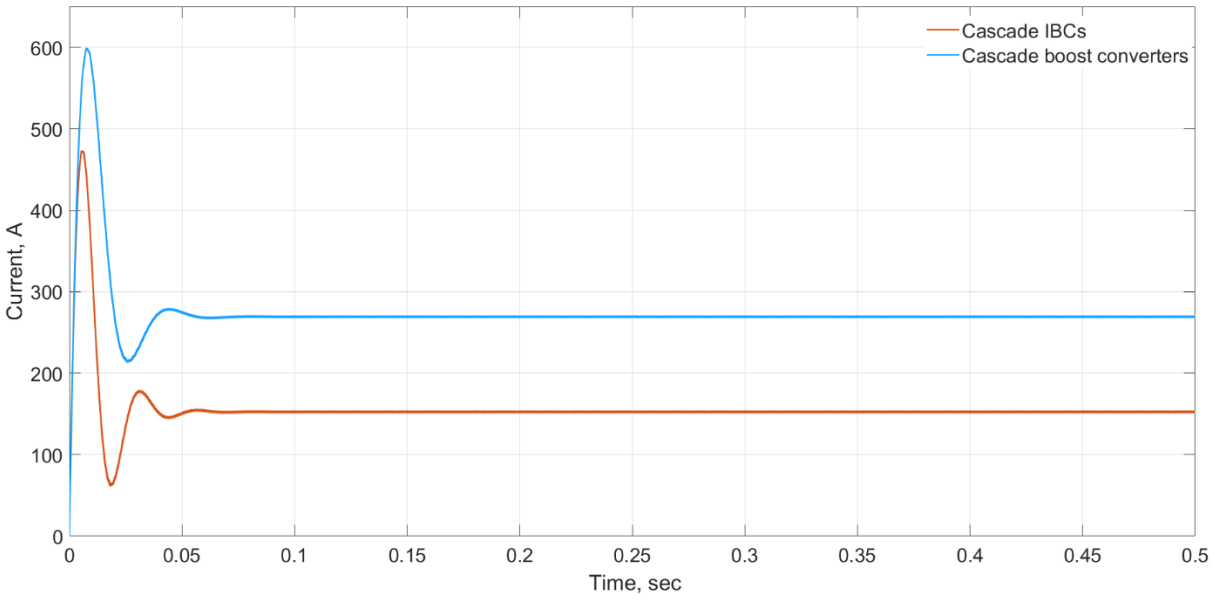

Figure 4.3 Inductor current.

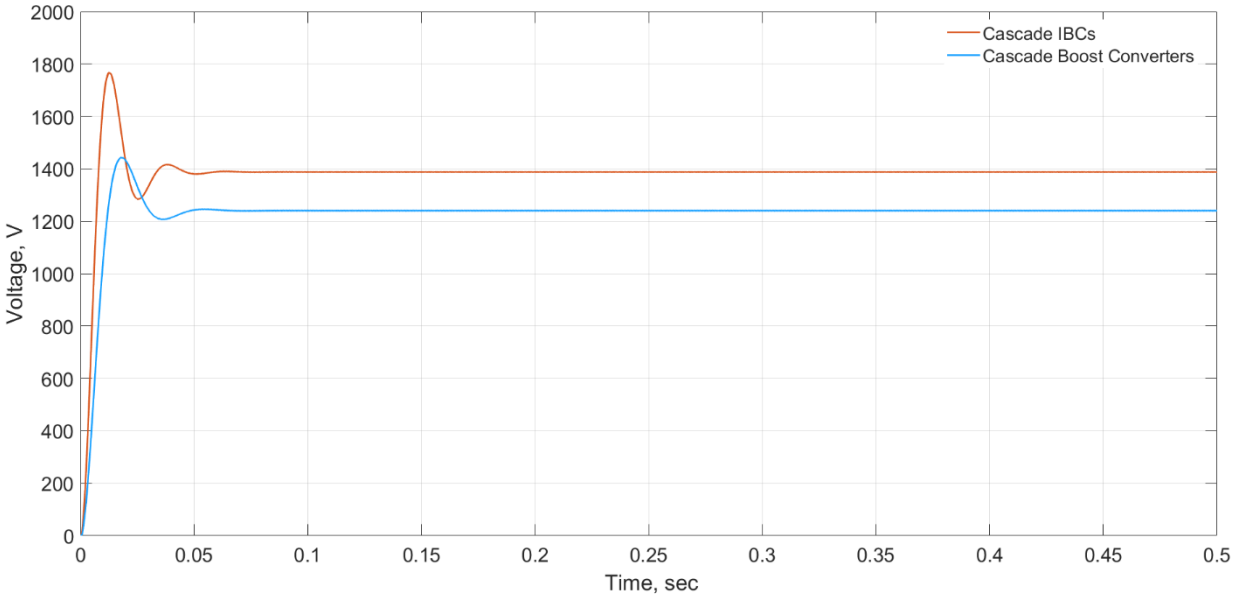

Figure 4.4 Output voltage.

For multi-level converter, two three-phase IBCs are connected in parallel and compared with two boost converters. Figure 4.5. shows the output current comparison and Figure 4.6. shows the output voltage comparison. The IBCs show higher output current and voltage, less overshot and fast steady state response. The systems specifications are listed on Table 4.1.

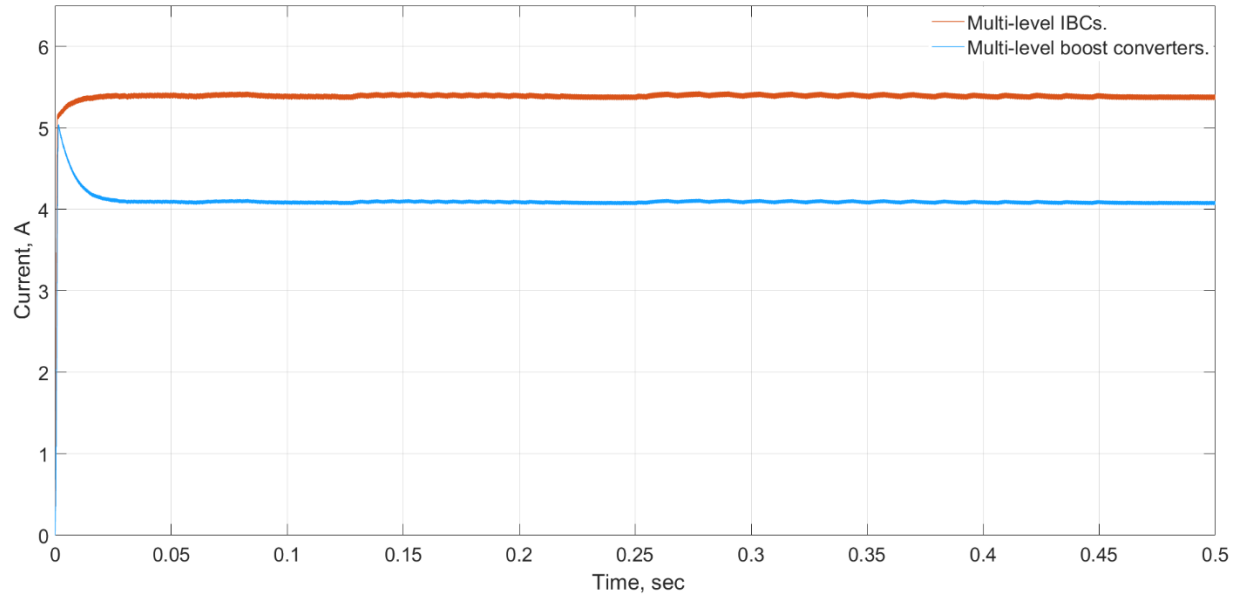

Figure 4.5 Output current.

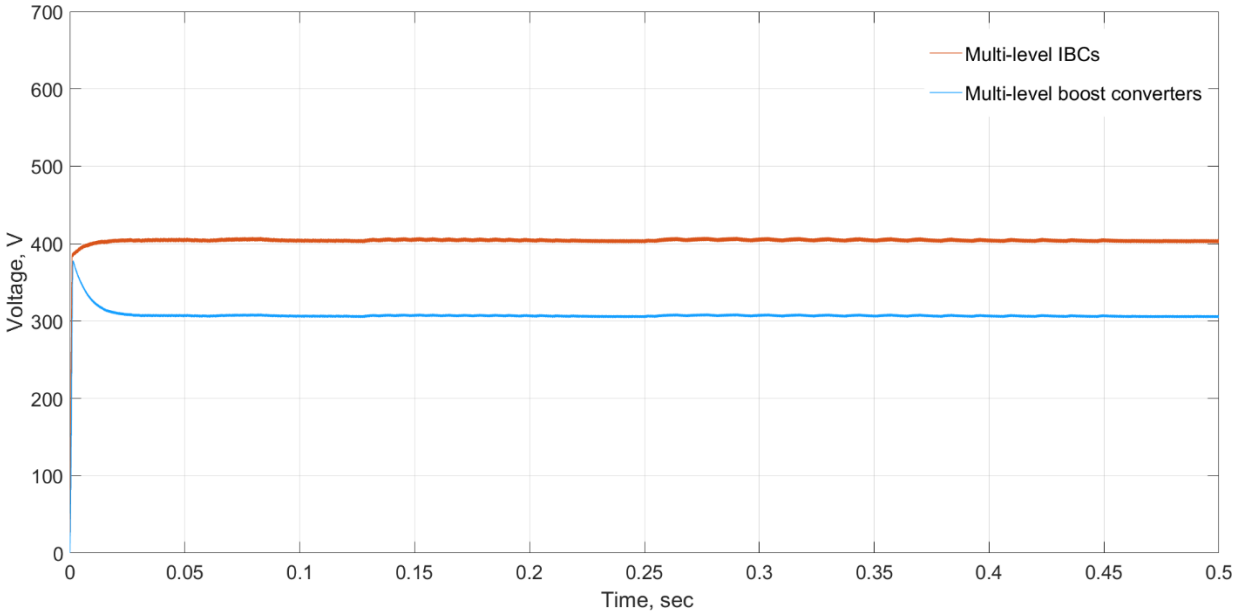

Figure 4.6 Output voltage.

Table 4.1 Systems Specification

	Parameters	**Values**
Cascade system	Input voltage, V_i	100 V
	First-stage $L\_b=L\_IBC1=L\_IBC2$ $C_{b\_o1}=C\_ibc\_o1$	560 μH 100 μF
	Second-stage $L\_b=L\_IBC3=L\_IBC4$ $C_{b\_o}=C\_ibc\_o$	860 μH 200 μF
	Switching frequency, f_s	25 *KHz*
	Duty cycle, d	0.75
	Output resistance, R_o	75 Ω
Multi-level system	Input voltage, V_i	100 V
	$L\_b=L\_IBC1=L\_IBC2$ $C_b=C\_ibc$	560 μH 100 μF
	Duty cycle, d	0.5
	Switching frequency, f_s	5000 *Hz*
	Output resistance, R_o	75 Ω

4.5 Stability

4.5.1 Stability and CPL

Cascade IB converter in power electronic system could react as Constant Power Loads (CPL) in a multi converter system (cascade converters) that pursue as a negative impedance characteristic ($dV/dI < 0$) as displayed in Figure 4.8 which discussed in [92] and [93]. The behavior of CPL may affect the stability of the system. Control system engineers have studied and analyzed that the boost converter is unstable when connected with a CPL, but Constant Voltage Load (CVL) should be observed to reach the stability. The parallel CVL with CPL, diode and inductor of the source converter has an effect which is mathematically calculated and estimated on system stability and was discussed in [94],[95], [96].

The performance of each converter when they are cascaded may decreased or become unstable. CPL technique is applied mainly to test the stability and assure constant power is delivered as shown in Figure 4.7. In general, the open loop systems interconnected CPL are unstable but can be turned into stable by applying a feedback control system [96].

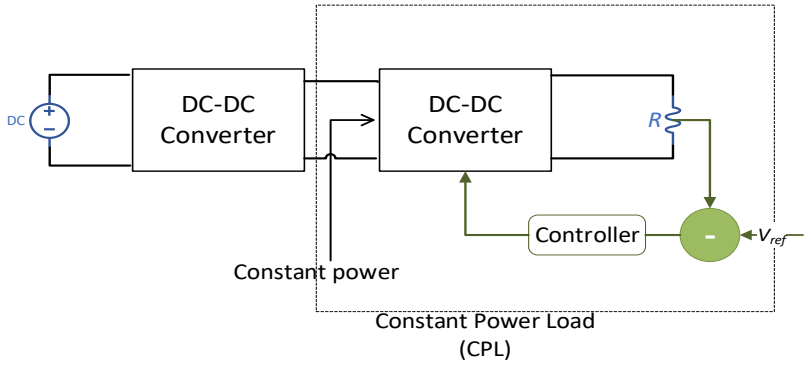

Figure 4.7 CPL for multi converter.

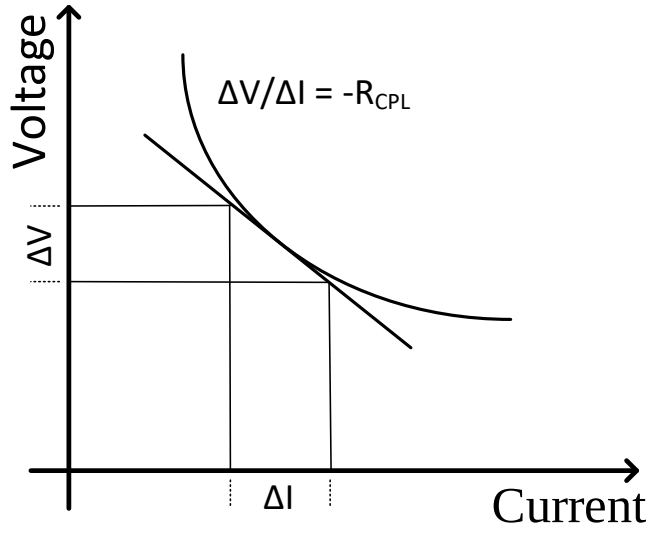

Figure 4.8 Negative impedance characteristic of CPL.

4.5.2 Stability Analysis of Interleaved Boost Converter with CPL

The interleaved boost converter running in continuous conduction mode, *CCM* connected with a CPL with switching period, *T* and duty cycle, *D* is displayed in Figure 4.9. The control to output transfer function ($\frac{\hat{v}_o(s)}{\hat{d}(s)}$) is determined using averaging technique to deliver the state-space.

When the switches (Q_1 *and* Q_2 = ON, the state-space equations of boost converter with a CPL when can be written as:

$$\frac{di_{L_1}}{dt} = \frac{1}{L_1} v_i \tag{4.3}$$

$$\frac{di_{L_2}}{dt} = \frac{1}{L_2} v_i \tag{4.4}$$

$$\frac{dv_c}{dt} = \frac{-1}{C}\frac{v_c}{R} = \frac{-1}{C}\frac{P}{v_c}. \tag{4.5}$$

When the switches (Q_1 *and* Q_2 = OFF), the state-space equations can be written as:

$$\frac{di_{L_1}}{dt} = \frac{1}{L_1}(v_i - v_c) \tag{4.6}$$

$$\frac{di_{L_2}}{dt} = \frac{1}{L_2}(v_i - v_c) \tag{4.7}$$

$$\frac{dv_c}{dt} = \frac{1}{C}(i_L - \frac{P}{v_c}). \tag{4.8}$$

The transformer function is given by,

$$\frac{\hat{v}_o(s)}{\hat{d}(s)} = \frac{\frac{1}{L_1 C} v_i}{s^2 + \frac{P}{CV^2} s + \frac{1}{L_1 C}}. \tag{4.9}$$

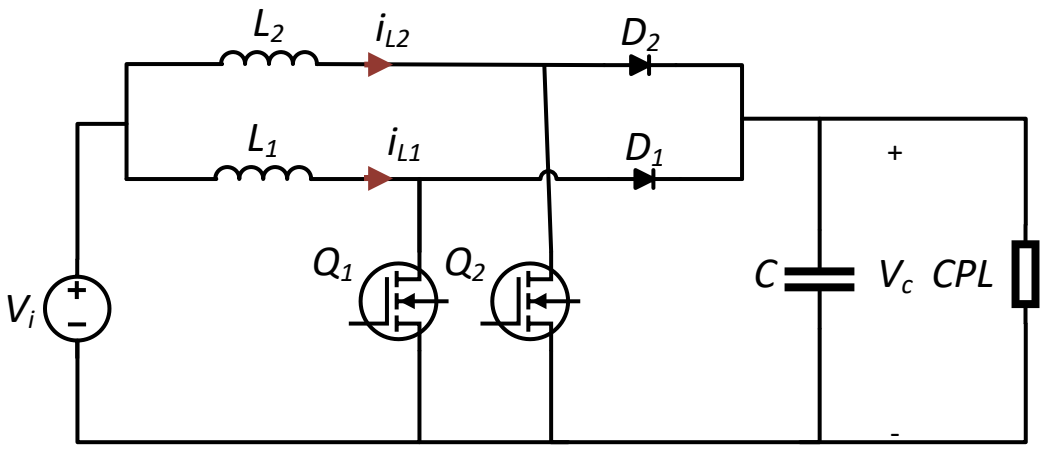

Figure 4.9 Interleaved boost converter with CPL.

For an interleaved boost converter with parameters listed in Table 4.2, the poles as shown in Figure 4.10 are located on the right half plane indicates that the system is unstable.

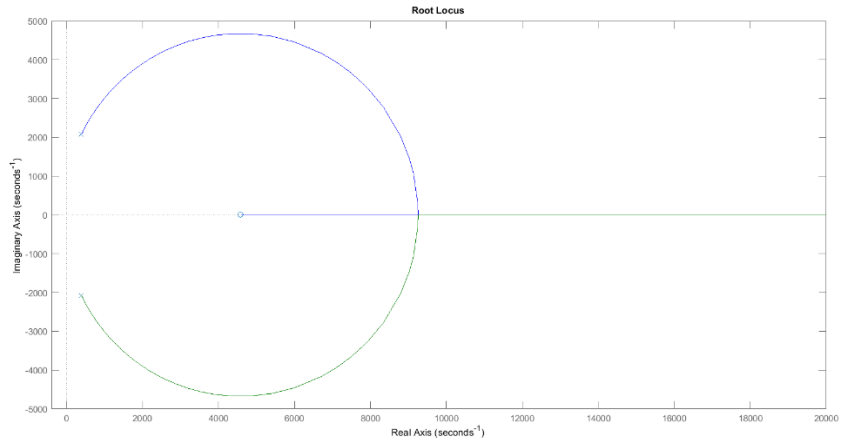

Figure 4.10 Poles of boost converter with CPL.

Table 4.2 System specifications.

Parameter	Value
V_i	20 V
L	560×10^{-6}H
C	100×10^{-6}F
P	140W

4.5.3 Stability Issue of Cascade Converters

The instability issue of cascade converters comes from the interaction between them even they are well designed and worked perfect individually [97]. There are many techniques that investigate the stability issue. One of the best methods is Middlebrook's stability criterion.

4.5.3.1 Middlebrook's Stability Criterion

Middlebrooks's stability criterion is a technique that applied for cascade systems to prove that system is stable [92]. Connecting power converters in series (cascaded) is one of the basic configurations of DC distributed power systems [98]. The instability issue could be float from

impedance interaction between single converters at several stages even though each converter in the stage is perfectly designed and individually stable [97],[99]. One of the most utilized methods of impedance/admittance criteria is the Middlebrook criterion, which states that the system that contain cascade power converters will remain stable if the Nyquist contour of Z_{o1}/Z_{i2} lies within the unit circle [97][100]. Middlebrook clarified that the cascaded system is stable if the first-stage and the second-stage converters, as displayed in Figure 4.11, are individually stable, and the output impedance of first-stage converter, Z_{o1} , is lower than the input impedance of second-stage converter, Z_{i2} , for the valid frequency domain [16]. Based on Middlebrook Criteria [101], to secure the stability of cascaded system, the cut-off frequency of the first stage should be greater than the cut-off frequency of the second-stage converter and $|Z_{o1}|$ and $|Z_{i2}|$ is not intersected; and to secure that $Z_{o1} < Z_{i2}$ in the valid frequency domain [102], and |Zo1,peak| must satisfies $|Z_{o1,\text{peak}}| \leq |V_{o1}^2/P_{o2}|$ [103].

The output impedance of the source converter is

$$Z_{os}(s) = \frac{V_i G_c(s) G(s)}{1 + V_i G_c(s) G(s)}, \tag{4.10}$$

where V_i is the steady state of the source voltage, $G_c(s)$ is the transfer function of the output voltage control, $G(s)$ is the transfer function from duty cycle to output control ($V_o(s)/d(s)$). Within the bandwidth of the closed loop:

$$\left\| G_c(jw) G(jw) \right\| \gg 1 \text{ , and} \tag{4.11}$$

$$\left\| \frac{V_i G_c(jw) G(jw)}{1 + V_i G_c(jw) G(jw)} \right\| \approx 1. \tag{4.12}$$

Middlebrook's stability criterion

$$\left\|Z_{o_1}(s)\right\| < \left\|Z_{i_2}(s)\right\|, \text{ is performed.} \tag{4.13}$$

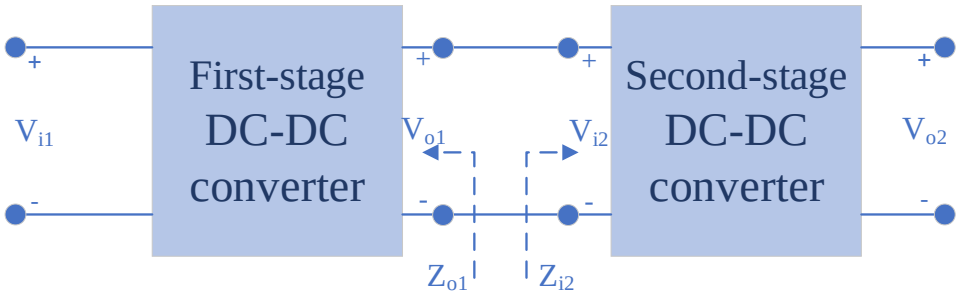

Figure 4.11 Cascade power converters.

4.5.3.2 Hamiltonian function:

Hamiltonian technique or (energy function) [23] is to investigate the stability of cascade power converters. The passivity properties and the Port-Controlled Hamiltonian (PCH) based on the evident system structure, where the system energy interpretation is allowed [104]. The dynamic behavior of the interactions between the source converter and the load converter could be analyzed in PCH models [105]. The Passivity-based control (PBC) is a property that can be used to design controllers for cascade systems [38]. The technique is investigated by using root-locus method to examine the complete system stability based on the following state-space system for cascade IBC shown in Figure 4.12.

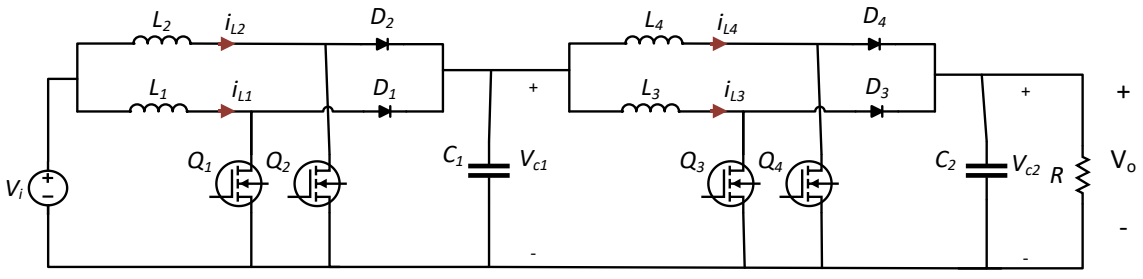

Figure 4.12 Cascade IBC.

System Model:

The derivative of the inductors current and the capacitor voltage of the source IBC converter can be written as the following equations:

$$\frac{di_{L_1}}{dt} = \frac{V_i - (1-d)v_{c_1}}{L_1} \tag{4.14}$$

$$\frac{di_{L_2}}{dt} = \frac{V_i - (1-d)v_{c_1}}{L_2} \tag{4.15}$$

$$\frac{dv_{c_1}}{dt} = \frac{(1-d)i_1 - i_{o_1}}{C_1}. \tag{4.16}$$

The derivative of the inductors current and capacitor voltage of the load IBC converter can be written as the following equations:

$$\frac{di_{L_3}}{dt} = \frac{V_{o_1} - (1-d)v_{c_2}}{L_3} \tag{4.17}$$

$$\frac{di_{L_4}}{dt} = \frac{V_{o_1} - (1-d)v_{c_2}}{L_4} \tag{4.18}$$

$$\frac{dv_{c_2}}{dt} = \frac{(1-d)i_2 - \frac{V_o}{R_o}}{C_2}. \tag{4.19}$$

The energy control provides the reference voltage (or reference current). The controller law is provided as:

$$\frac{dS_e}{dt} = \frac{1}{2}C_2(V_{ref}^2 - V_o^2) \tag{4.20}$$

$$V_{ref} = \frac{P_o}{I_o}, \tag{4.21}$$

where S_e denotes the integral actions in the energy voltage loop.

The voltage control provides the duty cycle of the system, d, and is connected to control the output voltage (or output current). The controller law is written as

$$\frac{dS_i}{dt} = V_{ref} - V_o, \tag{4.22}$$

where S_i denotes the integral actions in the voltage control loop.

The nonlinear state-space model can be determined by using small signal theory as:

$$\frac{d}{dt}\begin{bmatrix} i_{L_1} \\ i_{L_2} \\ i_{L_3} \\ i_{L_4} \\ v_{c_1} \\ v_{c_2} \\ S_i \\ S_e \end{bmatrix} = \begin{bmatrix} \frac{V_i - (1-d)v_{c_1}}{L_1} \\ \frac{V_i - (1-d)v_{c_1}}{L_2} \\ \frac{V_{o_1} - (1-d)V_o}{L_3} \\ \frac{V_{o_1} - (1-d)V_o}{L_4} \\ \frac{(1-d)i_1 - i_{o_1}}{C_1} \\ \frac{(1-d)i_{o_1} - i_o}{C_2} \\ V_{ref} - V_o \\ \frac{1}{2}C_2(V_{ref}^2 - V_o^2) \end{bmatrix}. \tag{4.23}$$

Root-locus or pole-placement techniques could be used to investigate the dynamic system stability.

4.5.4 Stability of Parallel Converters

The stability of multi-level converters could be investigated by using root-locus method to examine the complete system stability based on the following state-space system for two parallel IBCs as shown in Figure 4.13 [106][107]:

$$\frac{d}{dt}\begin{bmatrix} i_{L_1} \\ i_{L_2} \\ i_{L_3} \\ i_{L_4} \\ v_{c_1} \\ v_{c_2} \end{bmatrix} = \begin{bmatrix} 0 & 0 & 0 & 0 & \frac{-(1-d)}{L_1} & 0 \\ 0 & 0 & 0 & 0 & \frac{-(1-d)}{L_2} & 0 \\ 0 & 0 & 0 & 0 & 0 & \frac{-(1-d)}{L_3} \\ 0 & 0 & 0 & 0 & 0 & \frac{-(1-d)}{L_4} \\ \frac{1-d}{C_1} & 0 & 0 & 0 & 0 & 0 \\ 0 & \frac{1-d}{C_2} & 0 & 0 & 0 & 0 \end{bmatrix} \begin{bmatrix} i_{L_1} \\ i_{L_2} \\ i_{L_3} \\ i_{L_4} \\ v_{c_1} \\ v_{c_2} \end{bmatrix} + \begin{bmatrix} \frac{1}{L_1} \\ \frac{1}{L_2} \\ \frac{1}{L_3} \\ \frac{1}{L_4} \\ 0 \\ 0 \end{bmatrix} V_i \qquad (4.24)$$

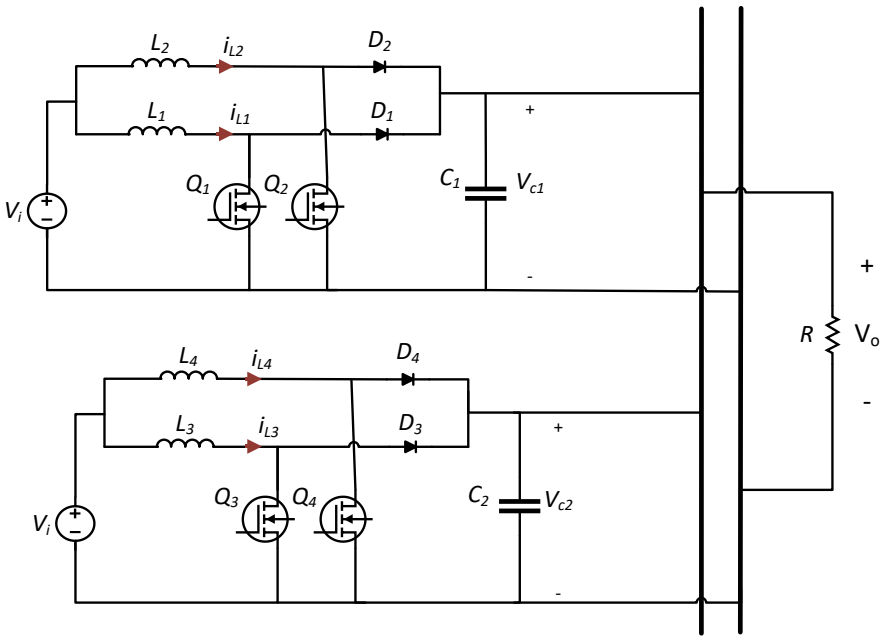

Figure 4.13 DC microgrid structure.

4.6 A Novel Multi-stage Interleaved Boost Converter for PV Application

Multi-stage IBC are three IBCs connected in series to reach a high voltage level with less output current for PV application as depicted in Figure 4.14. Normally, the PV output current is high that needs a high inductor value which result in bulky size of the system. Using the IBC could reduce the size and the input current ripple and increase the system efficiency. The stability between the two converters is one of the main issues for cascade converter. The first-stage is designed as a four-phase IBC to handle the high PV output current as displayed in Figure 4.15.

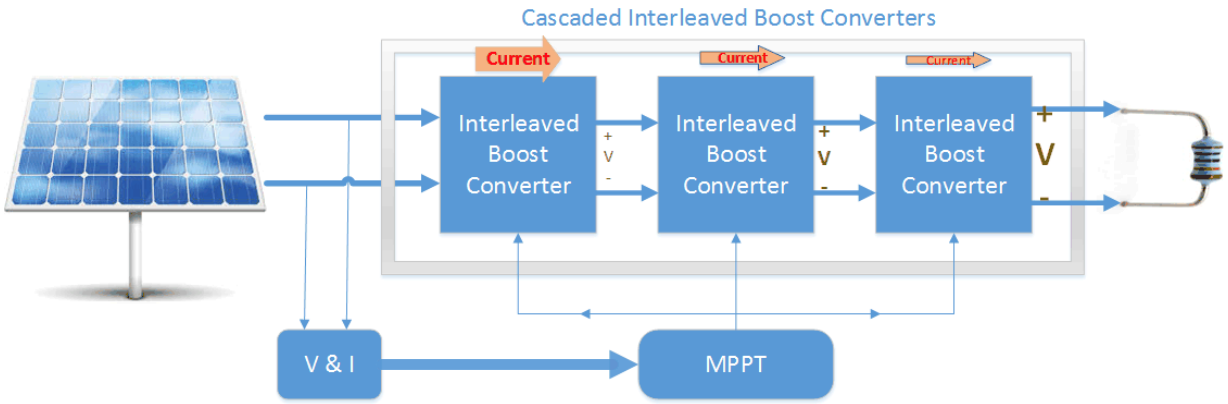

Figure 4.14 Multi-stage multi-phase IBCs for PV application.

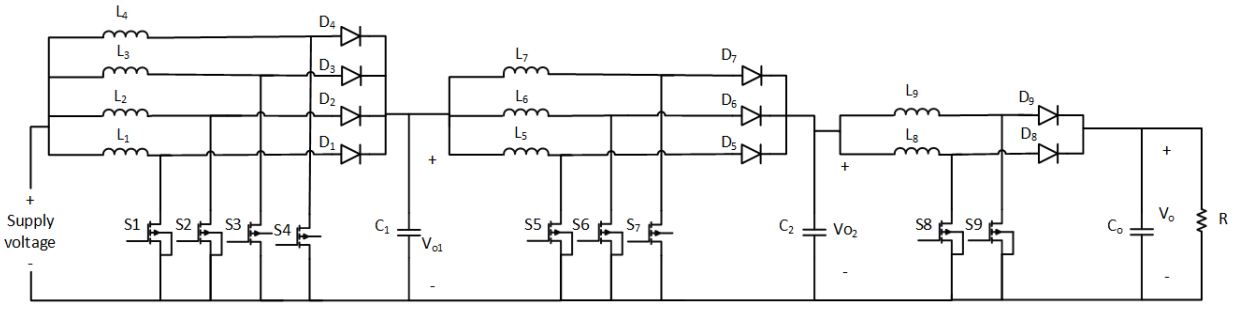

Figure 4.15 Multi-stage multi-phase IBCs.

The individual IBC in each stage is to design separately based on regular design criteria [64], [40]. For the first-stage, four-phase IBC is designed to meet the high input current and to

transfer the highest power with reduced input current ripple, small component size less stress on power devices and better efficiency [108]. The waveform for S_1, S_2, S_3 and S_4 are delayed by 90^o as shown in Figure 4.16. For the second-stage, three-phase IBC is chosen as the current is reduced. The switches S_5, S_6 and S_7 are delayed by 120^o as shown in Figure 4.17. For the third-stage, two-phase IBC is chosen. The switches S_8 and S_9 are delayed by 180^o as shown in Figure 4.18. Transport delay tools are used to adjust the phase shift for each stage. IBCs work in continuous conductance mode. PWM pulse generator is used to generate the pulses for each switch based on the reference signal produced by the InC MPPT controller. The output capacitor is selected large enough to consider the high voltage applied. The power ratio of multi-stage IBCs is

$$\frac{V_o}{V_i} = \left(\frac{1}{1-d}\right)^m, \tag{4.25}$$

where m is the number of stages and duty ratio is 0 < d < 1.

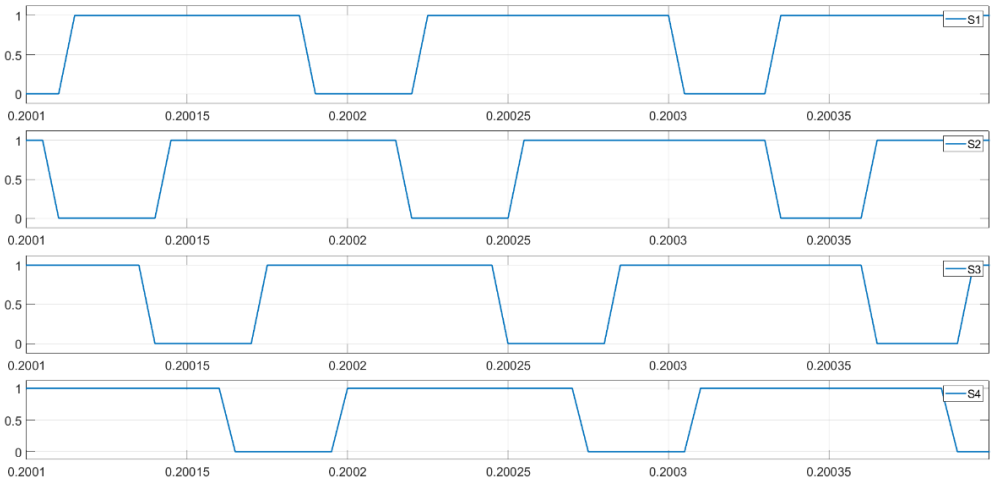

Figure 4.16 First-stage switches waveforms.

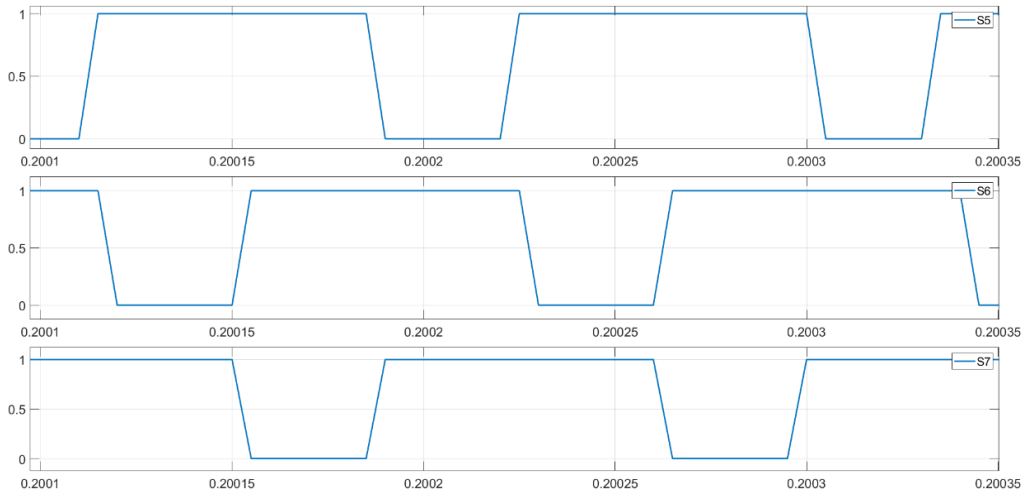

Figure 4.17 Second-stage switches waveforms.

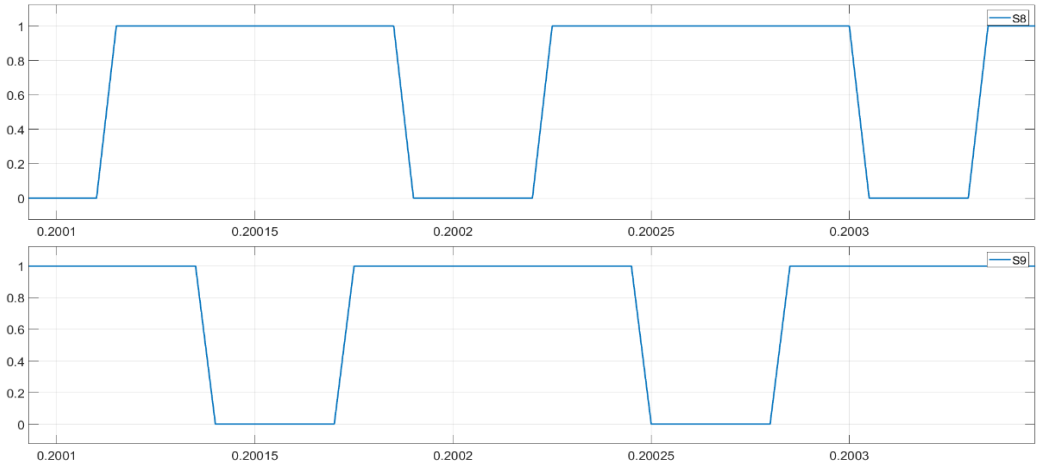

Figure 4.18 Third-stage switches waveforms.

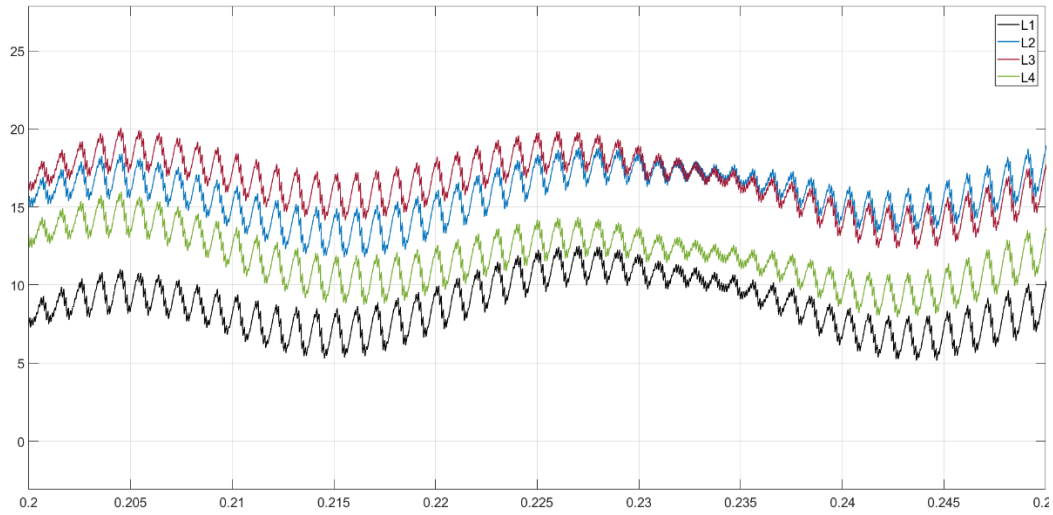

Figure 4.19 First-stage inductor current waveforms.

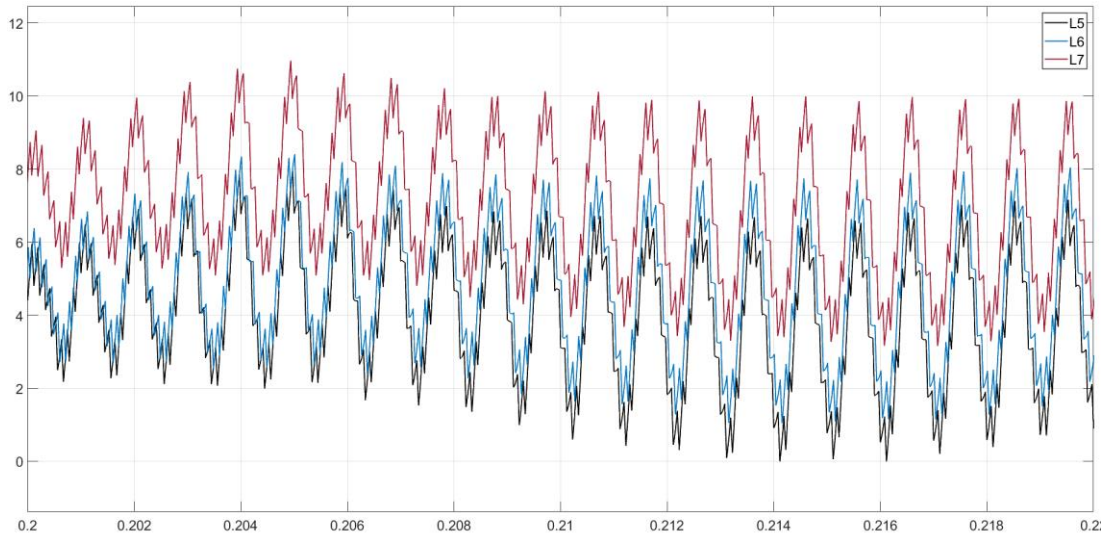

Figure 4.20 Second-stage inductor current waveforms.

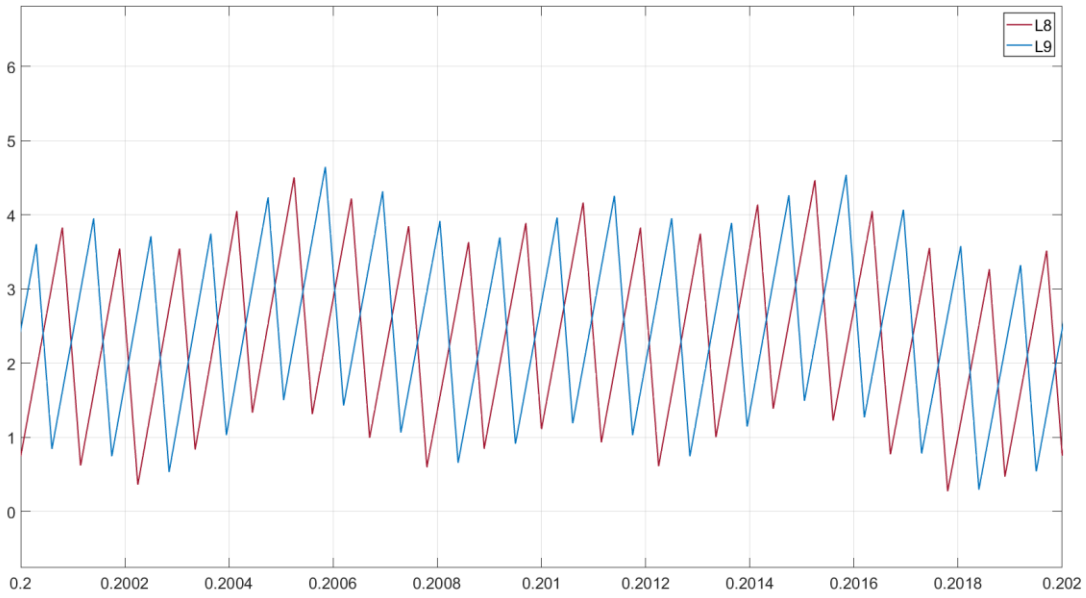

Figure 4.21 Third-stage inductor current waveforms.

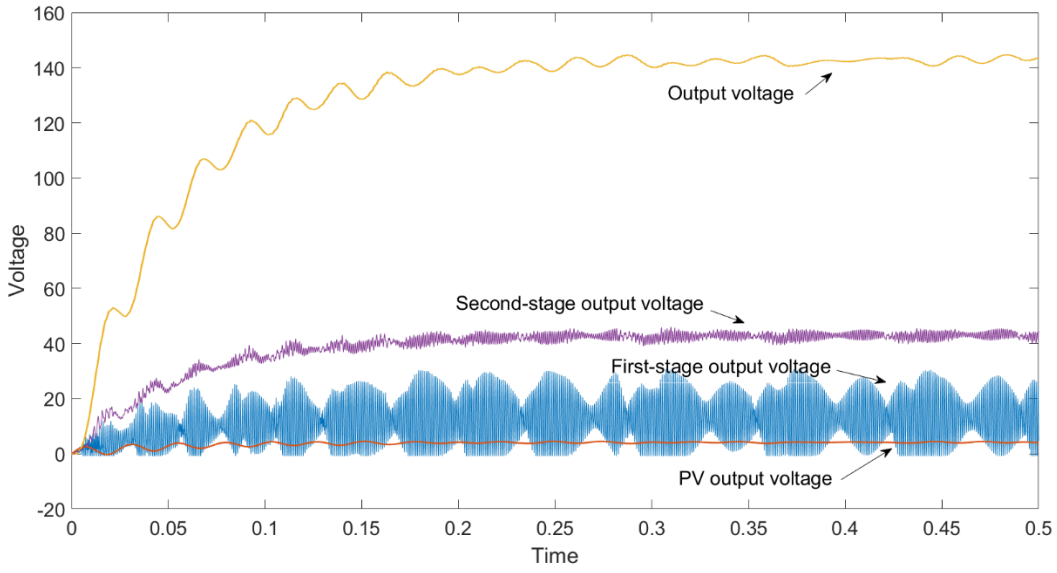

Figure 4.22 Output voltage waveforms.

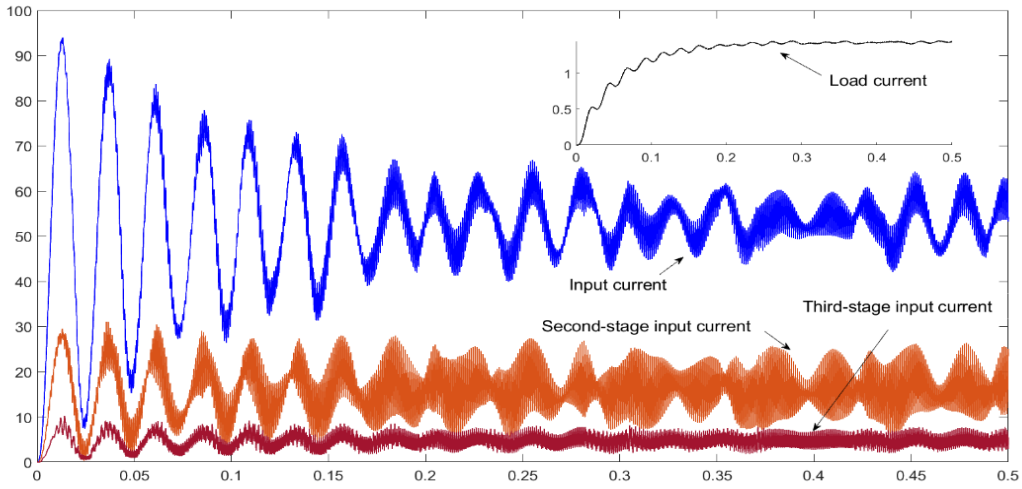

Figure 4.23 Output current waveforms.

CHAPTER 5

ROBUST CONTROL TECHNIQUE

This chapter presents the control technique and the control design problem for IBC using MATLAB/SIMULINK based on the linearized model of the multi-phase IBC converter presented in ch.2. The concept of modern robust control theory and μ-analysis and synthesis approach for robustness is provided is this chapter. The simulation results of IBC is discussed and validated by the experimental results.

5.1 Introduction

When George James and Bruce Francis introduced the importance of robustness in control systems in 1980s, the topic become a very interesting for control engineers which extended to more general problems [109]. Robust control design tends to emphasize *H*- technique for optimization of performance objectives. The process is based on the theory that sufficient gain and phase margin are provided by a suitable single-input single-output (SISO). Solving a linear matrix inequality constraint with a defined optimization cost function results in robust stability of closed-loop [110]. The development of the robust control has a great impact to guarantee stability and high performance of electrical power systems with respect to uncertainties, disturbance effect, and non-linearities [111]. The satisfied solutions can be achieved by using mixed sensitivity, H- loop shaping and μ -synthesis approaches. The μ-synthesis approach was provided by Doyle in 1982 to assess the impact of parametric uncertainty. The approach is a model for robust control and a successful technique for an efficient controller within structured and unstructured uncertainties and disturbance conditions [110]. In this research, an improved robust controller design method using μ-synthesis and H-infinity to achieve optimal voltage regulation for IBC output voltage and DC bus voltage for grid connected PV system.

5.2 DC-DC Boost converter control problem

DC-DC power boost converters are challenging to maintain stable due to the tendency to exit the stability region especially at high duty ratio and because of the right plane zero and the inherent operating characteristics of the semiconductor switch that cause the nonlinearity properties [112],[113]. The differences between real system and its nominal model, that is used to build the controller, is the main issue for converter control system and stability. One of the benefit of robust stability theory is the ability to determine stability boundary condition of uncertain system models that make it mimics the real system. Controlling Interleaved boost converter is another challenging as it contains multi boost converter in parallel and sharing the output.

5.3 Robust Controller Design:

5.3.1 Perturbation Models

Nominal models are used to illustrate the plant model wherein input voltage and load are related to dc gain, poles and RHP zeroes of the system but they are not representing the actual operation system as the inductor and capacitor values have electromagnetic properties that have small change with frequencies and the amount of current [114]. To cover the possible values of these changes, simple block perturbation (Figure 5.1) called input multiplication is applied to the nominal model as shown in eq. 1 where $\Delta(s)$ is a unity norm perturbation and $w(s)$ is an uncertainty weight [115],

$$G_{\Delta}(s) = G(s)[1 + \Delta(s)w(s)]. \tag{5.1}$$

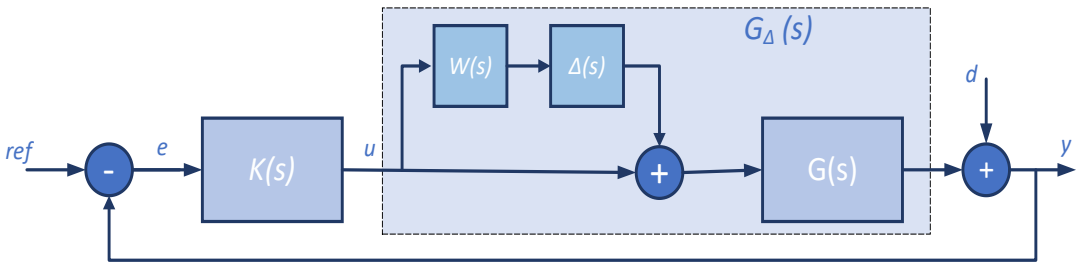

Figure 5.1 Multiplicative uncertainty.

The nominal model and possible values are listed in Table 5.1 and the Bode plot of uncertain system is shown in Figure 5.2. The uncertainty bound and possible multiplicative perturbation is displayed in Figure 5.3 where the uncertainty bound covers all possible values. Accurate calculations and uncertainty percentage mean safety stability margins for the controller. Robust controllers are able to cover the small changes between the nominal model and actual dynamic system. The uncertainty comes from:

1) Approximated parameters.
2) Model nonlinearity.
3) Sensors error and external noises.
4) High frequency effect and parasitic.
5) Age.
6) Temperature.
7) Part-part variation in manufacturing.

On robust control system design, it is necessary to consider the parameters changes to meet the operating system to mimic the real system

Table 5.1 IBC parameters with uncertainties.

Parameters	Values	Uncertainty
Input voltage, Vi	20V	[15 25]
Inductor value, $L_1=L_2=L_3=L_4$	560×10^{-6} H	±10%
Capacitor value, C	470×10^{-6} F	±10%
Resistance load, R	400 Ω	[200 500]

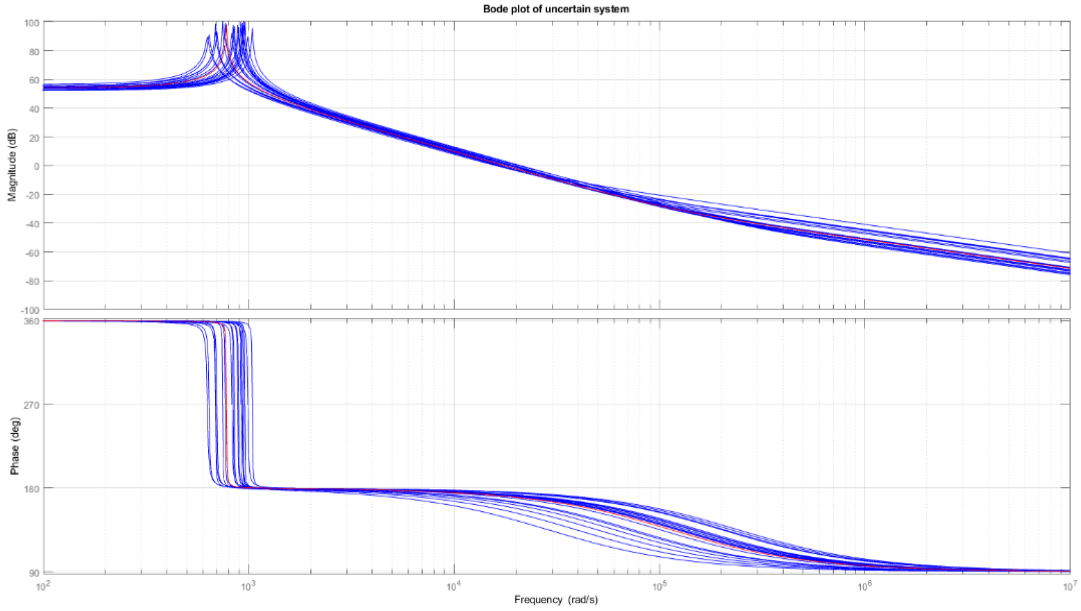

Figure 5.2 bode plot of uncertain system

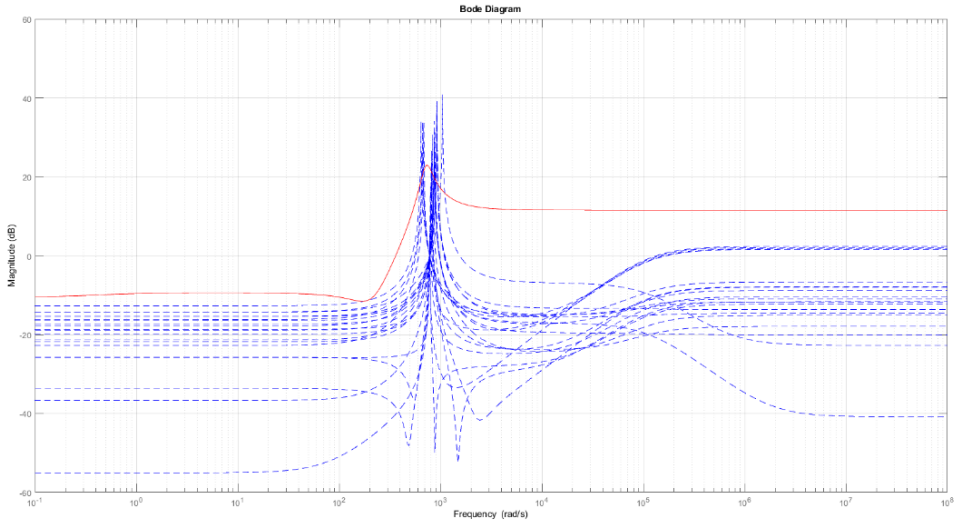

Figure 5.3 Uncertainty bound and input multiplicative perturbation.

5.3.2 H_∞ Method

The optimization H_∞ method has become an efficient robust control design method in the field of Linear Time Invariant LTI control systems since 1980s as explained in [116]. H_∞ technique based on norm-based optimization theory enables robust performance and intends to sufficient performance in worst-case disturbance cases. To include tracking and robustness, the design specifications used limitations on the singular values of loop transfer functions where loops can be shaped by weighting functions. H_∞ has the ability to assure the stability of closed-loop systems require and performance. First, H_∞ has the following condition that should be satisfied as

$$\|G\|_\infty = \sup_w \left|\bar{G}(jw)\right| \tag{5.2}$$

which results in minimum singular value of the bode diagram that shows the largest robust stability margin. H_∞ method includes performance conditions, disturbance rejection, control input constraints, and robustness achievements.

5.3.3 Mixed Sensitivity Problem

The system displayed in Figure 5.4 which include model uncertainties and possible perturbation must be satisfied by the nominal performance to ensure the robust stability and performance specification by mixed sensitivity problem as [117]:

$$\min_{\substack{K \\ Stabilizing}} \left\| \begin{matrix} S \\ R \\ T \end{matrix} \right\|_{\infty}, \tag{5.3}$$

which describes the closed-loop system with model uncertainities and possible perturbation. Here *S* is the sensitivity, *R* is the control effort, and *T* is is the complementary sensitivity functions. The three functions will be shaped by using mixed sensitivity method . The sensitivity is reflected the disturbance transfer function from the output d to the reference output *y* which will determine the steady-state behavior of the feedback system and the disturbance attenuation [118]. The sensitivity is designed small in magnitude to secure a perfect reference tracking and deminish the disturbance effect. The comeplementary sensitivity, *T*, is the disturbance transfer function to the control signal and is desired to limit the control signal, which is designed small at all frequance ranges to minimize the norm [119]. Here Δ represents the uncertainities.

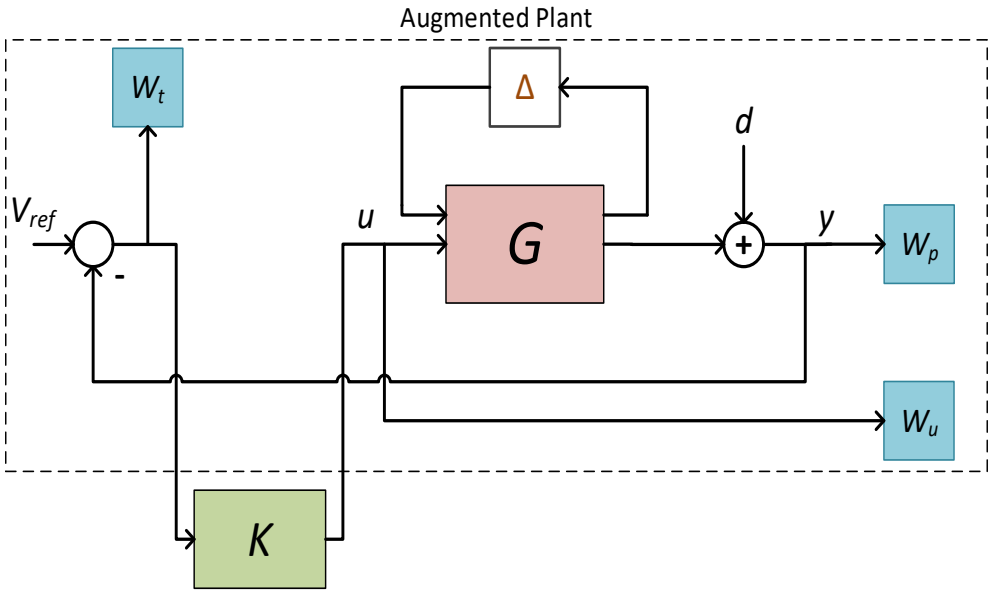

Figure 5.4 Typical diagram of a feedback control system.

Where w_p, w_u, w_t are the performance, control, and noise weight functions respectively. w_p forms sensitivity function that measures the disturbance rejection, steady-state error, and plant variations. W_u measures the control input limitation. w_t measures the system oscillations.

The controller, K can be found by using MATLAB robust control Toolbox's command [120]:

$$[K, CLP, gamma, \inf] = mixsyn(G, w_p, w_u, w_t). \tag{5.4}$$

The command penalizes the error signal, w_p, control signal, w_u, and noise signal, w_t to make the following closed loop transfer function:

$$T_{yu=} \begin{bmatrix} w_p \dfrac{1}{I+GK} \\ w_u \dfrac{GK}{I+GK} \\ w_t \dfrac{K}{I+GK} \end{bmatrix}. \tag{5.5}$$

The controller target is to design a stable controller that diminished the norm of transfer function:

$$\left\| \begin{matrix} w_p \dfrac{1}{I+GK} \\ w_u \dfrac{GK}{I+GK} \\ w_t \dfrac{K}{I+GK} \end{matrix} \right\|_\infty < 1. \tag{5.6}$$

5.3.4 Robust Modeling

The block diagram of robust control system with μ-analysis is displayed in Figure 5.5. Here, *w* is the disturbance inputs, *u* represents the control inputs, *z* is the error outputs (small value), *y* is the measurements outputs to the controller. The uncertain plant is constructed by building a state space model with uncertainties of parameters and dynamics.

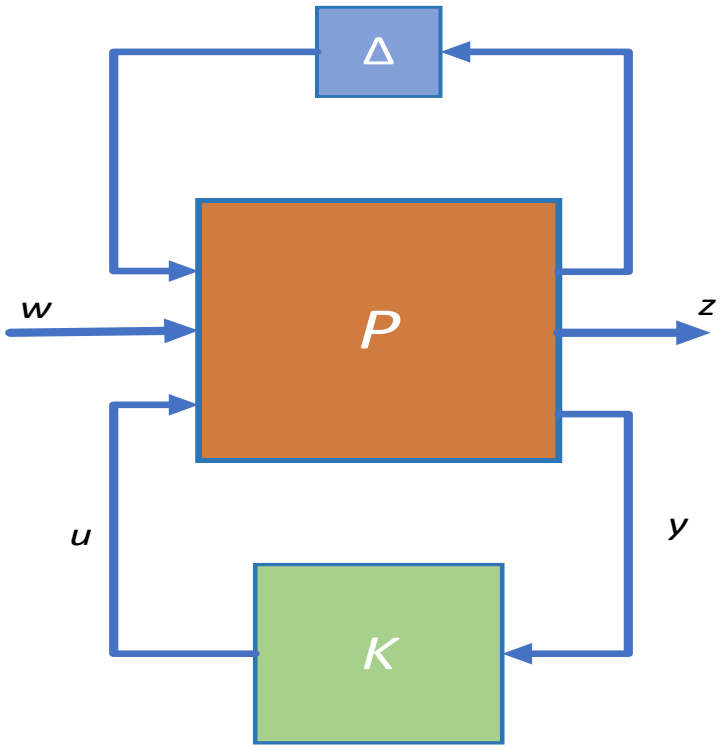

Figure 5.5 Block diagram for generalized plant.

Using the $F_l(P,K)$, the model can be reduced to N-Δ structure s displayed in Figure 5.6 which enables to assess the stability margins of uncertain systems using μ-analysis.

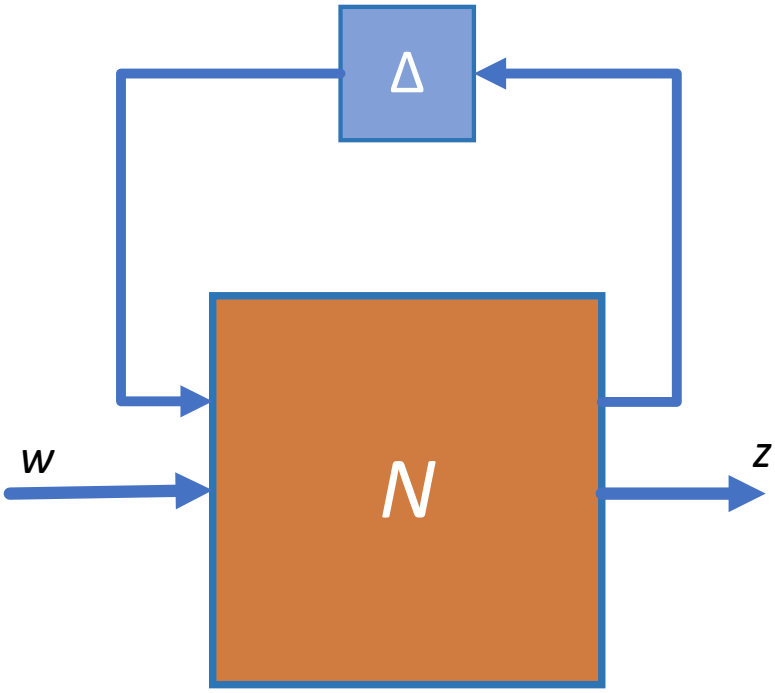

Figure 5.6 N-Δ structure.

Assume that:

$$N = \begin{bmatrix} N_{11} & N_{12} \\ N_{21} & N_{22} \end{bmatrix}. \tag{5.7}$$

To fulfill robust stability analysis, matrix M is defined as

$$M(s) = N_{11}(s), \tag{5.8}$$

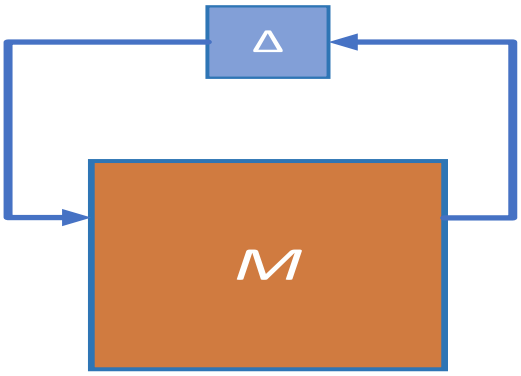

Figure 5.7 μ-analysis structure.

$$\begin{bmatrix} z \\ y \end{bmatrix} = \begin{bmatrix} P_{11} & P_{12} \\ P_{21} & P_{22} \end{bmatrix} \begin{bmatrix} w \\ u \end{bmatrix} \tag{5.9}$$

$$u = K(s)y\,. \tag{5.10}$$

The connection between robust control and the disturbance attenuation problem can be found by the input output transfer function which can be written as [121]:

$$T_{zw} = P_{11} + P_{12}K(I - P_{22}K)^{-1}P_{21}\,. \tag{5.11}$$

The lower linear fractional transformation (LFT) is determined as [121]:

$$N = F_l(P,K) = P_{11} + \frac{P_{12}K}{I - P_{22}K}P_{21}. \tag{5.12}$$

Here P is the nominal plant.

5.3.5 Robust design requirements

The control system goal is to provide robustness with respect to uncertainties. Uncertainty parameters are listed in Table 5.1. The control task is to maintain the closed loop system stable and to minimizes the maximum value of the sensitivity function to minimize the disturbance influence on the output as

$$\min_{K} \|S\|_{\infty} \tag{5.13}$$

or

$$\|T_{zw}\|_{\infty} = \left\| \begin{matrix} w_p S \\ w_u KS \\ w_t T \end{matrix} \right\|_{\infty} < 1. \tag{5.14}$$

5.3.6 Weighting functions selections

Weighting functions are low-pass and high-pass filters used to formulate the augmented plant for μ-synthesis to deal with system perturbation that lead to reach the desired controller performance by ensuring the norm of in eq. (5.12) is less than one. The purpose of the weighting functions is to measure the estimated indication of required performance criteria within particular frequency range [122]. One of the difficult tasks in robust control design is the selection of weighting functions to shape the desired performance criteria within certain frequency scope [123].

The general guidelines to choose the perfect weight functions are mentioned in [124],[111],[125] are:

$$w_p = \frac{\frac{s}{M_p} + w_b}{s + w_b A_b} \tag{5.15}$$

$$w_u = \frac{\sigma s + A_u}{\frac{\sigma s}{M_u} + 1}, \tag{5.16}$$

where M_p and M_u are high-frequency gains, A_p and A_u are low-frequency gains, w_b and σ are the cross-over frequencies. Trails and errors were done until the robust performance are obtained. In case of 4-phase IBC the weight functions are chosen as follows:

$$w_p = \frac{0.05s + 1250}{10s + 0.1}$$
$$w_u = \frac{0.01s + 1\times10^{-4}}{0.001s + 100}.$$

W_t is designed small constant (0.1) as a high pass filter to minimize the impact of disturbance and controller energy [118]. It is remarkable to say that weight functions are a key issue in the μ-synthesis control design and a suitable selection of weight transfer functions drives to a robust performance.

5.4 μ-synthesis analysis

μ-synthesis controller design technique is one of the robust control techniques to account for all performance limitations and plant uncertainty described by weight functions [126]. As the other regular controller design techniques don't utilize the uncertainty model during controller synthesis and take the uncertainty model which gives the μ-synthesis an advantage [110]. The procedure is to diminish the structured singular value of N, μ(N(K)) over all frequencies by locating a stabilizing controller. The controller design is achieved if the following condition is satisfied:

$$\mu(N) < 1, \tag{5.17}$$

where

$$N = \begin{bmatrix} -w_t T & w_t KS \\ -w_p GS & w_p S \\ -w_. T & w_. KS \end{bmatrix}. \tag{5.18}$$

The goal of test is to ensure this norm are nominal stability NS and nominal performance NP and to reach robust stability RS and robust performance RP.

The μ-synthesis algorithm is complex due to the SSV minimization is approached at all frequencies. Thus, MATLAB Robust Control Toolbox has utilized functions to do μ-synthesis.

The controller process is carried out with the command *musyn* to synthesizes the automated design.

Many iterations will be performed to get the μ-value. The μ-value should be less than one which means that the controller achieves the task and the system is robustly stable and the performance is robust. The controller objective is to achieve robust stability and robust performance.

5.5 Robust stability and performance

The system robustness requires the designed controller maintain a satisfactory performance and obtain the following conditions [127]:

- N is internally stable (Nominal stability, NS)
- The nominal performance, NP is gained if and only if $\|N_{22}\|_\infty < 1$ or $\|T_{wz}\|_\infty < 1$.
- Robust stability, RS is performed if and only if the system is internally stable (NS) for all parameters and $\|N_{11}\|_\infty < 1$ or $\mu_\Delta(N_{11}) < 1$.
- Robust performance, RP is approached if and only if $\|N\|_\infty < 1$ or $\mu_\Delta(N) < 1$ for all frequencies.

5.5 Control of boost converter

A robust controller design method using μ-synthesis is applied for dc-dc boost converter. The model is compared with the conventional PID controller. Step responses of PID versus μ-controllers is displayed in Figure 5.8. The robust stability and robust performance of μ-controller is shown in Figure 5.9 and Figure 5.10 respectively.

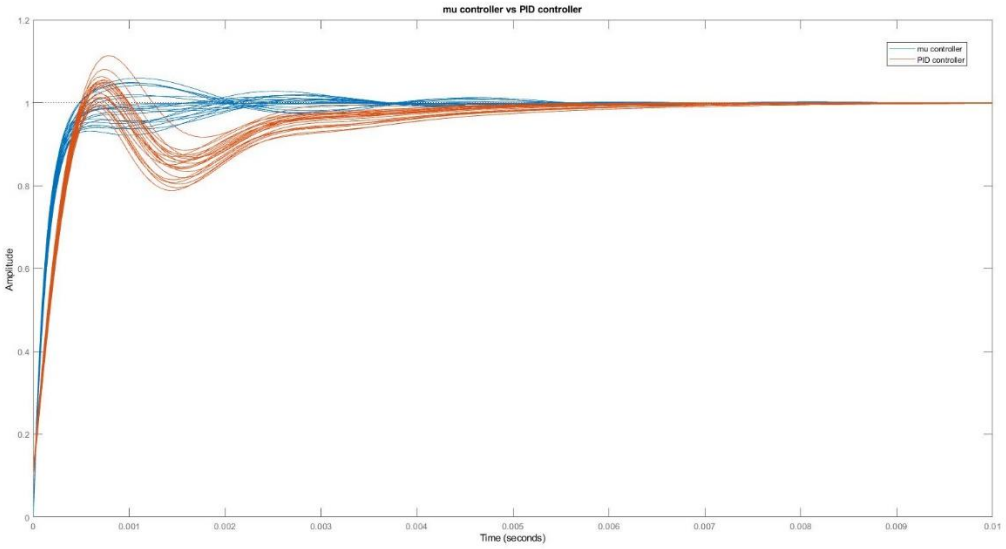

Figure 5.8 Comparison of PID and μ-controller.

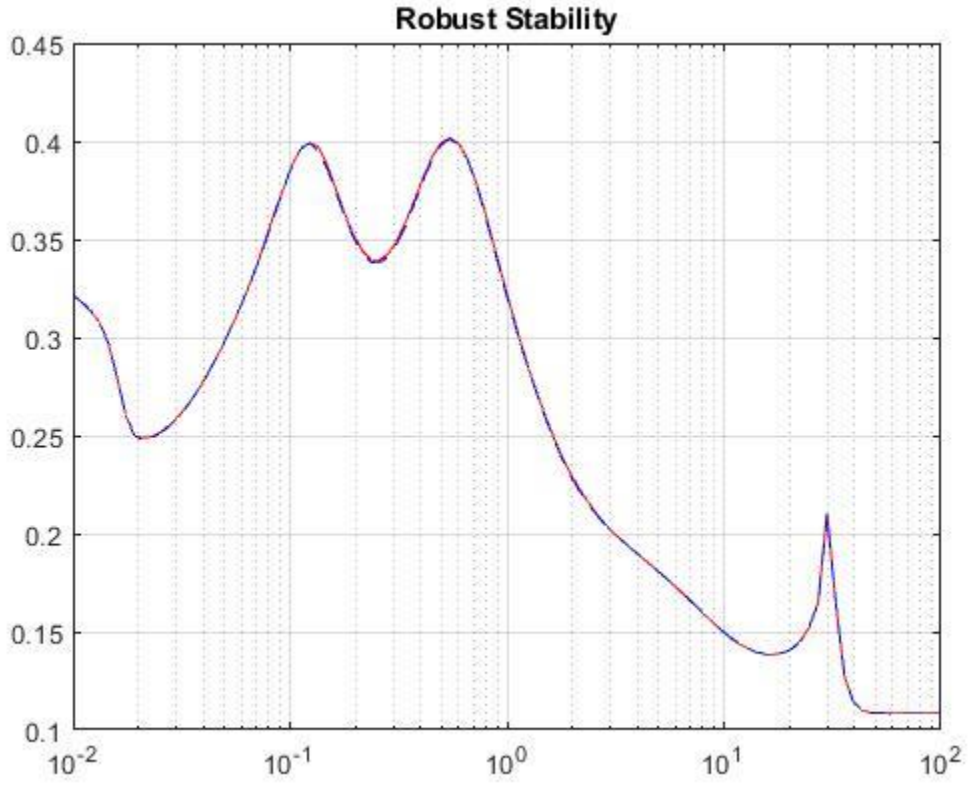

Figure 5.9 Robust stability.

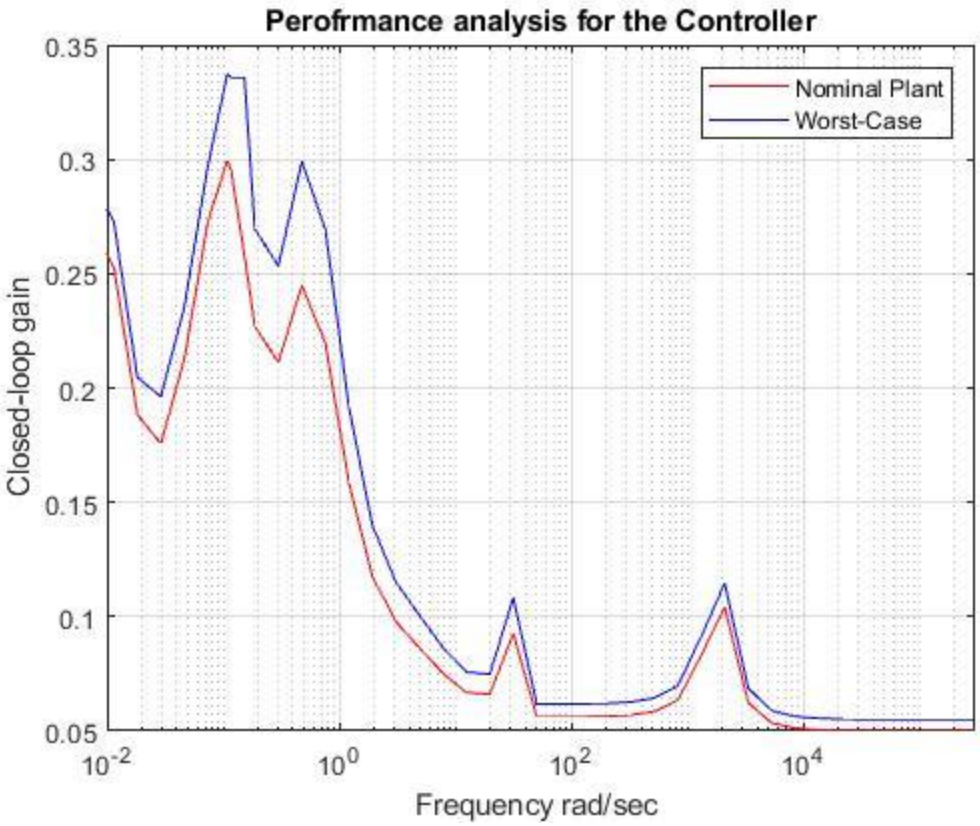

Figure 5.10 Robust performance.

The μ-controller exhibits more improvements compared to the PID controller such as fast step response, and less overshoot voltage.

5.6 Control of IBC

The DC/DC interleaved boost converter is regulated by feedback control to provide a constant output voltage or constant output current.

5.6.1 Robust Voltage Control

The system is a second order system with a right half plane zero that results in a large phase shift which make it strict control design to maintain stability. Therefore, a robust controller is required to achieve stability and minimizes the influence of the disturbance on the output voltage. The control strategy is depicted in Figure 5.11.

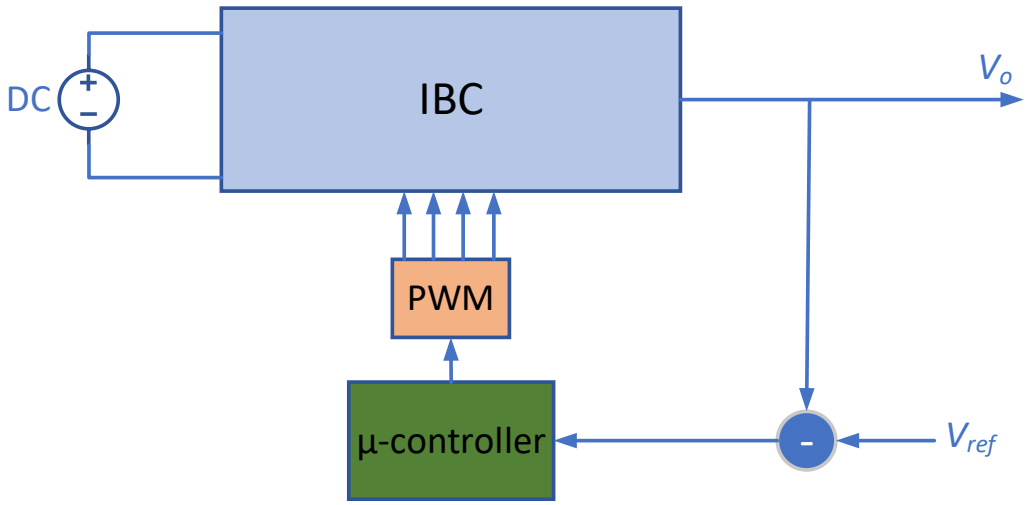

Figure 5.11 Voltage control strategy.

PID Voltage Control Design

PID control is the most method used to control the DC-DC converters output voltage where more than 95% of the control types are PID. Zigler-Nichols step response, which is based on the open loop step response, is one of the classical methods for PID controller design. The PID transfer function is:

$$K(s) = K_p + \frac{K_i}{s} + K_d s\,, \tag{5.19}$$

where K_p is the proportional gain to fix the open loop gain of the control system, K_i is the integral gain to cancel steady state error, and K_d is derivative gain to damp oscillation and to maintain accurate control. These parameters adjust the system dynamic responses.

The parameters for the designed PID controller are provided in Table 5.2.

Table 5.2 PID parameters

K_p	K_i	K_d
0.0395	5.95	2.0102e-5

Rise time, overshoot and settling time are the factors that characterize the closed loop step response to reach system stability. The values of these factors and robustness are listed in Table 5.3.

Table 5. 3 PID performance and robustness

Parameters	**Values**
Rise time	0.000415 seconds
Settling time	0.00842 seconds
Overshoot	14.7%
Gain margin	27.1 dB @$1.51x10^5$ rad/s
Phase margin	70 deg @ $3.2x10^3$ rad/s

5.6.2 Robust Current Control

The inductor current among the multi-phase IBC should remain in balance to have equal current. A robust controller is required to achieve stability and minimizes the influence of the disturbance on the output current. The control strategy in depicted Figure 5.12.

The controller tasks are determined as follows:

1) Maintain equal current in the IBC phases.
2) Ensure robust stability and performance.

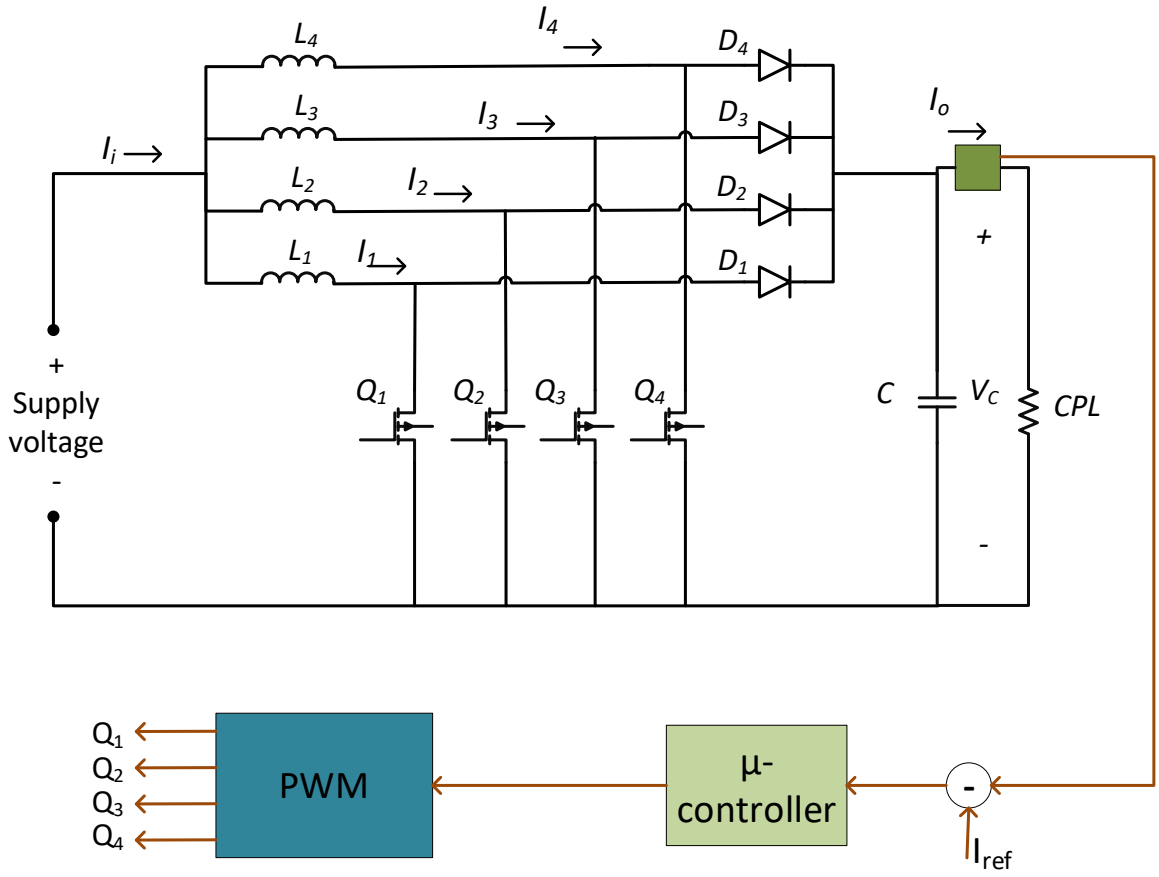

Figure 5.12 Current control strategy.

An average current sharing for four-phase IBC is presented in this section based on μ-synthesis approach to track the output current and to provide equal current for the inductors. The transfer function used to design the current controller is [7]:

$$\frac{\hat{i}_L}{\hat{d}} = \frac{\frac{2(d+3)}{1-d}(1+\frac{RC}{d+3})s}{RLCs^2+2Ls+2R(1-d)^2}. \qquad (5.20)$$

The controller performance is tested by changing the load from 100Ω to 67Ω at 1.0 sec. The supply is step changed from 20 to 25 V at 2.1 sec. The controller achieved good tracking to the reference

current which was change from 1 to 1.2 at 2.1sec. The simulation results is displayed in Figure 5.13. The inductor current is equal as shown in Figure 5.14.

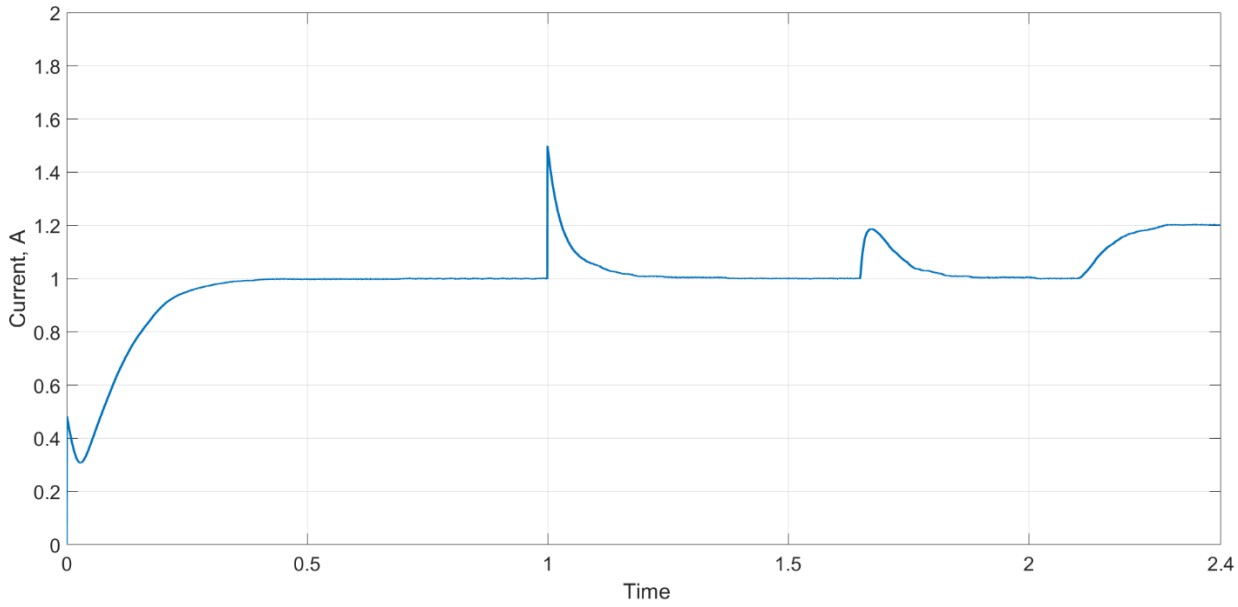

Figure 5. 13 Output current of IBC.

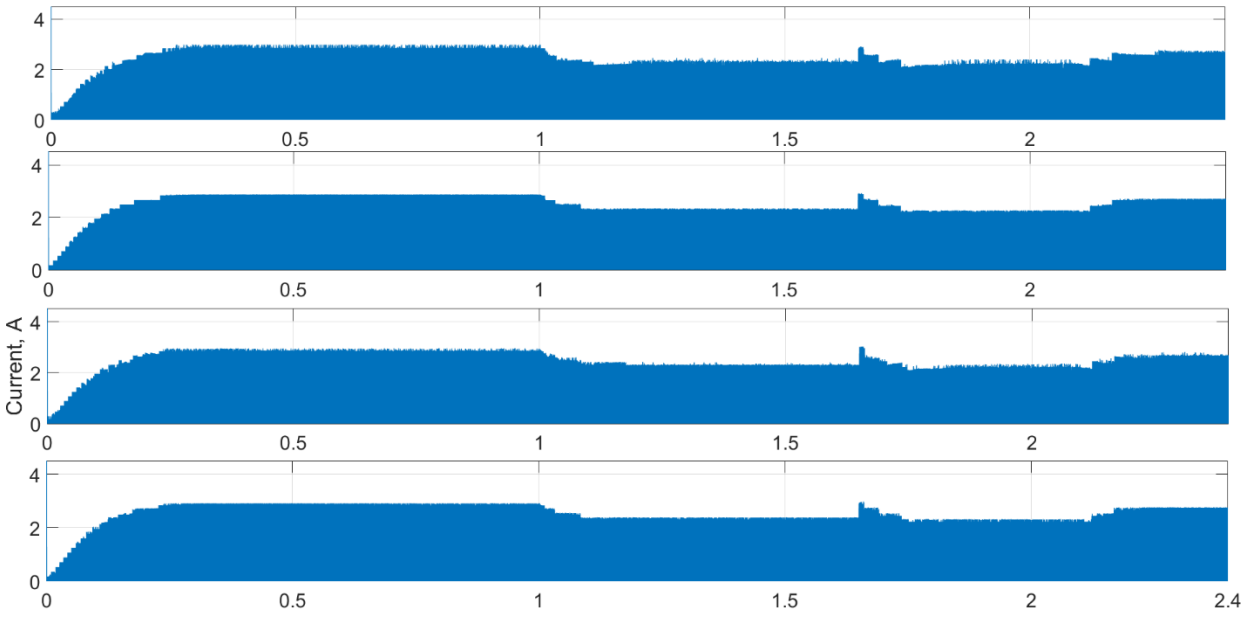

Figure 5.14 Inductor current for each phase.

5.6.3 Voltage Control Simulation Results

Four-phase IBC is designed and simulated using MATLAB/Simulink software as displayed in Figure 5.15 with parameters displayed in Table 5.4. The model is tested for open loop at different gate signals and for closed loop. For open loop, the converter is tested for duty ratio of 0.25, 0.5 and 0.75. Figure 5.16 shows the output voltage waveforms. The μ-controller is implemented to achieve high performance and track the reference voltage and the variation of the load, reference voltage and input supply. To determine the disturbance effect on the controller, the input voltage of the IBC is step changed from 10 to 15 V at (t= 4 sec). and the load is changed from 510 to 306 Ω at (t= 1.4 sec). Reference voltage is changed from 74 to 56 V to check the controller response at (t= 2.7). Simulation results are displayed in Figure 5.17. The controller is compared by PID controller as in Figure 5.18 which shows higher overshot voltage and the PID controller is not able to keep the output voltage constant when the load is changed compared with the μ-synthesis controller. The values of gain margin and phase margin are higher for μ-synthesis controller than the PID which means more stability

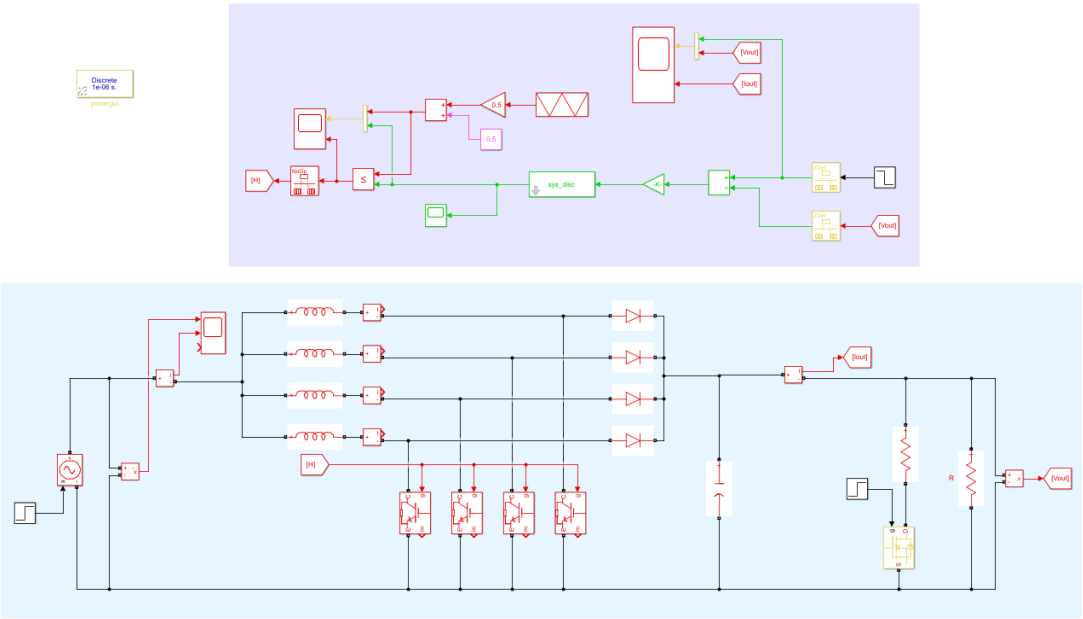

Figure 5.15 Simulation model for closed loop.

Table 5.4 Closed loop IBC parameters.

Parameters	Values
Input voltage, V_i	10, 15V
Inductor, L_1=L_2=L_3=L_4	560×10^{-6} H
Capacitor, C	470 ×10^{-6} F
Sampling time, T_s	100×10^{-6} sec
Switching frequency, f_s	10 KHz
Resistance load, R	510, 306 Ω
Reference voltage, V_{ref}	74, 56 V

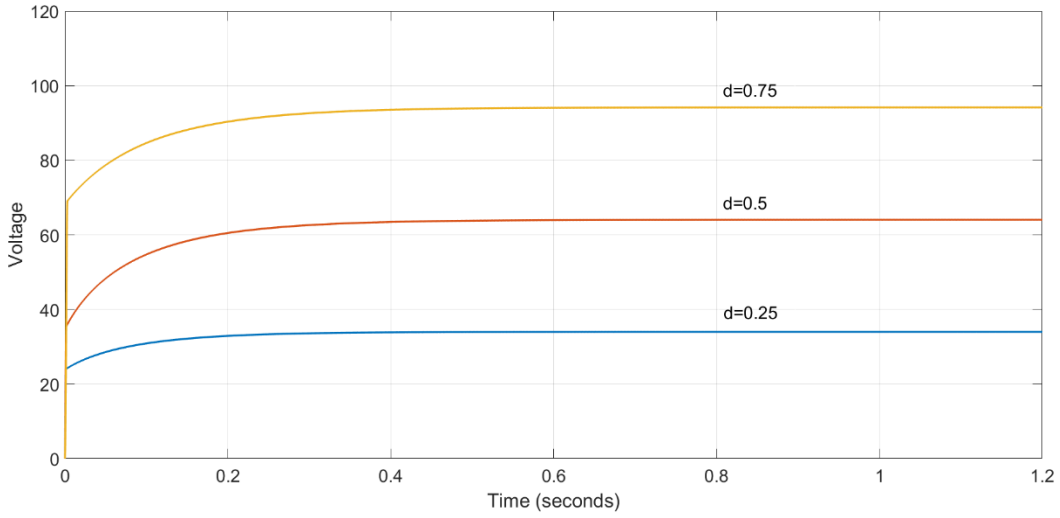

Figure 5.16 Output voltage at different duty cycles.

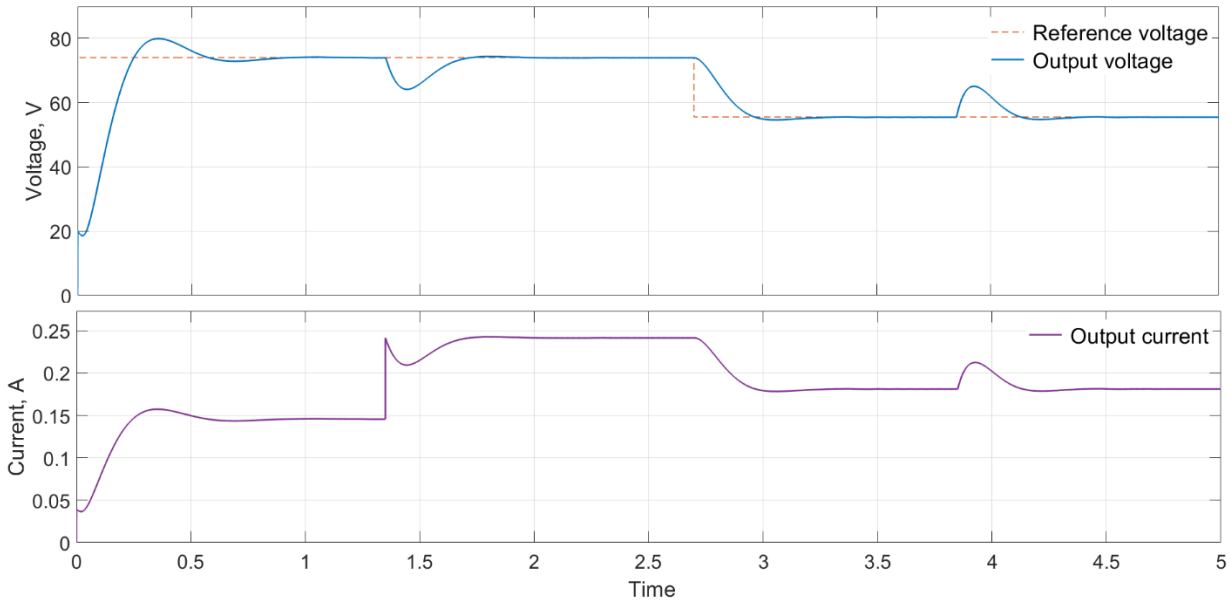

Figure 5.17 Closed loop output voltage and current.

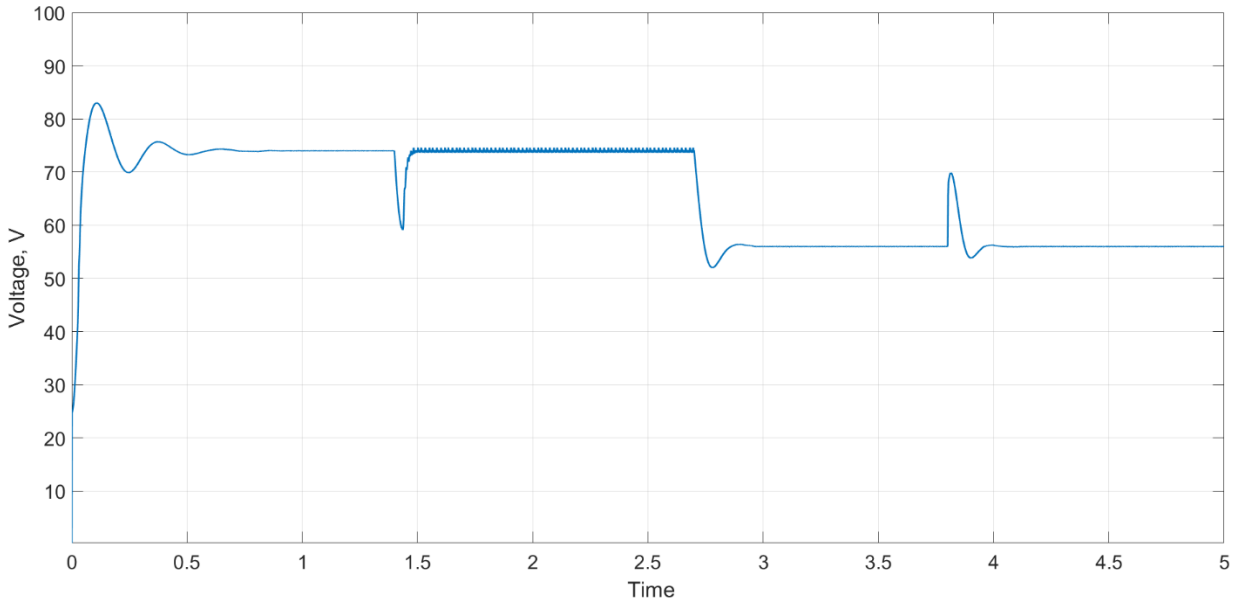

Figure 5.18 PID voltage response.

5.6.4 Experimental Results

5.6.4.1 Hardware Prototype Description

A prototype of a four-phase IBC has been designed and implemented in order to verify the simulation results with the experimental results. The set up of the hardware consists of three circuits; the power supply circuit, pulse generation circuit and main power circuit. The main power circuit includes four boost converters in parallel with IGBT transistors and SiC diodes. The gate driver is employed to produce the needed pulses to ignite the transistors with 10 kHz switching frequency. The complete prototype set up is shown in Figure 5.19.

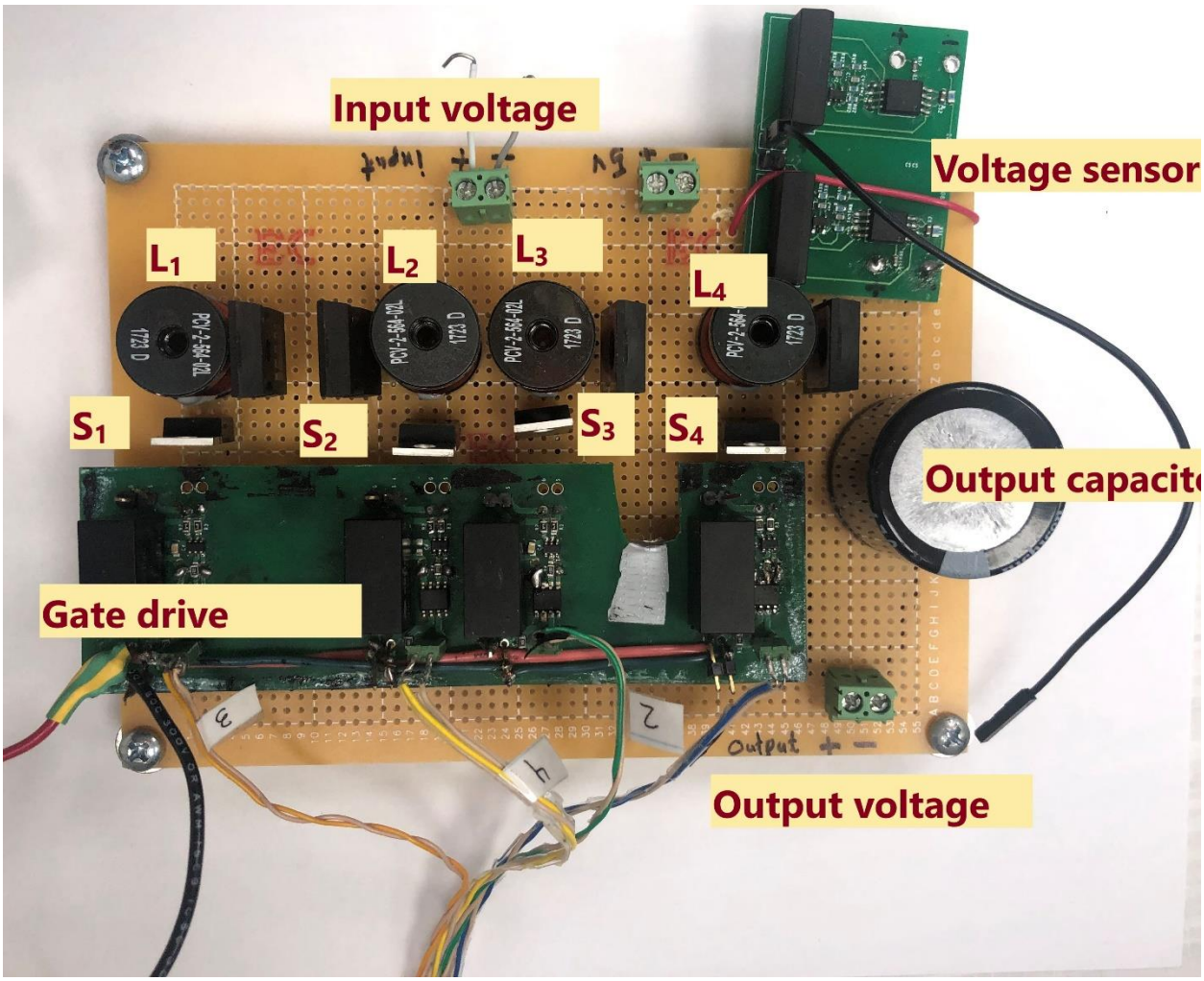

Figure 5.19 Prototype of four-phase IBC.

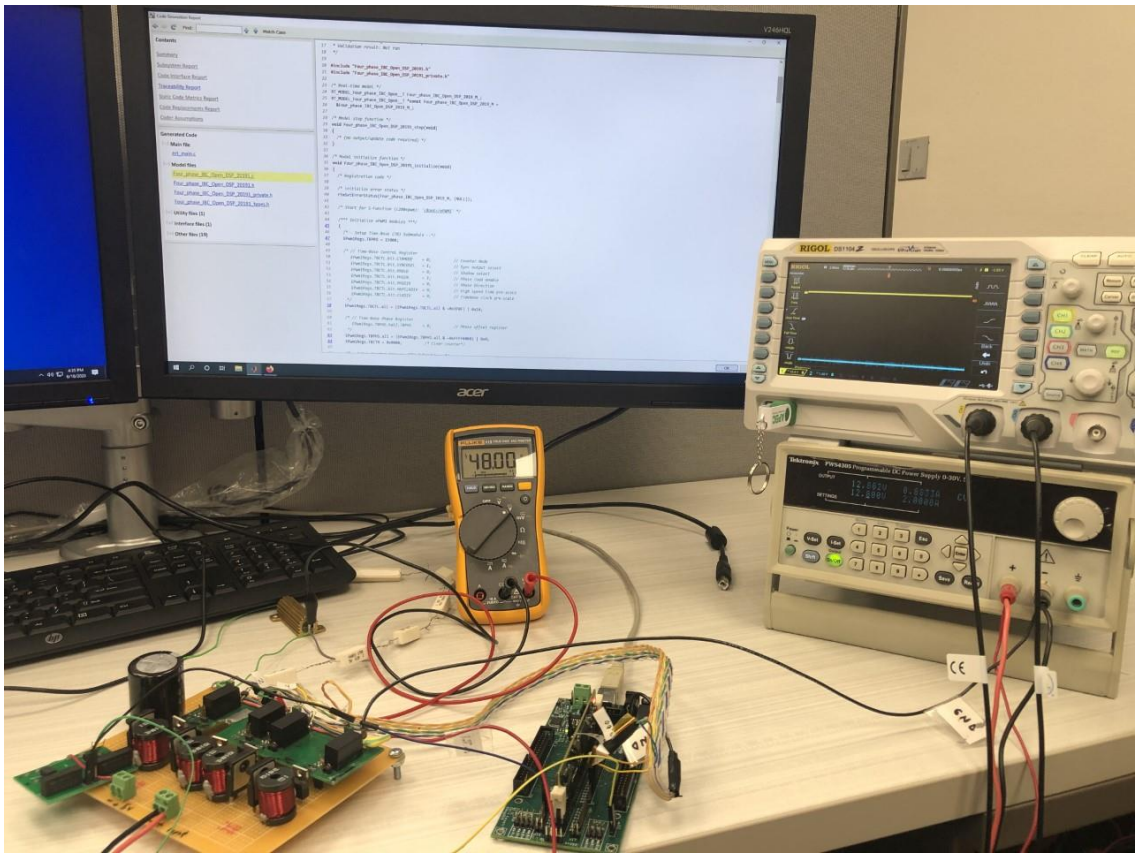

Figure 5.20 Experimental setup view.

The test on the four-phase IBC was carried out for open loop and closed-loop system. The test was operated with one signal for all switches and with phase shift of 90^{o}, 180^{o}, and 270^{o}. The parameters of the prototype are listed in Table 5.2. The open loop tests were carried out for the same gate signal with duty cycle values of 0.25, 0.5 and 0.75. The waveforms of the output voltage for these cases are shown in Figures 5.21, 5.22 and 5.23 respectively.

.

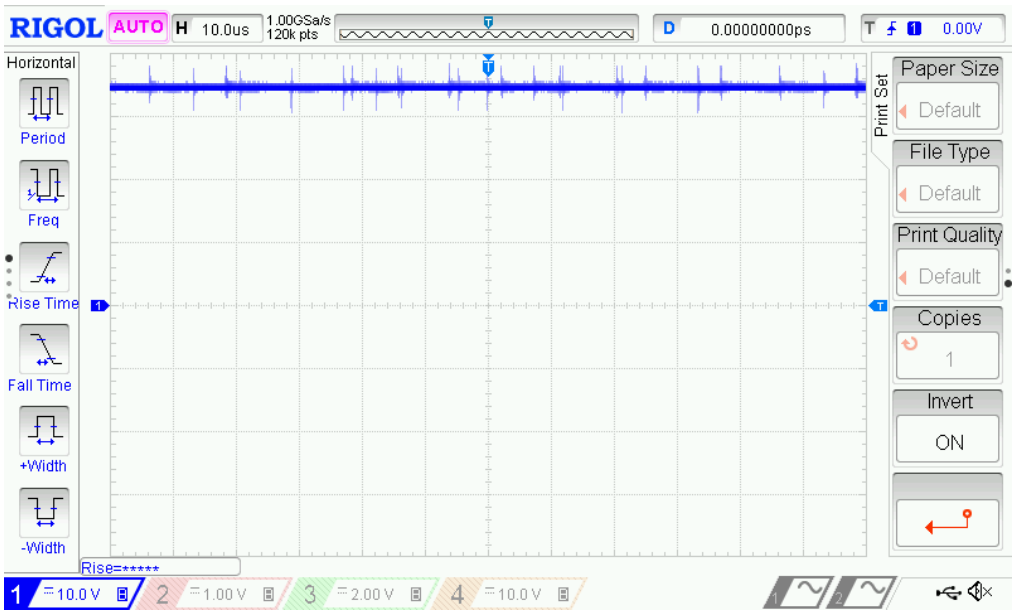

Figure 5.21 Output voltage (d=0.25).

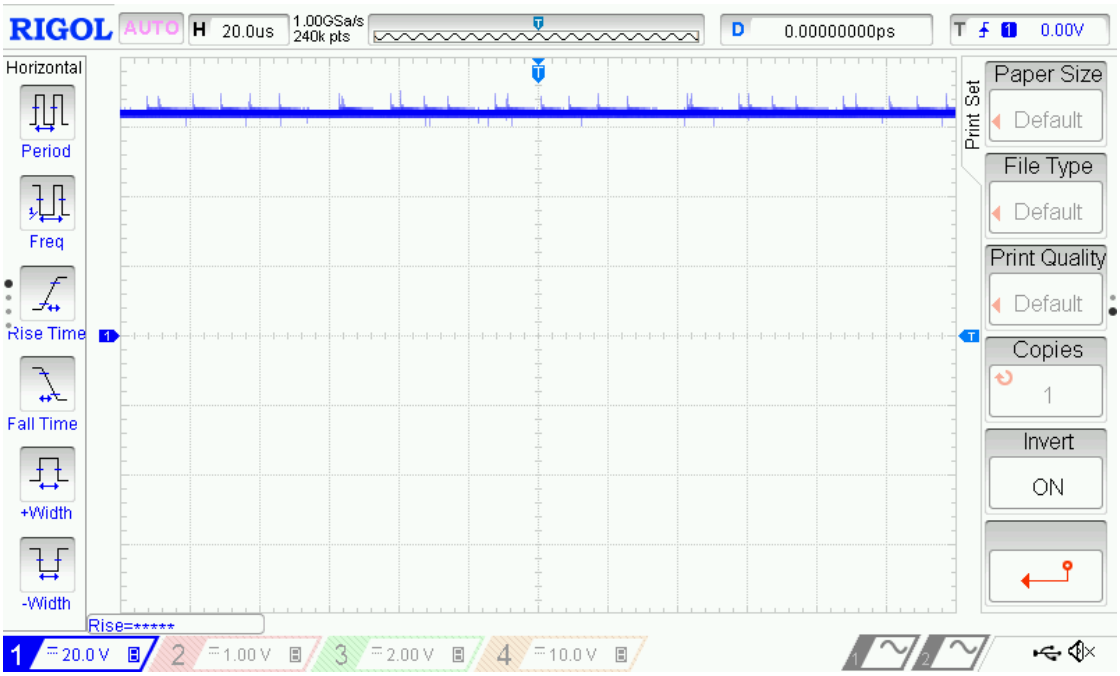

Figure 5.22 Output voltage (d=0.5).

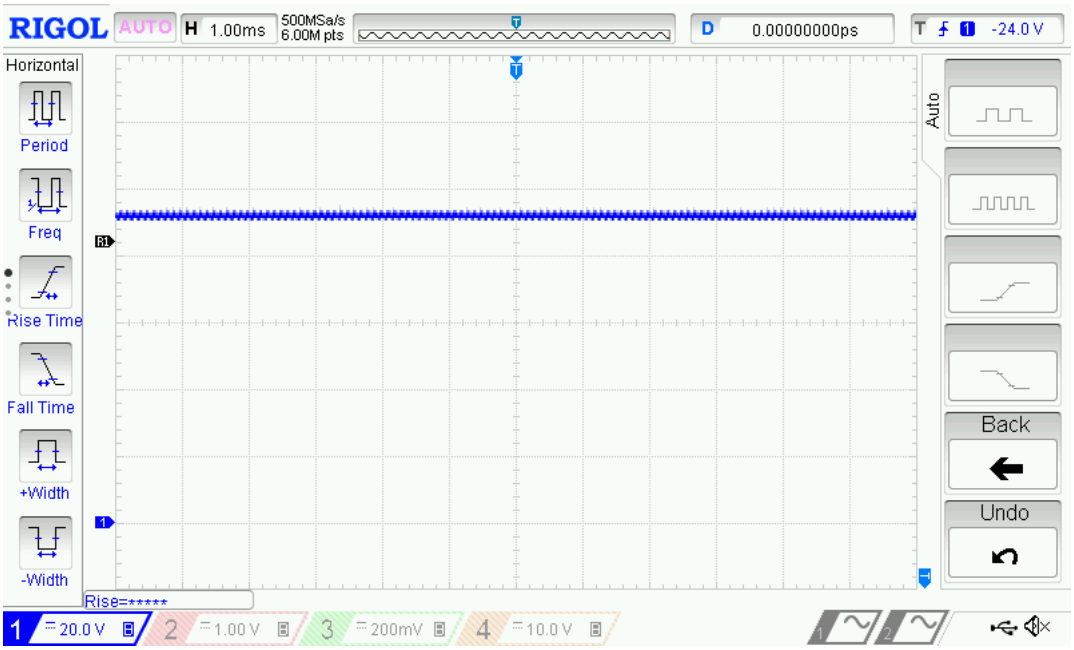

Figure 5.23 Output voltage (d=0.75).

The result of the experiment shows high voltage ratio and verifies the simulation results for both cases. The closed loop was carried out after generating the code into the control card (TI Delfino 28335) installed in the DSP by using MATLAB feature. The output voltage for the closed loop is shown in Figure 5.24. The system shows stable system and verifies the simulation result.

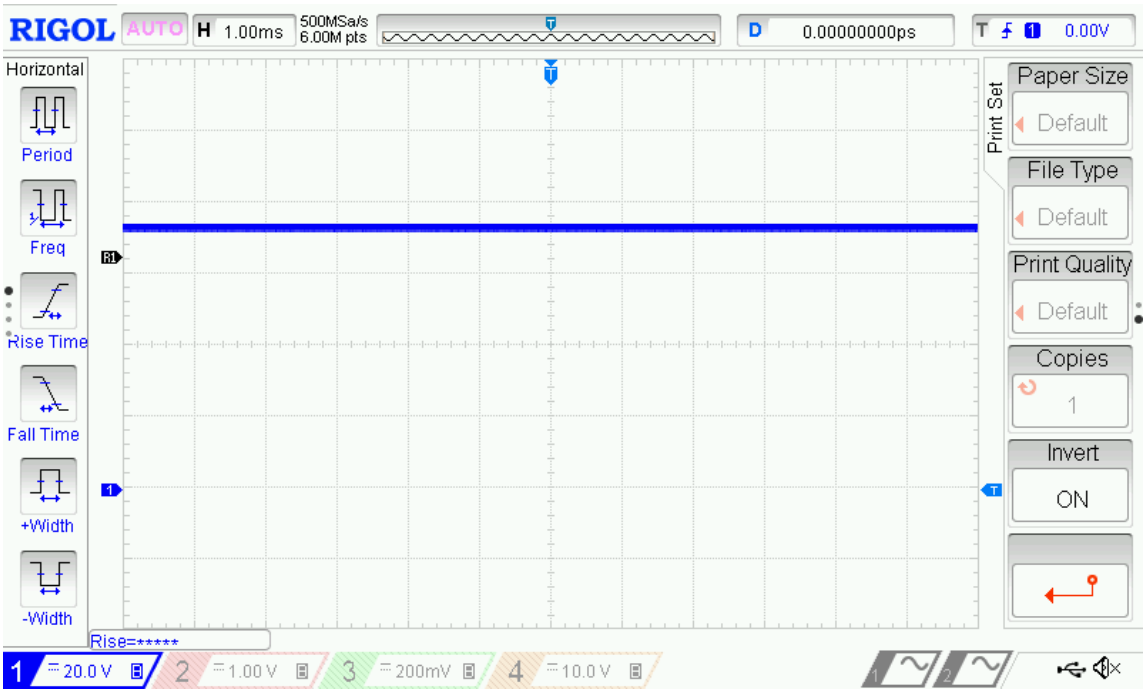

Figure 5.24 Output voltage of μ controller.

5.6.5.2 Shift-phase and Ripple Current

In order to study the effect of phase shift on input current ripple, the converter is derived a shifted gate signal with 45^{o}, 90^{o} and 135^{o} for duty cycle 0.5. The output voltage is shown in Figure 5.16 and the input current ripples is shown in Figures 5.25-5.27. It is observed that .

The topology was tested for the output voltage of each duty cycle. Output voltage and waveforms of PWM of each case are represented in Figures 5.28-5.30.

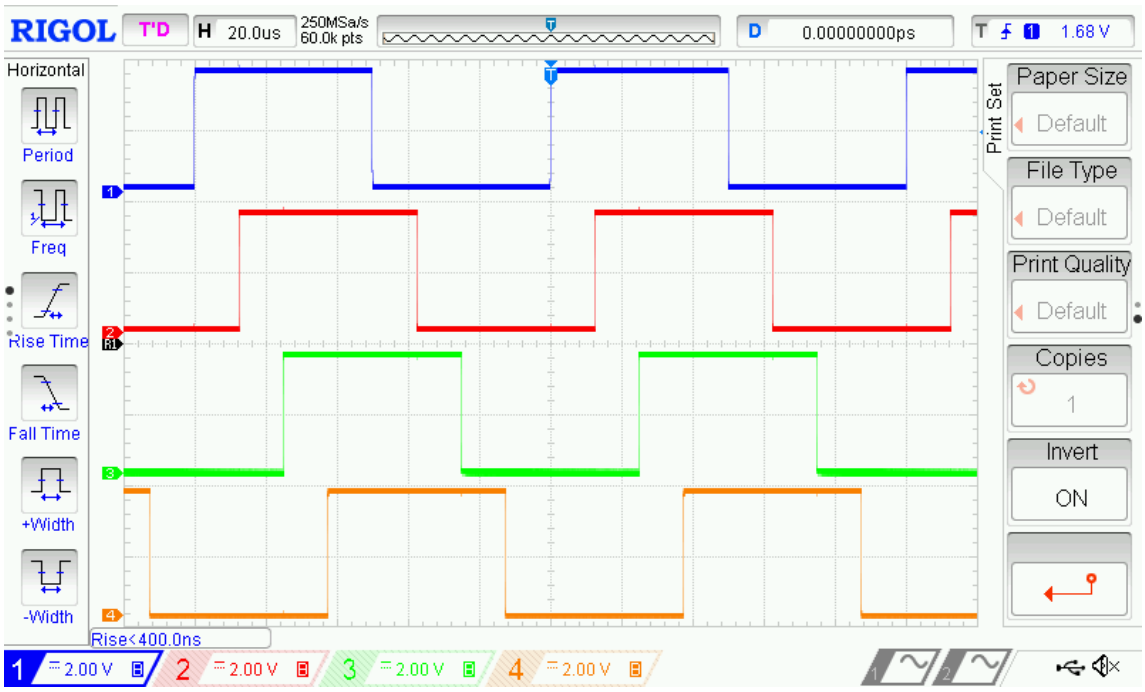

Figure 5.25 PWM waveform.

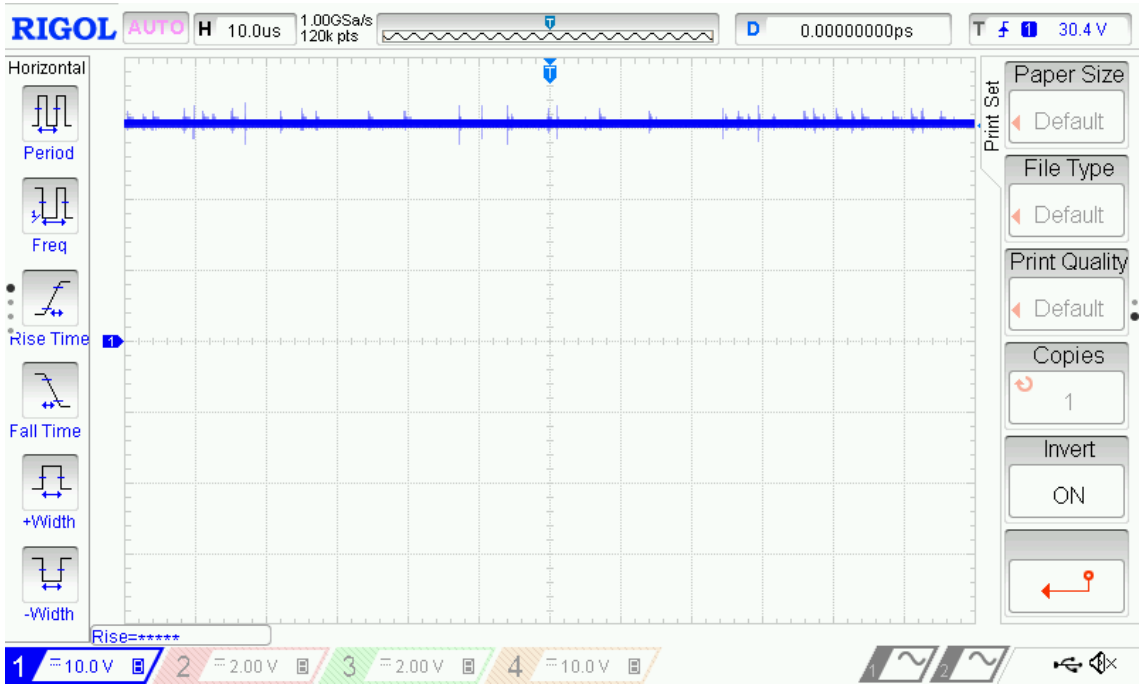

Figure 5.246 Output voltage with shift-phase 25% at d=0.5.

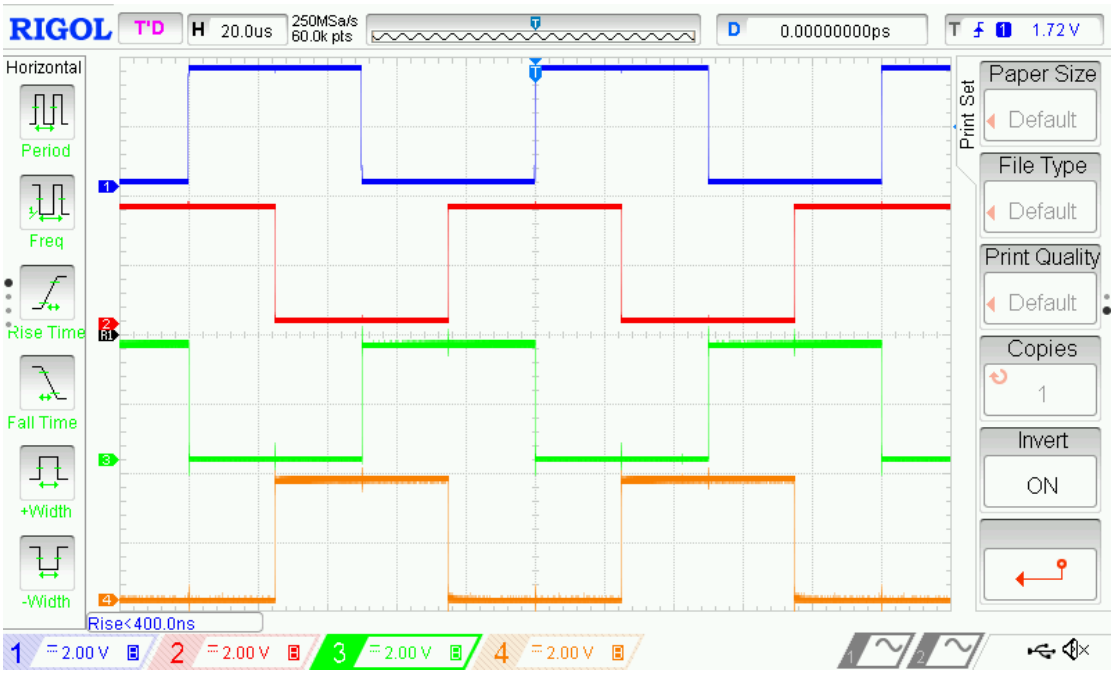

Figure 5.25 PWM waveform.

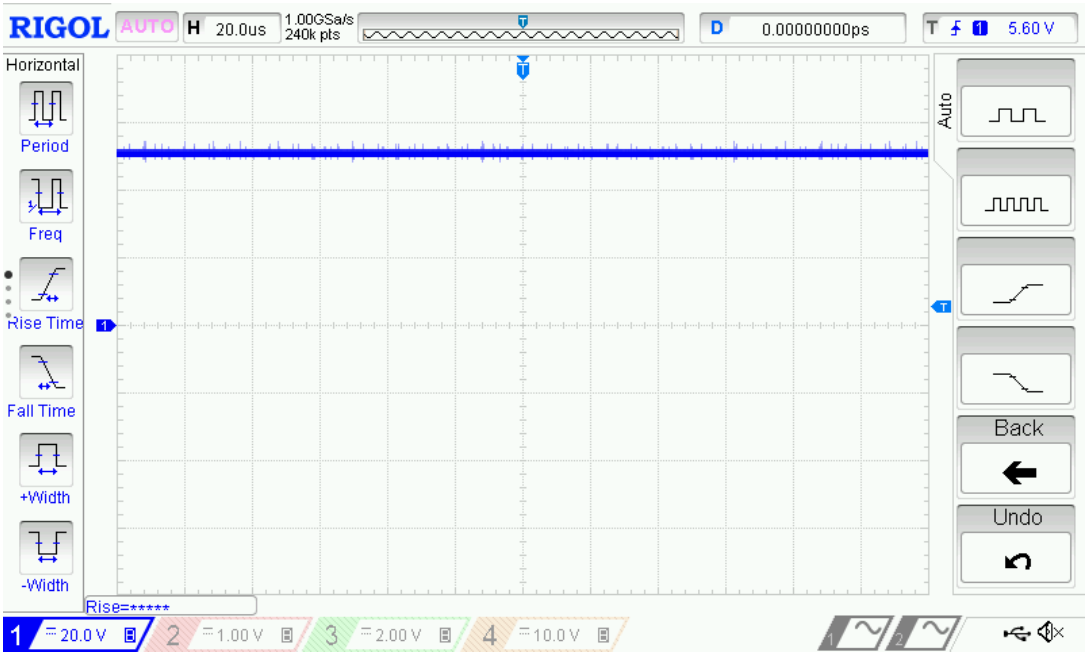

Figure 5.26 Output voltage with phase-shift 50% at d=0.5.

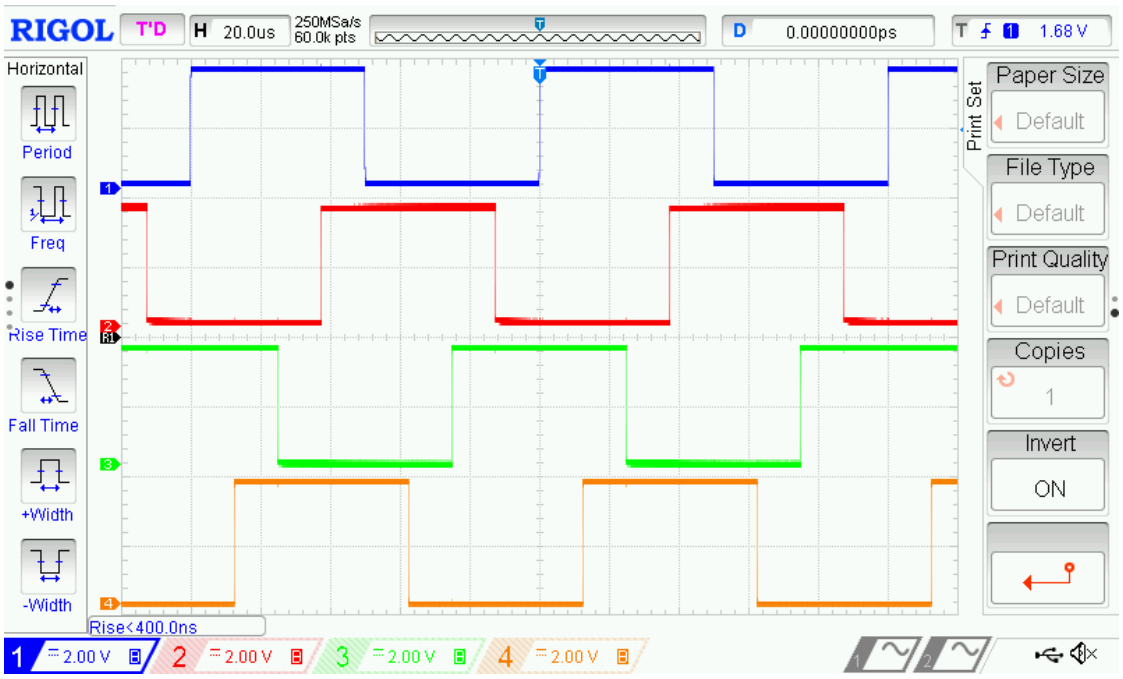

Figure 5.27 PWM waveform.

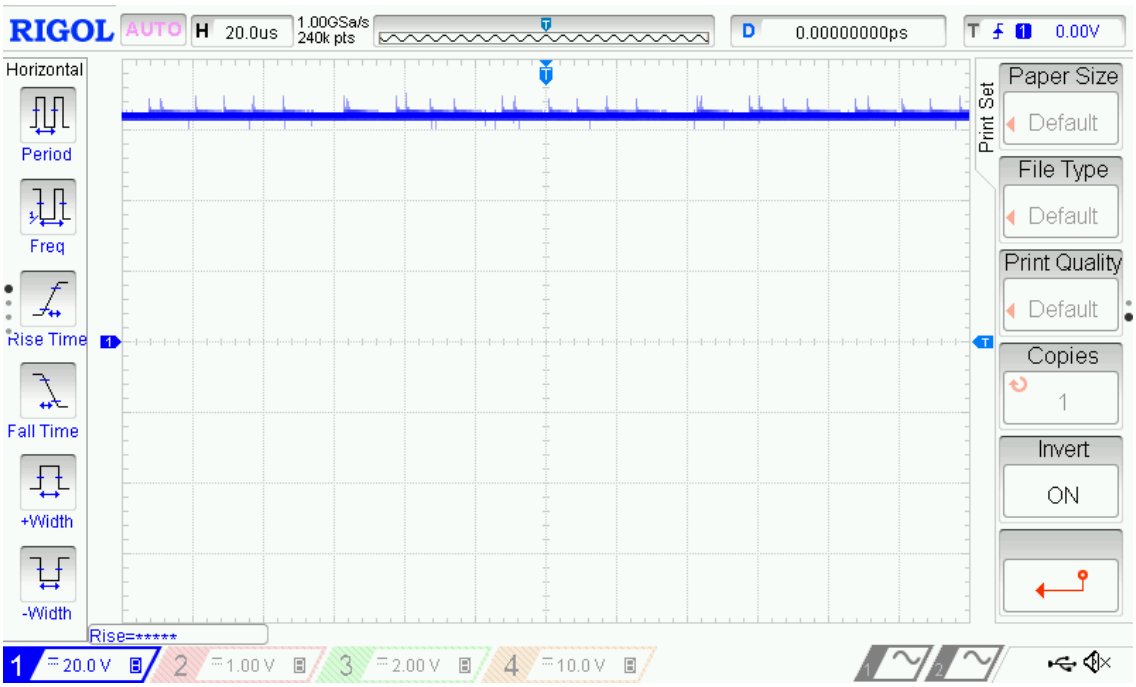

Figure 5.30 Output voltage with phase-shift 75% at d=0.5.

5.7 Conclusion

The design, control and implementation of μ-controller applied to multi-phase IBC is to guarantee robust performance under load variation and input supply changes and with the exist of disturbance is achieved with good reference tracking. It is demonstrated from the simulation and experimental results that μ-controller is affecting in regulating the output voltage under external disturbance. The controller has small overshoot, fast dynamic response, and high robustness.

From the simulation results, it can be concluded that μ-control technique obtains robust stability and robust performance under the uncertainty and external disturbance.

CHAPTER 6

RESEARCH RESULTS

6.1 Introduction

This chapter presents the design of robust controllers using μ-synthesis technique for multi-phase IBC using MATLAB/SIMULINK based on the linearized model of the multi-phase IBC converter in Ch.2. The performance is analyzed in the presence of load and input supply variations.

Multi-phase IBC is designed and simulated to verify the theoretical work proposed in this thesis. Several simulation models have been designed to validate the stability theories and control strategies proposed in chapter four and five.

The following tests are detailed in this Chapter:

- Control of AC-DC power system
- Control of cascade boost converter.
- Control of cascade IBC for PV system.
- Control of DC-link voltage for:
    - DC-Grid interconnected IBC.
    - PV-Grid interconnected IBC.

6.2 Control of AC-DC Power System using Cascade IBC.

Using the IBC for AC/DC converting is a solution for the limitation of high gain applications over the conventional boost converter, the power factor correction and improved THD. These features were tested to prove that IBC controlled by μ-synthesis as depicted in Figure 6.1.

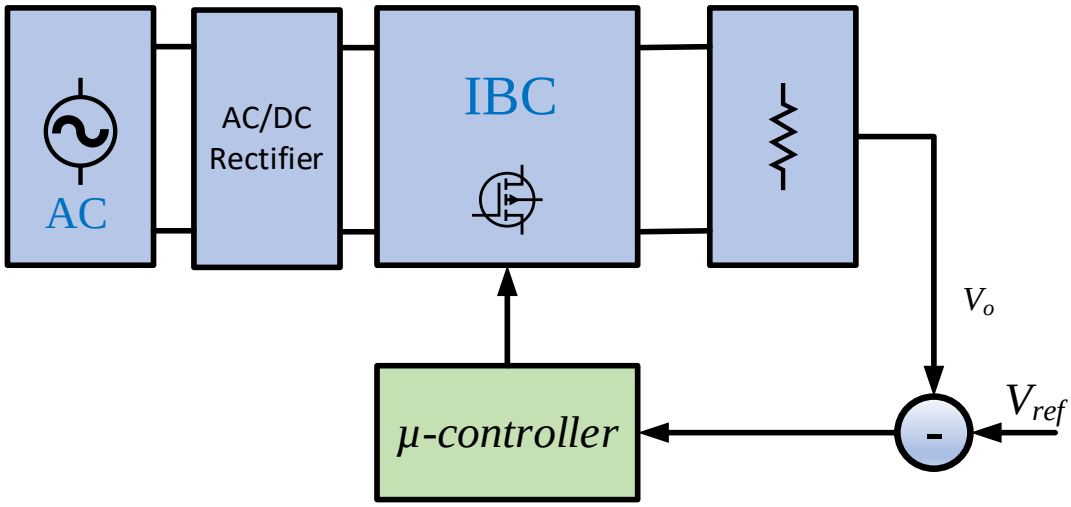

Figure 6.1 Block diagram of controlled cascade PFC system.

The system specification is listed in Table 6.1. The four-phase IBC is designed to meet the AC side. The system was interrupted by changing the load from 200 to 180 Ω at (t = 0.6 sec) and reference voltage was changed from 400 to 420 V at (t= 1 sec). Figure 6.2 shows voltage waveforms of each stage. Figure 6.3 shows the current waveform of each stage.

Table 6.1 Specification of AC/DC power system.

Parameters	Values
Input voltage, V_i	100 V, peak
AC frequency, f	50 Hz
Inductor, L_1=L_2=L_3=L_4	560×10^{-6} H
Capacitor, Co	900×10^{-6} F
Switching frequency, f_s	9 KHz
Resistance load, R	200, 182 Ω
Reference voltage, V_{ref}	400, 420 V

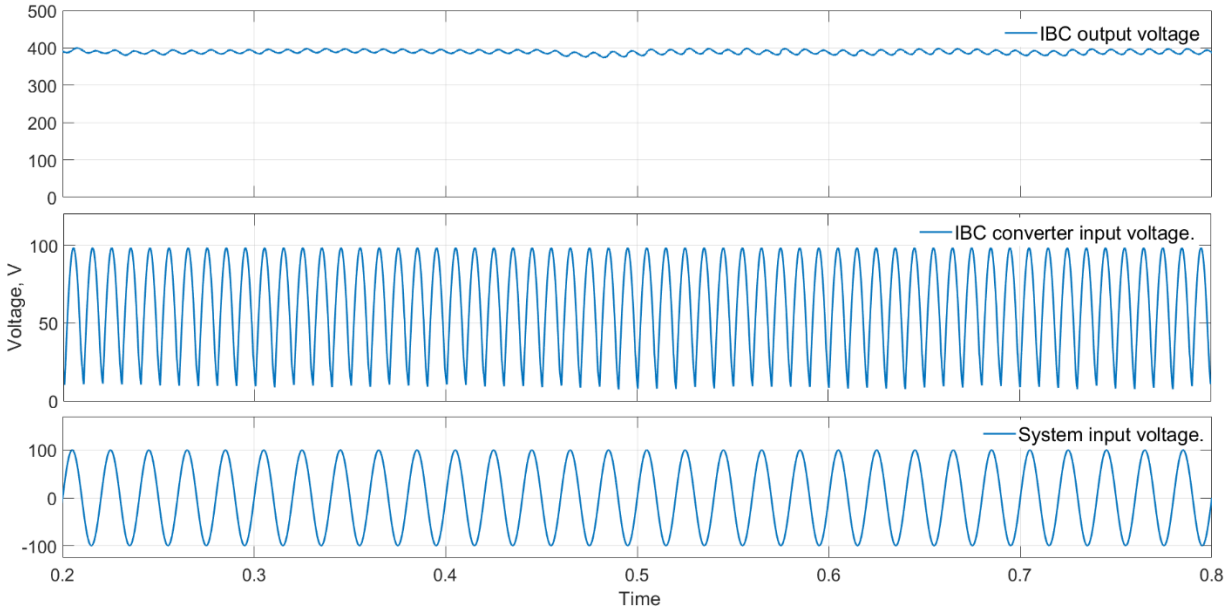

Figure 6.2 Voltage responses.

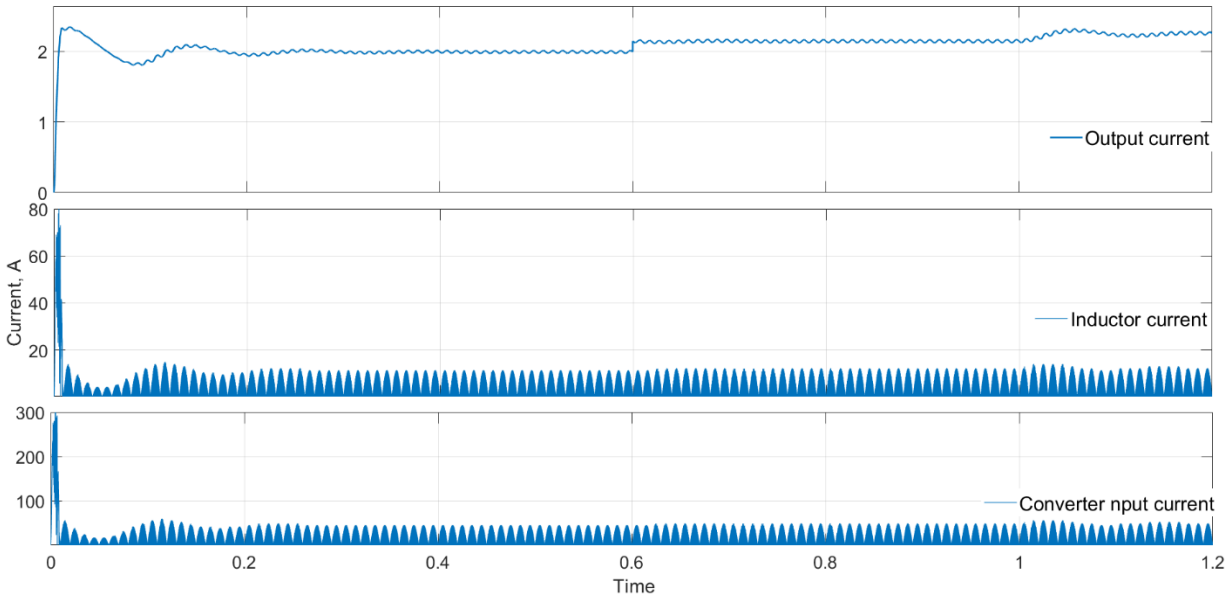

Figure 6.3Current responses.

The controller shows sufficient performance and good tracking.

6.3 Control of Cascade Boost Converter

In this section µ-controller is designed for closed loop cascade boost converter as depicted in Figure 6.4. to assure high performance under load and input supply variations and under uncertainty values to regulate the output voltage. The input supply is changed from 20to 25 V at (t= 0.2 sec.) and resistance load is changed from 20 to 15 Ω at (t= 0.35 sec.) and to 12 Ω at (t= 0.6 sec.) to interrupt the system while the reference voltage is changed from 100 to 120 V at (t=0.45 sec.). The controller responses is shown in Figure 6.5. The system efficiency is sufficient high as noticed from Figure 6.6.

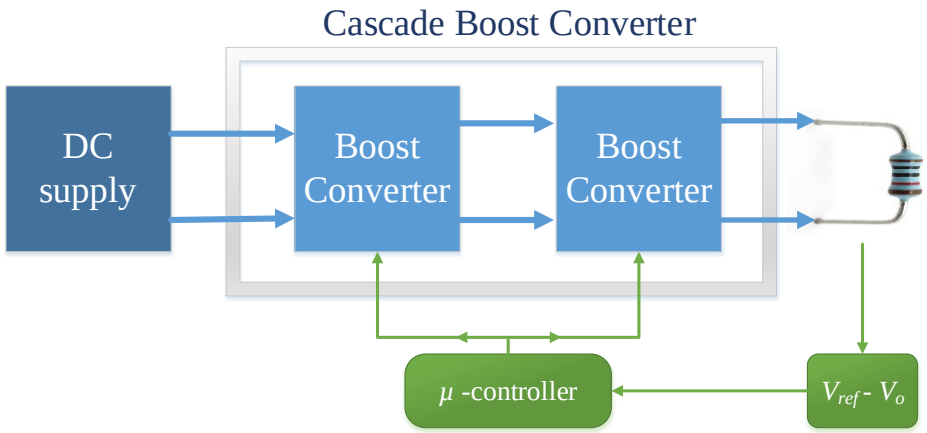

Figure 6.4 Block diagram of closed loop cascade boost converter.

Table 6.2 Cascade boost converter specifications.

Parameters	**Values**
Input voltage, V_i	20, 25V
Switching frequency, f_s	10kHz
Inductor, L_1	560μH
Inductor, L_2	860μH
Capacitor, C_1	100μF
Capacitor, C_2	300 μF
Load resistance, R	20, 15, 12 Ω
Series resistance, r_c=r_L	1mΩ
Output reference voltage, V_{ref}	100V, 120V

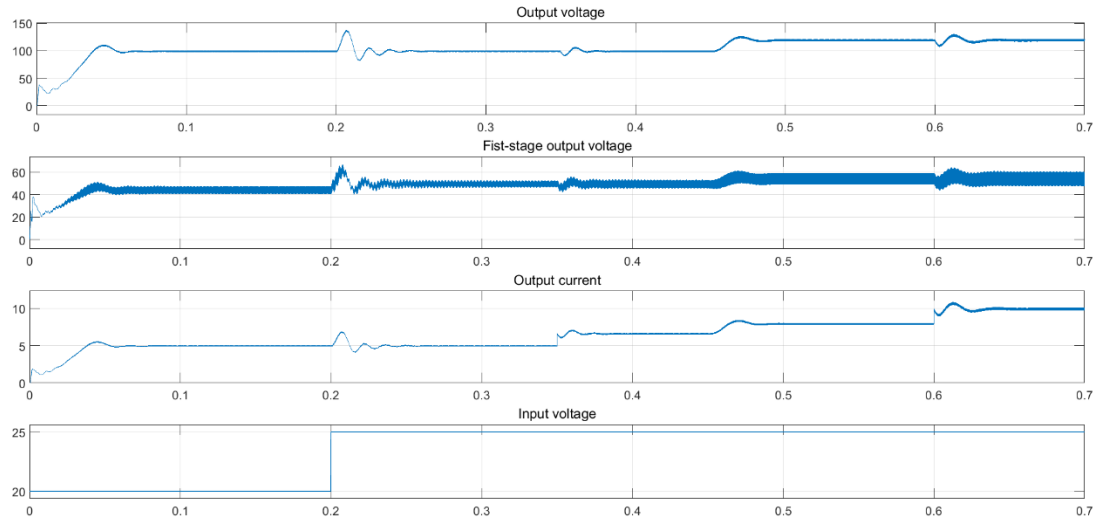

Figure 6.5 Waveforms of system responses.

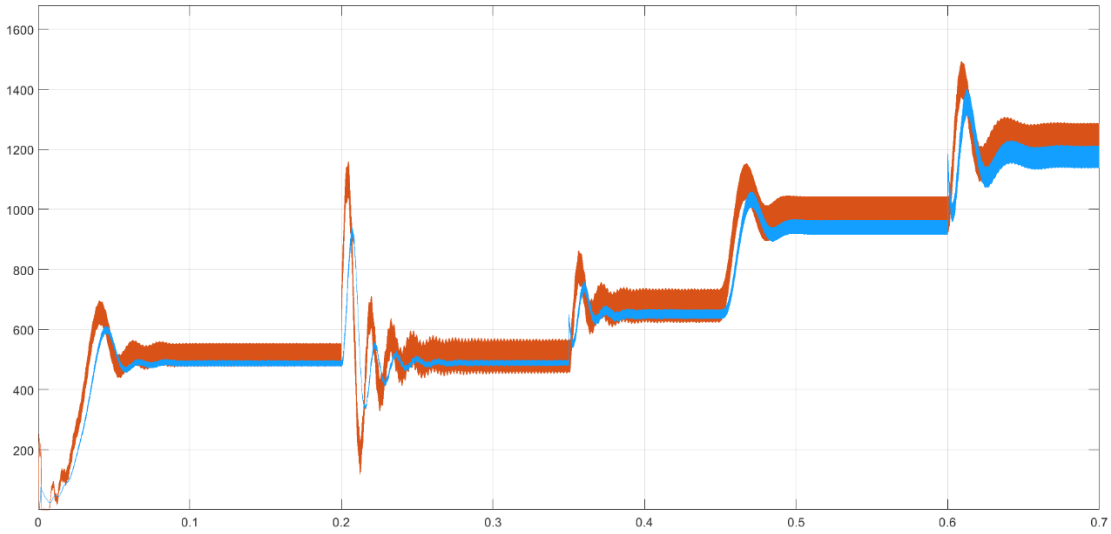

Figure 6.6 Power.

Simulation results show that µ-controller is able to achieve robust performance.

6.4 Control of CIBC for PV application

Designing the control system of converters connected in series or (cascaded converters) demands that the output impedance of the source converter is less than the input impedance of the load converter to achieve system stability [128] which might derive some challenging in the

converter design and the control system. The CIBC boosts the input voltage from 60 V to 500 V and steps-down the input current from 26 A to 2.9 A. The solar panel specification is provided in Table 6.3. The switches of PV-converter are pulsed with one signal which has the same switching frequency with phase shift $360/n = 90^o$. The circuit of CIBC is shown in Figure 6.7. Each IBC is designed individually based on regular design method that meets the two stages stability criteria. The PV-converter is to step up the PV output voltage from (60 V) to (233 V) and to step-down the input current from (26 A) to (15 A). It is designed with four-phase to handle the high input current, transfer the highest power and to reduce the input current ripple with better efficiency [40]. The waveform for Q_1, Q_2, Q_3 and Q_4 are phase-shifted by ($360/4 = 90^{o)}$ to drive the IGBTs switching devices. The pulses are generated by PWM generator based on InC MPPT controller. The load converter is to boost the output voltage of PV-converter from (233 V) to (500 V) and to step-down the current from (15 A) to (2.9 A). It is designed with two-phase to be regulated by µ-controller to promote the system stability. The switches Q_5 and Q_6 have the same pulse signal as displayed. The duty cycle ratio of CIBC is determined by the following equation:

$$d = (1 - \frac{V_i}{V_o}) \times m, \tag{5.21}$$

where m is the number of stages.

The parameters of PV-converter and load-converter are provided in Table 6.4. The cascade interleaved boost converter is modeled and simulated using MATLAB/Simulink software. The simulation circuit is depicted if Figure 6.8.

Table 6.3 Solar panel specifications.

Parameter	**Value**
Peak power, P_{mp}	305.226 W
Voltage at peak power, V_{mp}	54.7 V
Current at peak power, I_{mp}	5.58 A
Short circuit current, I_{sc}	5.96 A
Open circuit voltage, V_{oc}	64.2 V
Temperature coefficient of I_{sc}, K_i	0.061745
Cells per module, *Ncell*	96

Table 6.4 Converters specifications.

Parameters	**Value**
V_i	60 V
Capacitor, C_i	100×10^{-6} F
Inductor, L_1, L_2, L_3, L_4	560×10^{-6} H
Capacitor, C_1	100×10^{-6} F
Inductor, L_4=L_5	560×10^{-6} H
Capacitor, C_o	400×10^{-6} F
Resistance load, R_o	175Ω
Switching frequency, f_s	9kHZ

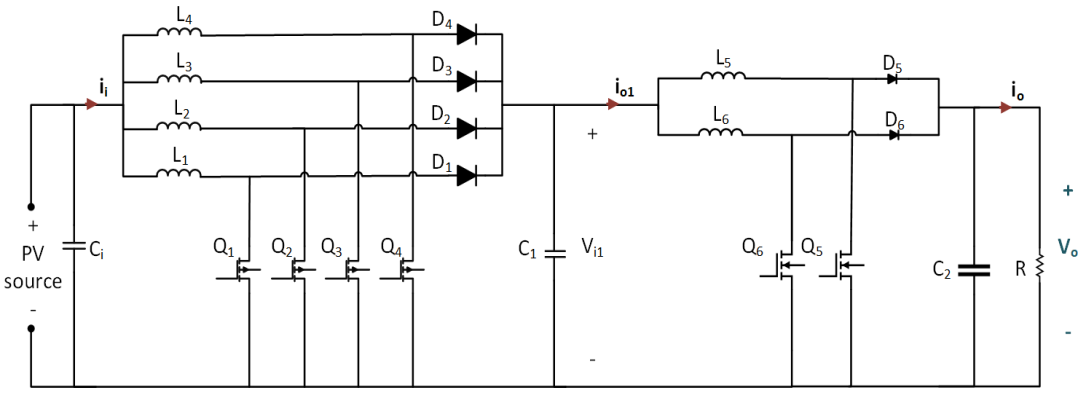

Figure 6.7 Cascade IBC for PV system.

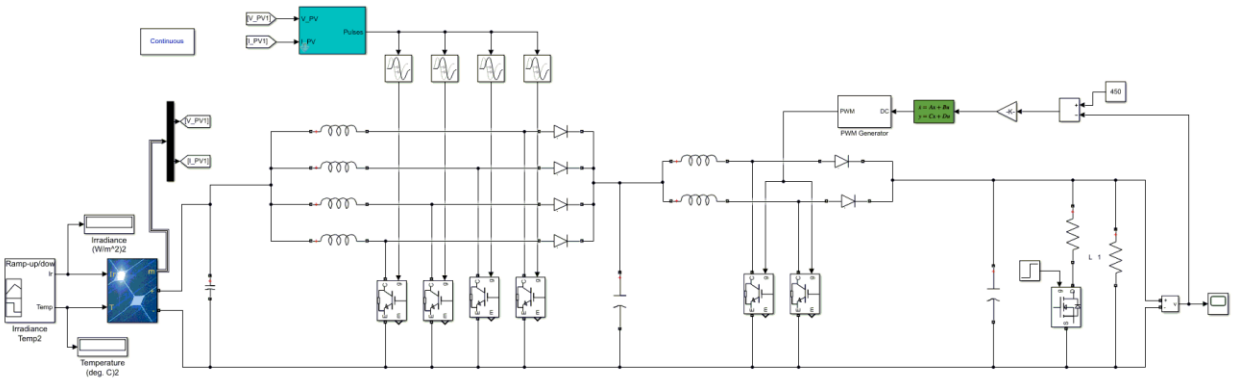

Figure 6.8 Simulation model.

The system performance of μ-controller is tested under load resistance changes with 25% at (t=0.3 sec.). The controller proves robust performance as shown if Figure 6.9 for the input voltage, PV-converter output voltage, and the load voltage. The system input current, load-converter input current and output current are shown in Figure 6.10. The output power is compared with the input power in Figure 6.11 where high efficiency is observed.

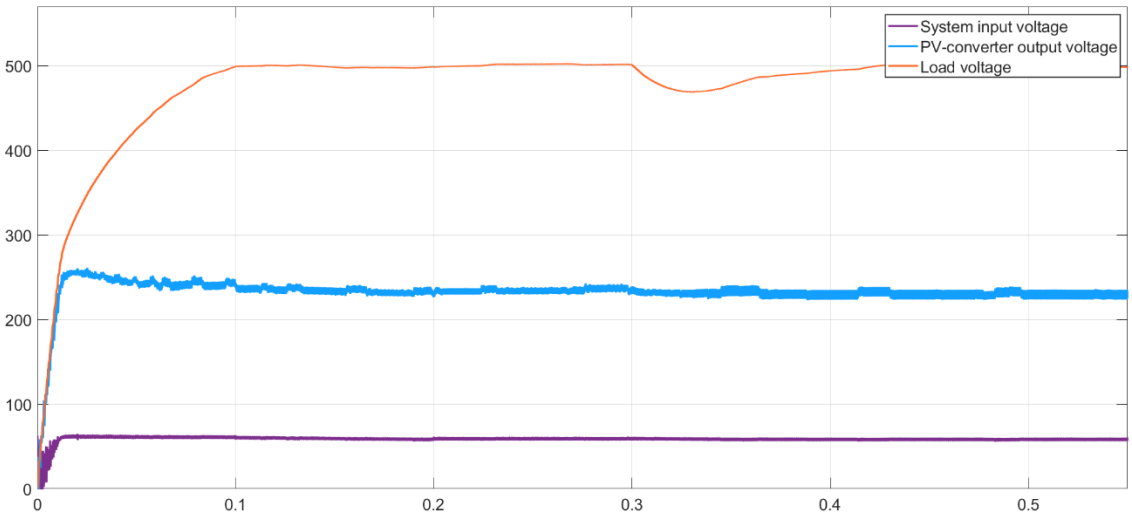

Figure 6.9 System input voltage and output voltage of each converter.

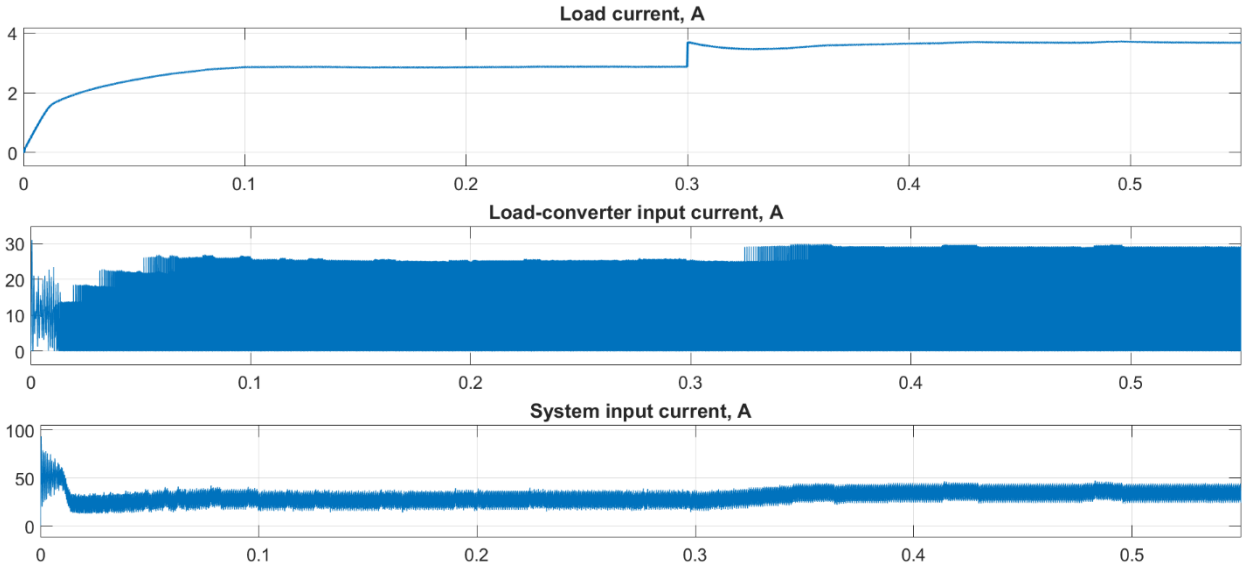

Figure 6.10 Load current and input current of each converter.

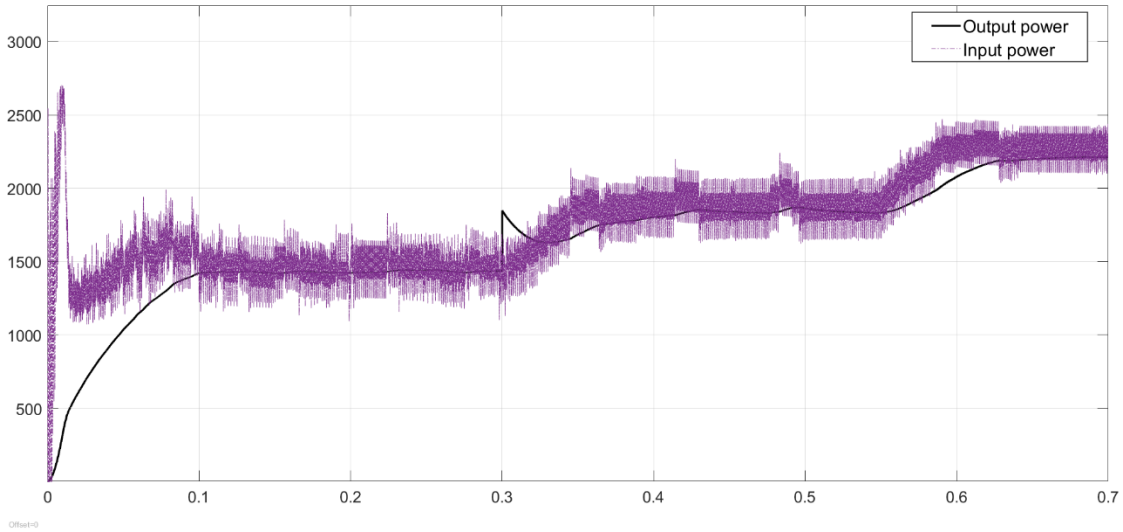

Figure 6.11 Power.

The operation of the proposed system is stable and efficient. The CIBC is able to produce the stable high voltage gain and deliver the maximum power with less ripple.

6.5 Control of DC-link voltage for:

For DC-link voltage, it is necessary to design a robust controller that can regulate the output voltage and maintain robust performance at disturbance conditions and load variation. In this section μ-synthesis technique is applied to regulate the DC-bus voltage and maintain system stability for grid system. The controller tasks are determined below:

1) Regulate the DC bus voltage and track the reference voltage.
2) Achieve robust stability and performance.

6.5.1 Control of DC-3AC Grid interconnected IBC

Recent power systems developments based smart grids have presented challenges to design new topologies of DC–DC power conversion systems which regulate several input energy sources to handle the input source variation, deliver a regulated and stable output for different applications.

IBC converters must be designed to meet their desired performance and specifications for harmonic distortion and remaining stable in terms of efficiency.

In this simulation, the 4-IBC converter is connected to grid side with frequency of 60 Hz in order to examine the proposed control along with the efficiency of the converter. The desired DC bus voltage is calculated based on the peak inverter voltage. Table 6.4 lists the main simulation parameters. The simulation control strategy is depicted in Figure 6.12. The strategy of Space Vector Pulse Width Modulation (SVPWM) is selected to generate the control signal of the inverter by using sine triangle modulation while the μ-synthesis is regulating the DC bus output voltage. Controlling the DC bus is challenging but it is the successful operation of the system where this helps the inverter to maintain the grid output voltage regulated.

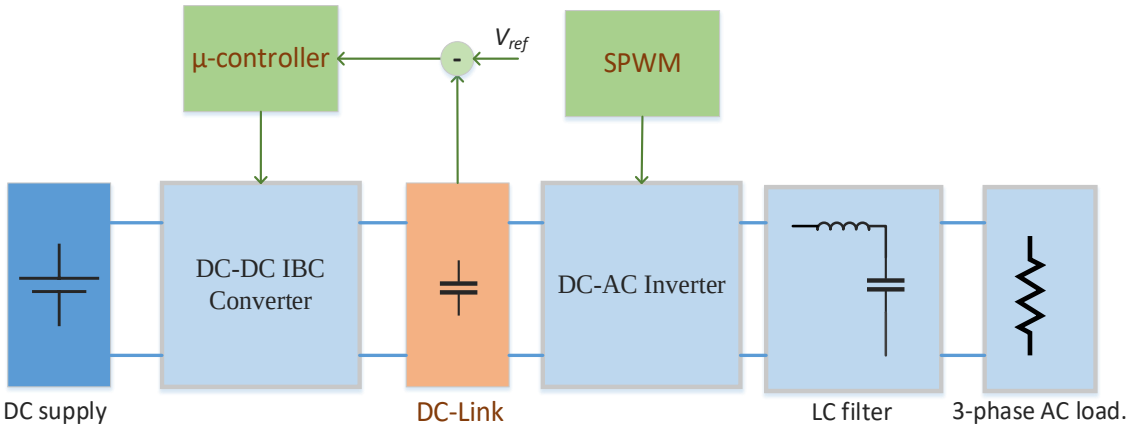

Figure 6.12 Schematic diagram of grid system.

The system responses for load variation from 100 to 80 Ω at (t= 0.35 sec.) and input supply changes from 100 to 110 V at (t= 0.7 sec.) are shown in Figure 6.13-6.15.

Table 6.5 Grid connected DC supply.

Parameters	Values
Input voltage, V_i	100, 110 V
Reference voltage of DC-link	400V
Switching frequency, f_s	9kHz
Capacitor, C	900×10^{-6} F
Inductor value, L	560×10^{-6} H
AC frequency, f	50 Hz
Filter values, L, C	8mH, 100µF
Resistance load, R	100, 80Ω
Load voltage, V_o	450 V (peak)

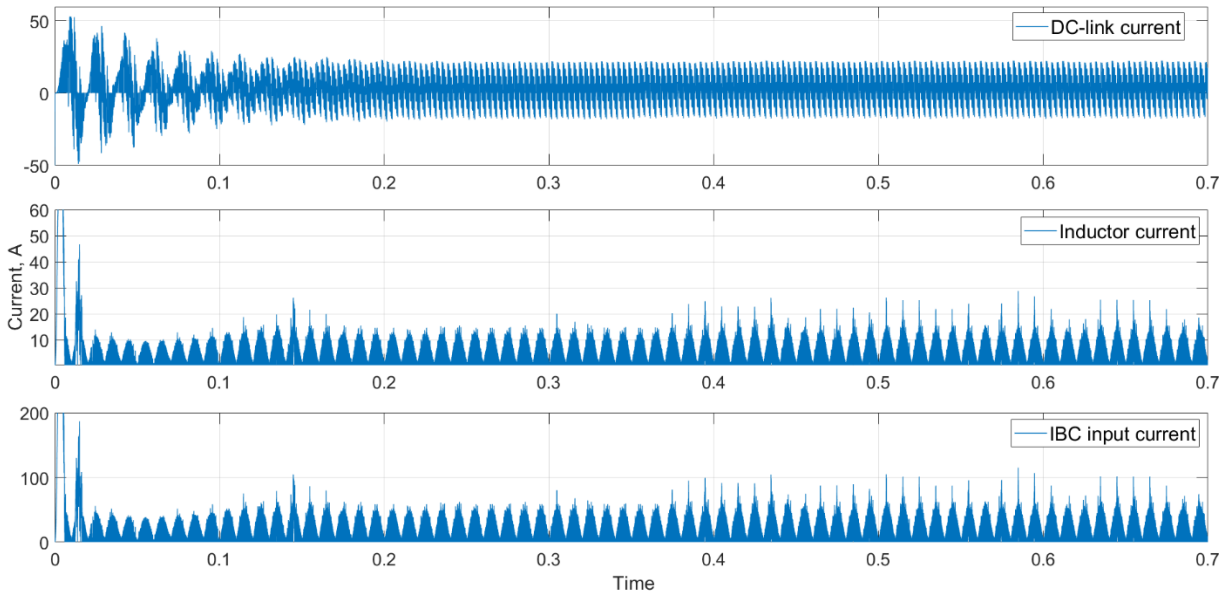

Figure 6.13Current waveforms.

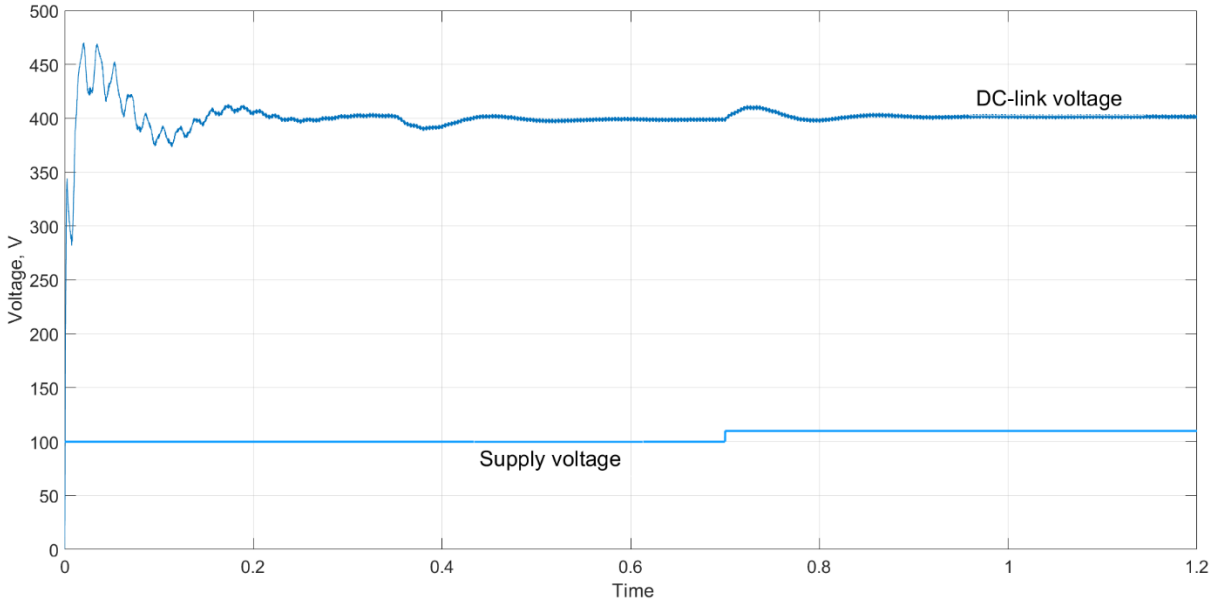

Figure 6.14 DC-link voltage.

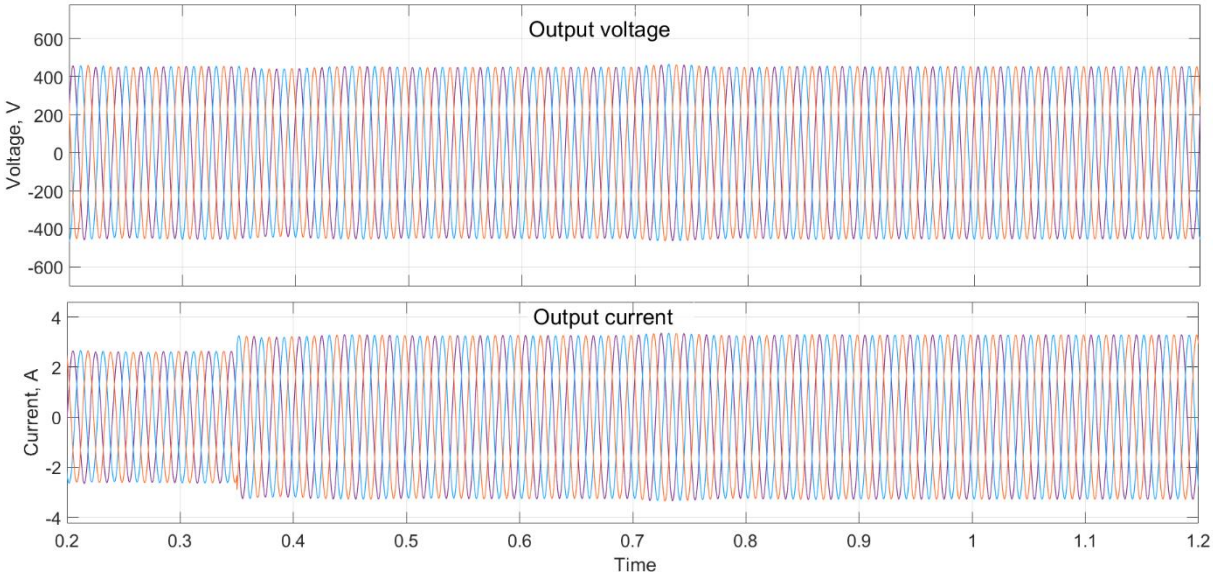

Figure 6.15 Output voltage and current.

6.5.2 Control of DC-3AC for PV Application intercommoned cascade multi-phase IBC.

IBC converters must be designed to meet their contractual obligations for available active and reactive power capability and to meet specifications for maximum power generation of PV panel and remaining competitive in terms of efficiency and to ensure stability [129]. The schematic

diagram of proposed system is displayed in Fig 6.16 and system specifications for grid connected PV source converters of is listed in Table 6.6.

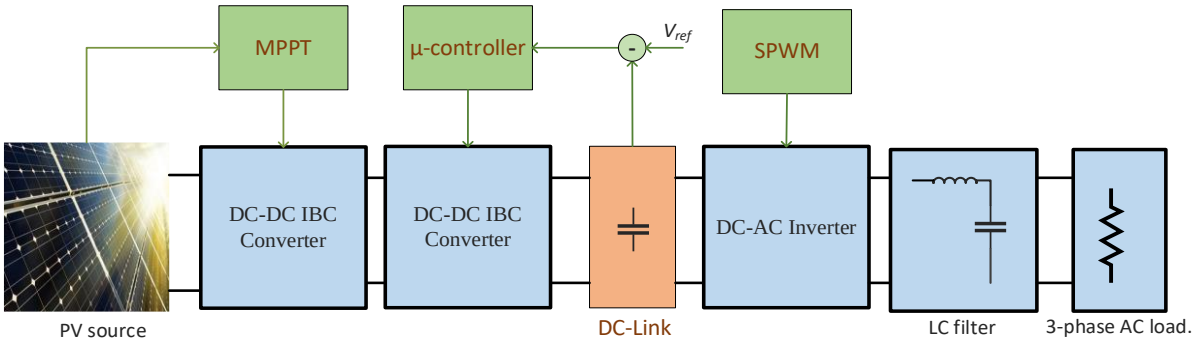

Figure 6.16 PV-grid interconnected cascade IBC.

Table 6.6 Grid connected solar PV source.

Parameters	Values
Reference voltage of DC-link	212 V
Switching frequency, f_s	9KHz
Input capacitor, C_i	100×10^{-6} F
First-stage inductor value, L	560×10^{-6} H
First-stage capacitor value, C_1	400×10^{-6} F
Second-stage inductor value, L	660×10^{-6} H
First-stage capacitor value, C_2	900×10^{-6} F
AC frequency, f	50 Hz
Filter values, L, C	8×10^{-3} H, 100×10^{-6} F
Resistance load, R	100, 82 Ω
Load voltage, V_o	230 V, (peak)

The system is interrupted by the effect of weather changes and the variation of resistance load from 100 to 82 Ω at (t= 0.55sec.). The DC-link voltage and current waveforms are shown in Figure 6.17. The grid responses is shown in Figure 6.18.

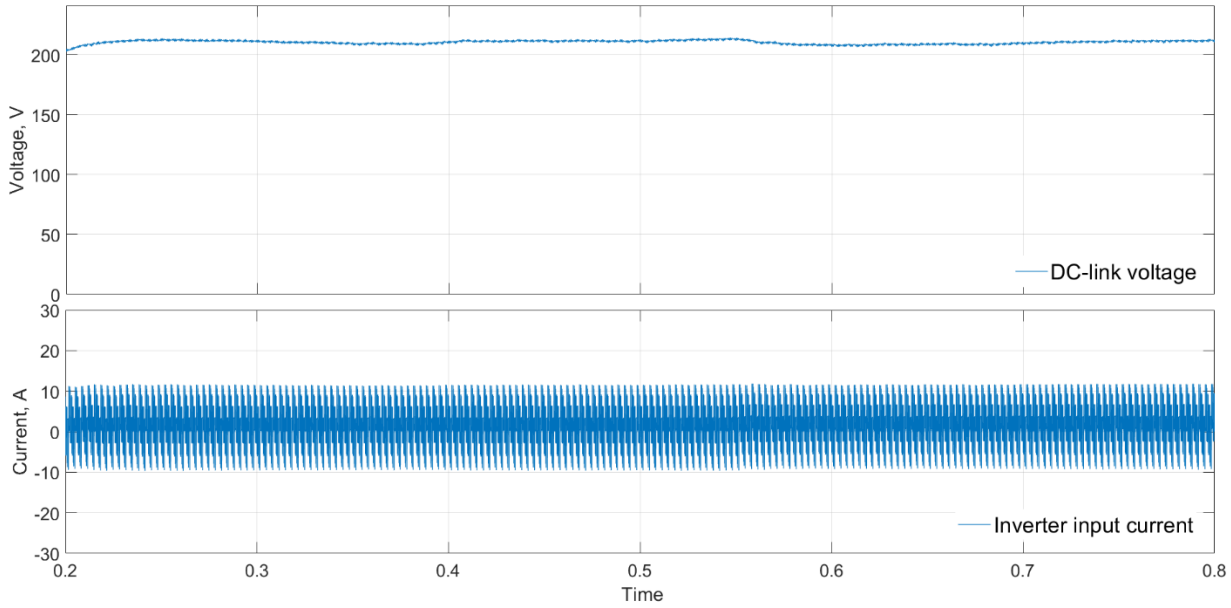

Figure 6.17 Current and voltage waveforms.

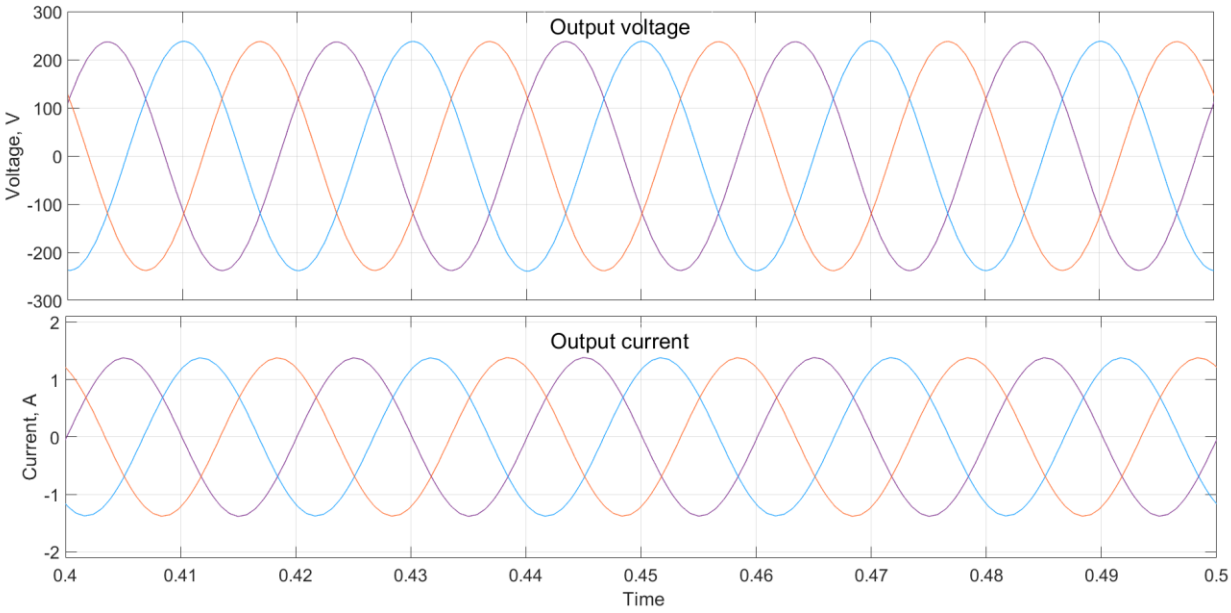

Figure 6.18 Grid output voltage and current.

6.5.3 Control of Grid system supplied by one phase AC system interconnected IBC.

One of the applications of IBC is to generate a high voltage ratio. In this section the converter is used to boost the input voltage into higher level and enhance the stability. The schematic diagram is depicted in Figure 6.19 and the system parameters is listed in Table 6.7. The system is interrupted by the changing the load from 100 to Ω 80 Ω at (t= 0.45 sec.).

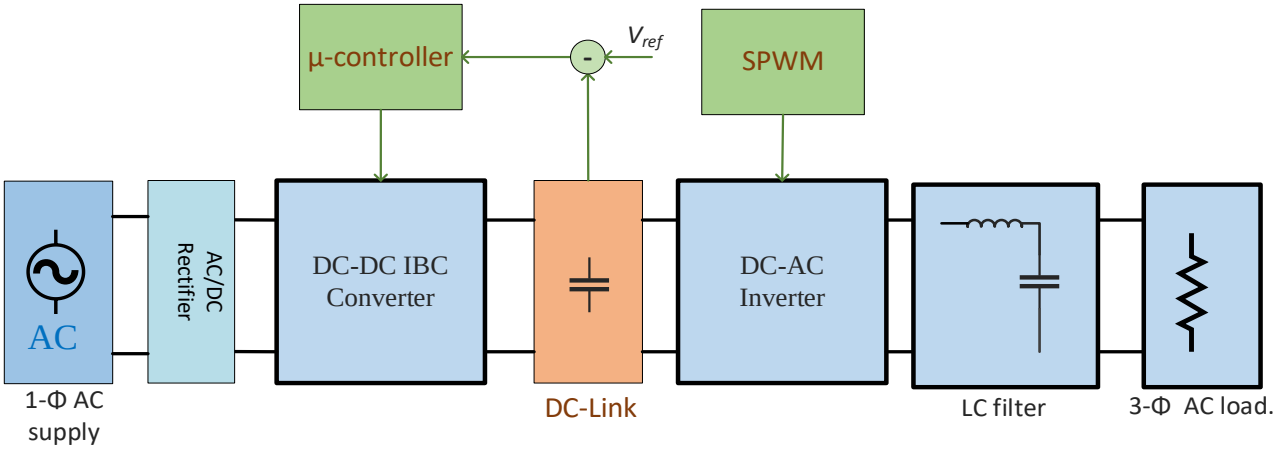

Figure 6.19 Schematic diagram of ac-grid interconnected IBC.

Table 6.7 Ac-3phase system specifications.

Parameters	Values
Input voltage, V_i	100 V, peak
AC frequency, f	50 Hz
Input capacitor, C_i	200×10^{-6} F
Switching frequency, f_s	9KHz
Inductor, L	560×10^{-6} H
Capacitor value, C	900×10^{-6} F
Reference voltage of DC-link	400 V
Filter values, L, C	8×10^{-3} H, 100×10^{-6} F
Resistance load, R	100, 80 Ω
Reference voltage, V_{ref}	400, 420 V

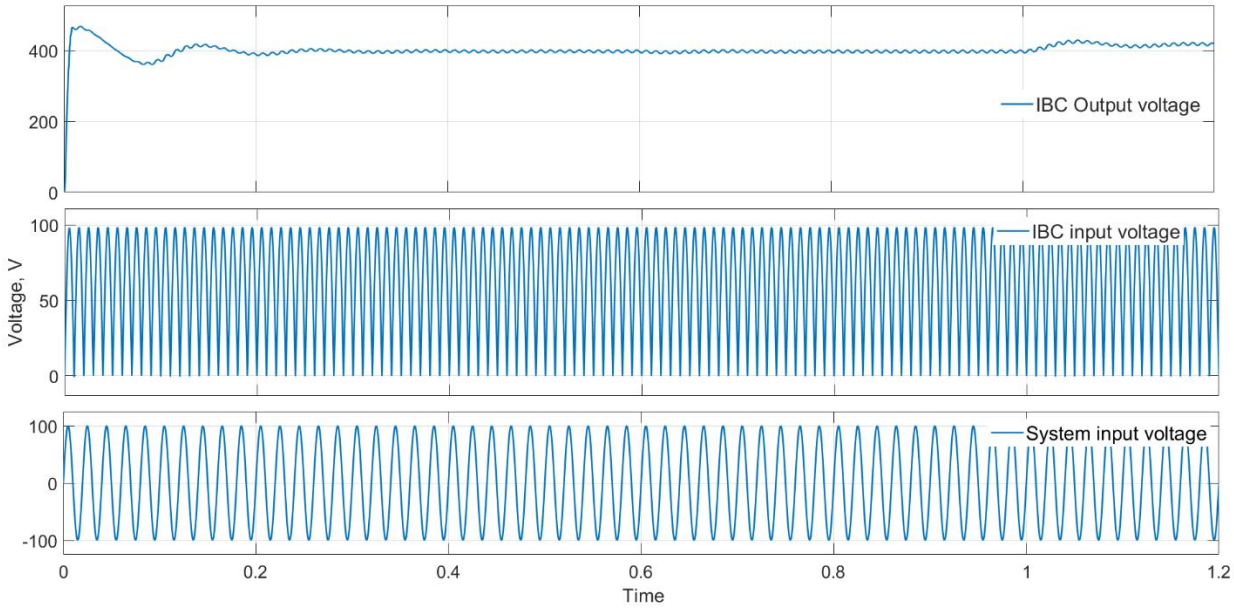

Figure 6.20 Voltage waveforms.

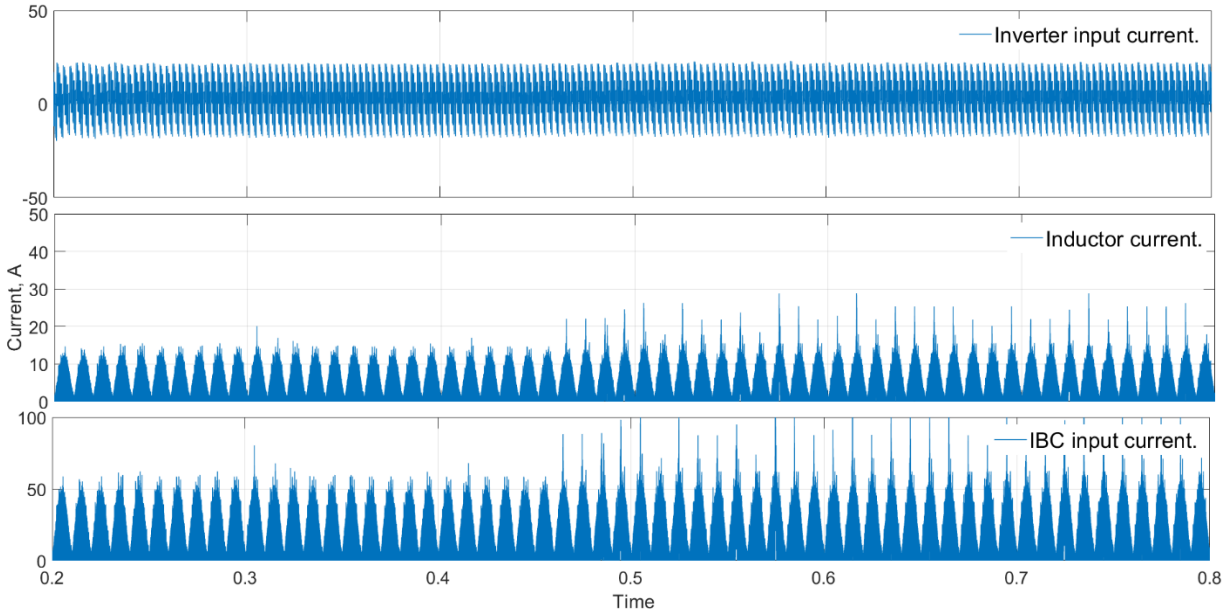

Figure 6.21 Current waveforms.

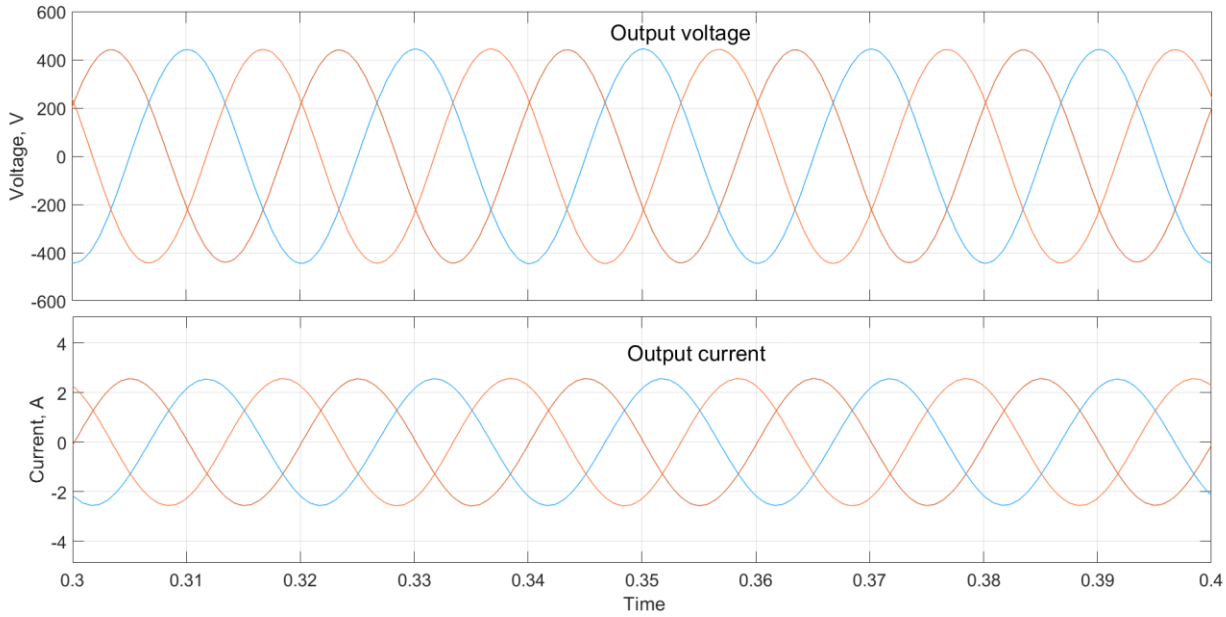

Figure 6.22 Grid voltage and current.

In summary, this chapter presented the simulation results of the μ-synthesis control technique in several applications. The controller performance showed sufficient performance and achieved robust stability.

CHAPTER 7

CONCLUSION

7.1 Summary

This dissertation has proposed a concept for an interleaved boost converter topology for different applications. The proposed topology is applied for single and cascade converters for DC load and AC load. The robust mu-synthesis controller applied to the four-phase IBC was able to stabilize objects in the desired case with the robust performance and the steady-state error.

The research on multi-phase interleaved boost converters for power distribution systems mainly on cascaded multilevel converters that are able to provide higher reliability.

It was shown that a novel multi-phase multi-stage interleaved boost converters for various type of power transmission systems are proposed. Analysis, design and experimental verification for the proposed topologies have been presented. The objective of the proposed converters is to reduce the input current ripple and component size in the converter and also to enhance the system stability.

7.2 Conclusion

The goal of this research was to apply robust control technique using μ-synthesis analysis to define the robust stability margins of a non-linear system of an interleaved boost converter over wide range of operating situations for different power applications.

The research handles the design, control and implementation of multi-phase interleaved boost converters for power distribution systems mainly on cascaded multilevel converters that are able to provide higher reliability. In order to tune the mu-synthesis controller, the weight functions were designed to achieve a robust voltage controller. The response of the controller was illustrated and

obtained in this research. The controller responses and performance of the output voltage in different cases are satisfactory in case of constant load and load variations and the reference voltage as well as the input voltage. In sum, the four-phase interleaved boost converter using μ -synthesis control is highly effective for controlling the output voltage in actual systems and has showed robust stability and robust performance to parameter variation. The converter has promising features such as the reduced input ripple, reduced passive components size, and less power devices stresses that improve the efficiency. The μ -synthesis controller guaranteed a robust performance against variation of load and input voltage and track the reference voltage with disturbance rejection.

7.3 Further work

There are a number of directions that this research could be continued; two of the most promising are outlined below.

i) Input current ripple to carry out at different phase-shift cases.

ii) Controller effect at variation of input voltage and load value.

iii) Cascade converter is to implement and tested under mu-controller for PV applications.

iv) Experimental work is conducted to test the mu-controller feasibility.

v) Apply μ -synthesis approach on the identification of fractional systems.

BIBLIOGRAPHY

[1] J.-M. Kwon, B.-H. Kwon, and K.-H. Nam, "Three-phase photovoltaic system with three-level boosting MPPT control," *IEEE Trans. Power Electron.*, vol. 23, no. 5, pp. 2319–2327, 2008.

[2] D. Coutellier, V. G. Agelidis, and S. Choi, "Experimental verification of floating-output interleaved-input DC-DC high-gain transformer-less converter topologies," in *2008 IEEE Power Electronics Specialists Conference*, 2008, pp. 562–568.

[3] O. Hegazy, J. Van Mierlo, and P. Lataire, "Analysis, modeling, and implementation of a multidevice interleaved DC/DC converter for fuel cell hybrid electric vehicles," *IEEE Trans. power Electron.*, vol. 27, no. 11, pp. 4445–4458, 2012.

[4] R. Seyezhai and B. L. Mathur, "Design and implementation of interleaved boost converter for fuel cell systems," *Int. J. Hydrogen Energy*, vol. 37, no. 4, pp. 3897–3903, 2012.

[5] N. S. Hasan, N. Rosmin, D. A. A. Osman, and A. H. Musta'amal, "Reviews on multilevel converter and modulation techniques," *Renew. Sustain. Energy Rev.*, vol. 80, pp. 163–174, 2017.

[6] I. Laoprom and S. Tunyasrirut, "Design of PI Controller for Voltage Controller of Four-Phase Interleaved Boost Converter Using Particle Swarm Optimization," *J. Control Sci. Eng.*, vol. 2020, 2020.

[7] R. Saadi, M. Y. Hammoudi, O. Kraa, M. Y. Ayad, and M. Bahri, "A robust control of a 4-leg floating interleaved boost converter for fuel cell electric vehicle application," *Math. Comput. Simul.*, vol. 167, pp. 32–47, 2020.

[8] G. Zames, "Feedback and optimal sensitivity: Model reference transformations, multiplicative seminorms, and approximate inverses," *IEEE Trans. Automat. Contr.*, vol. 26, no. 2, pp. 301–320, 1981.

[9] M. Kabalo, B. Blunier, D. Bouquain, M. G. Simões, and A. Miraoui, "Modeling and control of 4-phase floating interleaving boost converter," in *IECON 2011-37th Annual Conference of the IEEE Industrial Electronics Society*, 2011, pp. 3026–3032.

[10] L. Guo, J. Y. Hung, and R. M. Nelms, "Evaluation of DSP-based PID and fuzzy controllers for DC–DC converters," *IEEE Trans. Ind. Electron.*, vol. 56, no. 6, pp. 2237–2248, 2009.

[11] E. Arango, C. Ramos-Paja, J. Calvente, R. Giral, A. Romero, and L. Martinez-Salamero, "Fuel cell power output using a LQR controlled AIDB converter," in *2007 International Conference on Clean Electrical Power*, 2007, pp. 492–499.

[12] E. Vidal-Idiarte, L. Martinez-Salamero, H. Valderrama-Blavi, F. Guinjoan, and J. Maixe, "Analysis and design of H/sub/spl infin//control of nonminimum phase-switching converters," *IEEE Trans. Circuits Syst. I Fundam. Theory Appl.*, vol. 50, no. 10, pp. 1316–1323, 2003.

[13] Y.-X. Wang, D.-H. Yu, and Y.-B. Kim, "Robust time-delay control for the DC–DC boost converter," *IEEE Trans. Ind. Electron.*, vol. 61, no. 9, pp. 4829–4837, 2013.

[14] S.-K. Kim and K.-B. Lee, “Robust feedback-linearizing output voltage regulator for DC/DC boost converter,” *IEEE Trans. Ind. Electron.*, vol. 62, no. 11, pp. 7127–7135, 2015.

[15] T. Geyer, G. Papafotiou, and M. Morari, “Hybrid model predictive control of the step-down DC–DC converter,” *IEEE Trans. Control Syst. Technol.*, vol. 16, no. 6, pp. 1112–1124, 2008.

[16] R. Giral, L. Martinez-Salamero, R. Leyva, and J. Maixe, “Sliding-mode control of interleaved boost converters,” *IEEE Trans. Circuits Syst. I Fundam. Theory Appl.*, vol. 47, no. 9, pp. 1330–1339, 2000.

[17] W. Thammasiriroj, V. Chunkag, M. Phattanasak, S. Pierfederici, B. Davat, and P. Thounthong, “Nonlinear single-loop control of the parallel converters for a fuel cell power source used in DC grid applications,” *Int. J. Electr. Power Energy Syst.*, vol. 65, pp. 41–48, 2015.

[18] Y.-X. Wang, D.-H. Yu, S.-A. Chen, and Y.-B. Kim, “Robust DC/DC converter control for polymer electrolyte membrane fuel cell application,” *J. Power Sources*, vol. 261, pp. 292–305, 2014.

[19] S. Kapat, A. Patra, and S. Banerjee, “A current-controlled tristate boost converter with improved performance through RHP zero elimination,” *IEEE Trans. power Electron.*, vol. 24, no. 3, pp. 776–786, 2009.

[20] B. Abdessamad, K. Salah-Ddine, and C. E. Mohamed, “Design and Modeling of DC/DC Boost Converter for Mobile Device Applications,” *Int. J. Sci. Technol.*, vol. 2, no. 5, pp. 394–401, 2013.

[21] F. Slah, A. Mansour, M. Hajer, and B. Faouzi, “Analysis, modeling and implementation of an interleaved boost DC-DC converter for fuel cell used in electric vehicle,” *Int. J. Hydrogen Energy*, vol. 42, no. 48, pp. 28852–28864, 2017.

[22] J. Imaoka, M. Yamamoto, and T. Kawashima, “High-power-density three-phase interleaved boost converter with a novel coupled inductor,” *IEEJ J. Ind. Appl.*, vol. 4, no. 1, pp. 20–30, 2015.

[23] E. Sanchis *et al.*, “High-power battery discharge regulator for space applications,” *IEEE Trans. Ind. Electron.*, vol. 57, no. 12, pp. 3935–3943, 2010.

[24] W. Li, J. Wu, D. Wang, Y. Deng, and X. He, “A family of interleaved DC/DC convert deduced from a basic cell with winding-coupled inductors for high step-up/step-down conversions,” in *2007 IEEE Power Electronics Specialists Conference*, 2007, pp. 2335–2340.

[25] N. Rana, M. Kumar, A. Ghosh, and S. Banerjee, “A novel interleaved tri-state boost converter with lower ripple and improved dynamic response,” *IEEE Trans. Ind. Electron.*, vol. 65, no. 7, pp. 5456–5465, 2017.

[26] M. Z. Hossain and N. A. Rahim, “Recent progress and development on power DC-DC converter topology, control, design and applications: A review,” *Renew. Sustain. Energy Rev.*, vol. 81, pp. 205–230, 2018.

[27] B. Akhlaghi and H. Farzanehfard, “Family of ZVT interleaved converters with low number of components,” *IEEE Trans. Ind. Electron.*, vol. 65, no. 11, pp. 8565–8573, 2018.

[28] M. O’Loughlin, “An interleaving PFC pre-regulator for high-power converters,” *Texas Instruments*, pp. 1–14, 2006.

[29] N.-J. Park and D.-S. Hyun, “IBC using a single resonant inductor for high-power applications,” *IEEE Trans. Ind. Electron.*, vol. 56, no. 5, pp. 1522–1530, 2008.

[30] E. Pazouki, J. A. De Abreu-Garcia, and Y. Sozer, “Fault tolerant control method for interleaved DC-DC converters under open and short circuit switch faults,” in *2017 IEEE Energy Conversion Congress and Exposition (ECCE)*, 2017, pp. 1137–1142.

[31] E. Pazouki, J. A. De Abreu-Garcia, and Y. Sozer, “A Novel Fault-Tolerant Control Method for Interleaved DC–DC Converters Under Switch Fault Condition,” *IEEE Trans. Ind. Appl.*, vol. 56, no. 1, pp. 519–526, 2019.

[32] R. Crews, “An-1820 lm5032 interleaved boost converter,” *Texas Instruments Inc., Dallas, TX, App. Rep. SNVA335A*, 2013.

[33] W. Li and X. He, “Review of nonisolated high-step-up DC/DC converters in photovoltaic grid-connected applications,” *IEEE Trans. Ind. Electron.*, vol. 58, no. 4, pp. 1239–1250, 2010.

[34] L. Zhou, B. Zhu, Q. Luo, and S. Chen, “Interleaved non-isolated high step-up DC/DC converter based on the diode–capacitor multiplier,” *IET Power Electron.*, vol. 7, no. 2, pp. 390–397, 2013.

[35] K. L. Shenoy, C. G. Nayak, and R. P. Mandi, “Design and Implementation of Interleaved Boost Converter,” *Int. J. Eng. Technol.*, vol. 9, no. 3, 2017.

[36] P.-W. Lee, Y.-S. Lee, D. K. W. Cheng, and X.-C. Liu, “Steady-state analysis of an interleaved boost converter with coupled inductors,” *IEEE Trans. Ind. Electron.*, vol. 47, no. 4, pp. 787–795, 2000.

[37] K. Musasa, M. N. Gitau, and R. C. Bansal, “Analysis of a DC collector-based power converter topology for an offshore wind farm,” *Electr. Power Components Syst.*, vol. 43, no. 8–10, pp. 1113–1121, 2015.

[38] A. Dòria-Cerezo, C. Batlle, and G. Espinosa-Pérez, “Passivity-based control of a wound-rotor synchronous motor,” *IET Control theory Appl.*, vol. 4, no. 10, pp. 2049–2057, 2010.

[39] G. Calderon-Lopez, A. Villarruel-Parra, P. Kakosimos, S. Todd, and A. J. Forsyth, “Comparison of digital PWM control strategies for high power interleaved DC-DC converters,” 2016.

[40] F. L. Luo and H. Ye, *Essential Dc/Dc Converters*. CRC Press, 2018.

[41] P. Chitra and R. Seyezhai, “Basic design and review of two phase and three phase interleaved boost converter for renewable energy systems,” *Int. J. Appl. Sci.*, vol. 1, no. 1, pp. 1–26, 2014.

[42] F. Yang, C. Li, Y. Cao, and K. Yao, “Two-Phase Interleaved Boost PFC Converter With Coupled Inductor Under Single-Phase Operation,” *IEEE Trans. Power Electron.*, vol. 35, no. 1, pp. 169–184, 2019.

[43] C. Li, F. Yang, Y. Cao, K. Yao, B. Fang, and H. Li, “Two-phase interleaved boost PFC converter with coupled inductor under single-phase operation,” in *2018 IEEE Energy Conversion Congress and Exposition (ECCE)*, 2018, pp. 606–613.

[44] V. Viswanatha, “A Complete Mathematical Modeling, Simulation and Computational Implementation of Boost Converter Via MATLAB/Simulink.”

[45] D. W. Hart, *Power electronics*. Tata McGraw-Hill Education, 2011.

[46] R. Ma, L. Xu, R. Xie, D. Zhao, Y. Huangfu, and F. Gao, “Advanced Robustness Control of DC–DC Converter for Proton Exchange Membrane Fuel Cell Applications,” *IEEE Trans. Ind. Appl.*, vol. 55, no. 6, pp. 6389–6400, 2019.

[47] Y.-Y. Hsu and L. Wang, “Damping of a parallel ac-dc power system using PID power system stabilizers and rectifier current regulators,” *IEEE Trans. Energy Convers.*, vol. 3, no. 3, pp. 540–547, 1988.

[48] C.-L. Shen, L.-Z. Chen, and Y.-S. Shen, “Interleaving-based converter system with features of external auxiliary triggering and universal line input for driving medical laser equipment,” *J. Eng.*, vol. 2019, no. 8, pp. 5379–5390, 2019.

[49] G. Niranjani and N. Subashini, “Power Factor Correction And THD Minimization Using Interleaved Boost Converter In Continuous Conduction Mode,” *ARPN J. Eng. Appl. Sci.*, vol. 12, no. 11, 2017.

[50] D. Raveendhra and M. K. Pathak, “Three-Phase Capacitor Clamped Boost Inverter,” *IEEE J. Emerg. Sel. Top. Power Electron.*, vol. 7, no. 3, pp. 1999–2011, 2018.

[51] J. D. van Wyk and F. C. Lee, “On a future for power electronics,” *IEEE J. Emerg. Sel. Top. Power Electron.*, vol. 1, no. 2, pp. 59–72, 2013.

[52] P. T. Krein, “Data center challenges and their power electronics,” *CPSS Trans. Power Electron. Appl.*, vol. 2, no. 1, pp. 39–46, 2017.

[53] V. A. K. Prabhala, P. Fajri, V. S. P. Gouribhatla, B. P. Baddipadiga, and M. Ferdowsi, “A DC–DC converter with high voltage gain and two input boost stages,” *IEEE Trans. Power Electron.*, vol. 31, no. 6, pp. 4206–4215, 2015.

[54] T. Jenkins, “A brief history of... semiconductors,” *Phys. Educ.*, vol. 40, no. 5, p. 430, 2005.

[55] IEA, “World Energy Outlook 2019.” https://www.iea.org/reports/tracking-power-2019/solar-pv.

[56] T. Wang, “Global investment in solar energy technologies 2004-2018,” 2019. https://www.statista.com/statistics/186823/global-investment-in-solar-technology-since-2004/.

[57] M. R, Hannah and R, “Renewable Energy,” 2020. https://ourworldindata.org/renewable-

energy#citation.

[58] I. Anand, S. Senthilkumar, D. Biswas, and M. Kaliamoorthy, “Dynamic power management system employing a single-stage power converter for standalone solar PV applications,” *IEEE Trans. Power Electron.*, vol. 33, no. 12, pp. 10352–10362, 2018.

[59] A. Hussain, M. M. Garg, M. P. Korukonda, S. Hasan, and L. Behera, “A parameter estimation based mppt method for a pv system using lyapunov control scheme,” *IEEE Trans. Sustain. Energy*, vol. 10, no. 4, pp. 2123–2132, 2018.

[60] J. Patel and G. Sharma, “Modeling and simulation of solar photovoltaic module using matlab/simulink,” *IJRET Int. J. Res. Eng. Technol. ISSN*, pp. 1163–2319, 2013.

[61] L. El Chaar, “Photovoltaic system conversion,” in *Alternative Energy in Power Electronics*, Elsevier, 2011, pp. 155–175.

[62] J. D. Bastidas-Rodriguez, E. Franco, G. Petrone, C. A. Ramos-Paja, and G. Spagnuolo, “Maximum power point tracking architectures for photovoltaic systems in mismatching conditions: a review,” *IET Power Electron.*, vol. 7, no. 6, pp. 1396–1413, 2014.

[63] A. Pallavee Bhatnagar and B. R. K. Nema, “Conventional and global maximum power point tracking techniques in photovoltaic applications: A review,” *J. Renew. Sustain. Energy*, vol. 5, no. 3, p. 32701, 2013.

[64] T. Esram and P. L. Chapman, “Comparison of photovoltaic array maximum power point tracking techniques,” *IEEE Trans. energy Convers.*, vol. 22, no. 2, pp. 439–449, 2007.

[65] M. A. G. De Brito, L. Galotto, L. P. Sampaio, G. de A. e Melo, and C. A. Canesin, “Evaluation of the main MPPT techniques for photovoltaic applications,” *IEEE Trans. Ind. Electron.*, vol. 60, no. 3, pp. 1156–1167, 2012.

[66] N. Femia, D. Granozio, G. Petrone, G. Spagnuolo, and M. Vitelli, “Predictive & adaptive MPPT perturb and observe method,” *IEEE Trans. Aerosp. Electron. Syst.*, vol. 43, no. 3, pp. 934–950, 2007.

[67] N. Femia, G. Petrone, G. Spagnuolo, and M. Vitelli, “Optimization of perturb and observe maximum power point tracking method,” *IEEE Trans. power Electron.*, vol. 20, no. 4, pp. 963–973, 2005.

[68] W. Xiao and W. G. Dunford, “A modified adaptive hill climbing MPPT method for photovoltaic power systems,” in *2004 IEEE 35th annual power electronics specialists conference (IEEE Cat. No. 04CH37551)*, 2004, vol. 3, pp. 1957–1963.

[69] Y.-T. Hsiao and C.-H. Chen, “Maximum power tracking for photovoltaic power system,” in *Conference Record of the 2002 IEEE Industry Applications Conference. 37th IAS Annual Meeting (Cat. No. 02CH37344)*, 2002, vol. 2, pp. 1035–1040.

[70] M. A. Elgendy, B. Zahawi, and D. J. Atkinson, “Assessment of the incremental conductance maximum power point tracking algorithm,” *IEEE Trans. Sustain. energy*, vol. 4, no. 1, pp. 108–117, 2012.

[71] N. E. Zakzouk, M. A. Elsaharty, A. K. Abdelsalam, A. A. Helal, and B. W. Williams,

"Improved performance low-cost incremental conductance PV MPPT technique," *IET Renew. Power Gener.*, vol. 10, no. 4, pp. 561–574, 2016.

[72] M. Rakhshan, N. Vafamand, M.-H. Khooban, and F. Blaabjerg, "Maximum power point tracking control of photovoltaic systems: A polynomial fuzzy model-based approach," *IEEE J. Emerg. Sel. Top. Power Electron.*, vol. 6, no. 1, pp. 292–299, 2017.

[73] M. A. A. M. Zainuri, M. A. M. Radzi, A. C. Soh, and N. A. Rahim, "Development of adaptive perturb and observe-fuzzy control maximum power point tracking for photovoltaic boost dc–dc converter," *IET Renew. Power Gener.*, vol. 8, no. 2, pp. 183–194, 2013.

[74] N. S. D'Souza, L. A. C. Lopes, and X. Liu, "An intelligent maximum power point tracker using peak current control," in *2005 IEEE 36th Power Electronics Specialists Conference*, 2005, p. 172.

[75] T. Kitano, M. Matsui, and D. Xu, "Power sensor-less MPPT control scheme utilizing power balance at DC link-system design to ensure stability and response," in *IECON'01. 27th Annual Conference of the IEEE Industrial Electronics Society (Cat. No. 37243)*, 2001, vol. 2, pp. 1309–1314.

[76] T. Hiyama and K. Kitabayashi, "Neural network based estimation of maximum power generation from PV module using environmental information," *IEEE Trans. Energy Convers.*, vol. 12, no. 3, pp. 241–247, 1997.

[77] D. Apablaza and J. Munoz, "Laboratory Implementation of a Boost Interleaved Converter for PV Applications," *IEEE Lat. Am. Trans.*, vol. 14, no. 6, pp. 2738–2743, 2016.

[78] F. H. Aghdam and M. Abapour, "Reliability and cost analysis of multistage boost converters connected to PV panels," *IEEE J. photovoltaics*, vol. 6, no. 4, pp. 981–989, 2016.

[79] R. Seyezhai and B. L. Mathur, "A Comparison of Three-Phase Uncoupled and Directly Coupled Interleaved Boost Converter for Fuel Cell Applications," *Int. J. Electr. Eng. Informatics*, vol. 3, no. 3, p. 394, 2011.

[80] S. Rauf, A. Wahab, M. Rizwan, S. Rasool, and N. Khan, "Application of Dc-grid for Efficient use of solar PV System in Smart Grid," *Procedia Comput. Sci.*, vol. 83, pp. 902–906, 2016.

[81] G. Velasco-Quesada, F. Guinjoan-Gispert, R. Piqué-López, M. Román-Lumbreras, and A. Conesa-Roca, "Electrical PV array reconfiguration strategy for energy extraction improvement in grid-connected PV systems," *IEEE Trans. Ind. Electron.*, vol. 56, no. 11, pp. 4319–4331, 2009.

[82] S. Kouro *et al.*, "Recent advances and industrial applications of multilevel converters," *IEEE Trans. Ind. Electron.*, vol. 57, no. 8, pp. 2553–2580, 2010.

[83] B. K. Bose, "Power electronics and motor drives recent progress and perspective," *IEEE Trans. Ind. Electron.*, vol. 56, no. 2, pp. 581–588, 2008.

[84] J. Chang, "Advancement and trends of power electronics for industrial applications," in

IECON'03. 29th Annual Conference of the IEEE Industrial Electronics Society (IEEE Cat. No. 03CH37468), 2003, vol. 3, pp. 3021–3022.

[85] L. G. Franquelo, J. Rodriguez, J. I. Leon, S. Kouro, R. Portillo, and M. A. M. Prats, "The age of multilevel converters arrives," *IEEE Ind. Electron. Mag.*, vol. 2, no. 2, pp. 28–39, 2008.

[86] J. Rodriguez, J.-S. Lai, and F. Z. Peng, "Multilevel inverters: a survey of topologies, controls, and applications," *IEEE Trans. Ind. Electron.*, vol. 49, no. 4, pp. 724–738, 2002.

[87] W. Mcmurray, "Fast response stepped-wave switching power converter circuit." Google Patents, May 25, 1971.

[88] J. A. Dickerson and G. H. Ottaway, "Transformerless power supply with line to load isolation." Google Patents, Aug. 03, 1971.

[89] R. H. Baker, "High-voltage converter circuit." Google Patents, May 13, 1980.

[90] R. H. Baker, "Bridge converter circuit." Google Patents, May 26, 1981.

[91] E. Babaei, "A cascade multilevel converter topology with reduced number of switches," *IEEE Trans. power Electron.*, vol. 23, no. 6, pp. 2657–2664, 2008.

[92] R. D. Middlebrook, "Input filter considerations in design and application of switching regulators," *IAS'76*, 1976.

[93] F. Zhang and Y. Yan, "Start-up process and step response of a DC–DC converter loaded by constant power loads," *IEEE Trans. Ind. Electron.*, vol. 58, no. 1, pp. 298–304, 2010.

[94] M. K. AL-Nussairi, R. Bayindir, S. Padmanaban, L. Mihet-Popa, and P. Siano, "Constant power loads (cpl) with microgrids: Problem definition, stability analysis and compensation techniques," *Energies*, vol. 10, no. 10, p. 1656, 2017.

[95] E. Hossain, R. Perez, A. Nasiri, and S. Padmanaban, "A comprehensive review on constant power loads compensation techniques," *Ieee Access*, vol. 6, pp. 33285–33305, 2018.

[96] R. Patel and R. Chudamani, "Stability analysis of the main converter supplying a constant power load in a multi-converter system considering various parasitic elements," *Eng. Sci. Technol. an Int. J.*, 2020.

[97] X. Zhang, X. Ruan, and Q.-C. Zhong, "Improving the stability of cascaded DC/DC converter systems via shaping the input impedance of the load converter with a parallel or series virtual impedance," *IEEE Trans. Ind. Electron.*, vol. 62, no. 12, pp. 7499–7512, 2015.

[98] H. Piquet, N. Roux, B. Nahid-Mobarakeh, S. Pierfederici, P. Magne, and J. Faucher, "Quality and stability of embedded power DC Networks," *Syst. Des. Methodol. Electr. Energy Syst. Anal. Synth. Manag.*, pp. 159–222, 2012.

[99] Y. Xia and R. Ayyanar, "Influence of bi-directional power flow on impedance and stability of cascaded systems," in *IECON 2014-40th Annual Conference of the IEEE Industrial Electronics Society*, 2014, pp. 1542–1548.

[100] J. M. Zhang, X. G. Xie, D. Z. Jiao, and Z. Qian, “Stability problems and input impedance improvement for cascaded power electronic systems,” in *Nineteenth Annual IEEE Applied Power Electronics Conference and Exposition, 2004. APEC’04.*, 2004, vol. 2, pp. 1018–1024.

[101] A. Riccobono and E. Santi, “Comprehensive review of stability criteria for DC power distribution systems,” *IEEE Trans. Ind. Appl.*, vol. 50, no. 5, pp. 3525–3535, 2014.

[102] X. Zhang, X. Ruan, H. Kim, and K. T. Chi, “Adaptive active capacitor converter for improving stability of cascaded DC power supply system,” *IEEE Trans. Power Electron.*, vol. 28, no. 4, pp. 1807–1816, 2012.

[103] B. M. Alharbi, M. A. Alhomim, and R. A. McCann, “A High Voltage Ratio Three-stage Cascaded Interleaved Boost Converters for PV Application,” in *2020 IEEE Power and Energy Conference at Illinois (PECI)*, 2020, pp. 1–5.

[104] S. Pang *et al.*, “Interconnection and Damping Assignment Passivity-Based Control Applied to On-Board DC–DC Power Converter System Supplying Constant Power Load,” *IEEE Trans. Ind. Appl.*, vol. 55, no. 6, pp. 6476–6485, 2019.

[105] X. Liu and X. Liao, “Fixed-Time $\mathcal {H} _ {\infty} $ Control for Port-Controlled Hamiltonian Systems,” *IEEE Trans. Automat. Contr.*, vol. 64, no. 7, pp. 2753–2765, 2018.

[106] M. Wu and D. D.-C. Lu, “A novel stabilization method of LC input filter with constant power loads without load performance compromise in DC microgrids,” *IEEE Trans. Ind. Electron.*, vol. 62, no. 7, pp. 4552–4562, 2014.

[107] M. A. Hassan, E. Li, X. Li, T. Li, C. Duan, and S. Chi, “Adaptive passivity-based control of dc–dc buck power converter with constant power load in dc microgrid systems,” *IEEE J. Emerg. Sel. Top. Power Electron.*, vol. 7, no. 3, pp. 2029–2040, 2018.

[108] K. Mudliyar, K. Suryanarayana, and H. Rao, “Analysis of High Frequency Multi-Phase Multi-Stage Boost Converter,” *Int. J. Adv. Electr. Electron. Eng.*, vol. 2, no. 1, pp. 45–51, 2013.

[109] J. Doyle, “Analysis of feedback systems with structured uncertainties,” in *IEE Proceedings D-Control Theory and Applications*, 1982, vol. 129, no. 6, pp. 242–250.

[110] Z. Kemin and J. C. Doyle, “Essential of Robust Control,(1995).” Prentice Hall Inc, New Jersey.

[111] S. Skogestad and I. Postlethwaite, *Multivariable feedback control: analysis and design*, vol. 2. Wiley New York, 2007.

[112] S. Banerjee, A. Ghosh, and N. Rana, “Design and fabrication of closed loop two-phase interleaved boost converter with type-III controller,” in *IECON 2016-42nd Annual Conference of the IEEE Industrial Electronics Society*, 2016, pp. 3331–3336.

[113] S. Banerjee, A. Ghosh, and N. Rana, “An improved interleaved boost converter with PSO-based optimal type-III controller,” *IEEE J. Emerg. Sel. Top. Power Electron.*, vol. 5, no. 1, pp. 323–337, 2016.

[114] V. A. Oliveira, E. S. Tognetti, and D. Siqueira, “Robust controllers enhanced with design and implementation processes,” *IEEE Trans. Educ.*, vol. 49, no. 3, pp. 370–382, 2006.

[115] M. Baskin and B. Caglar, “μ-Approach based robust voltage controller design for a boost converter used in photovoltaic applications,” in *IECON 2015-41st Annual Conference of the IEEE Industrial Electronics Society*, 2015, pp. 135–140.

[116] P. A. Ioannou and J. Sun, *Robust adaptive control*. Courier Corporation, 2012.

[117] A. Piłat and P. Włodarczyk, “The μ-synthesis and analysis of the robust controller for the active magnetic levitation system,” *Autom. Górniczo-Hutnicza im. Stanisława Staszica w Krakowie*, vol. 15, no. 1, pp. 85–98, 2011.

[118] S. D. A. Sanjeewa and M. Parnichkun, “Control of rotary double inverted pendulum system using mixed sensitivity H∞ controller,” *Int. J. Adv. Robot. Syst.*, vol. 16, no. 2, p. 1729881419833273, 2019.

[119] B. Pal and B. Chaudhuri, “Mixed-sensitivity approach using linear matrix inequalities,” *Robust Control Power Syst.*, pp. 115–138, 2005.

[120] G. Balas, R. Chiang, A. Packard, and M. Safonov, “Robust Control Toolbox user’s guide,” *MathWorks Inc., Natick, MA*, 2007.

[121] M. M. Amini and M. R. J. Motlagh, “Using μ sγη approach for robust control of a spin stabilized seeker,” in *The 2nd International Conference on Control, Instrumentation and Automation*, 2011, pp. 138–143.

[122] E. Alfaro-Cid, E. W. McGookin, and D. J. Murray-Smith, “Optimisation of the weighting functions of an H∞ controller using genetic algorithms and structured genetic algorithms,” *Int. J. Syst. Sci.*, vol. 39, no. 4, pp. 335–347, 2008.

[123] D. C. Donha and R. M. Katebi, “Automatic cost weight selection in mixed sensitivity H∞ controller synthesis,” *IFAC Proc. Vol.*, vol. 37, no. 10, pp. 279–284, 2004.

[124] R. W. Beaven, M. T. Wright, and D. R. Seaward, “Weighting function selection in the H∞ design process,” *Control Eng. Pract.*, vol. 4, no. 5, pp. 625–633, 1996.

[125] K. Zhou, J. C. Doyle, and K. Glover, *Robust and optimal control*, vol. 40. Prentice hall New Jersey, 1996.

[126] D.-W. Gu, P. Petkov, and M. M. Konstantinov, *Robust control design with MATLAB®*. Springer Science & Business Media, 2005.

[127] G. F. Wallis and R. Tymerski, “Generalized approach for/spl mu/synthesis of robust switching regulators,” *IEEE Trans. Aerosp. Electron. Syst.*, vol. 36, no. 2, pp. 422–431, 2000.

[128] V. Mummadi and B. S. Singamaneni, “Stability analysis of cascaded DC–DC power electronic system,” *IEEJ Trans. Electr. Electron. Eng.*, vol. 4, no. 6, pp. 763–770, 2009.

[129] C. Oates, “Modular multilevel converter design for VSC HVDC applications,” *IEEE J. Emerg. Sel. Top. Power Electron.*, vol. 3, no. 2, pp. 505–515, 2014.

APPENDIX I

LIST OF PUBLISHED PAPERS

[1] M. A. Alhomim , B. M. Alharbi and R. A. McCann, “Decentralized Control of a Hybrid AC and DC Ring bus Microgrid System,” 50th Annual Frontiers of Power Conference(FPC), Oklahoma State University ,OK, USA, 2017.

[2] B. M. Alharbi, M. A. Alhomim and R. A. McCann, “Robust Control of DC-DC Boost Converter by using mu-synthesis approach,” International Federation of Automatic Control (IFAC), Jeju, Korea, Volume 52, Issue 4, 2019, Pages 200-205.

[3] M. A. Alhomim , B. M. Alharbi and R. A. McCann, ”A Fractional Order Approach for Modeling Nonlinear Behavior in Boost DC-DC Converters” 52nd Annual Frontiers of Power Conference(FPC), Oklahoma State University ,OK, USA, 2019.

[4] B. M. Alharbi, M. A. Alhomim and R. A. McCann, "Design and Simulation of Multi-phase Multi-stage Interleaved Boost Converters for Photovoltaic Application," 2020 IEEE Texas Power and Energy Conference (TPEC), College Station, TX, USA, 2020, pp. 1-4.

[5] B. M. Alharbi, M. A. Alhomim and R. A. McCann, “A High Voltage Ratio Three-Stage Cascaded Interleaved Boost Converters for PV Application” 2020 IEEE Power and Energy Conference at Illinois (PECI), Champaign, IL, 2020, pp. 1-5.

[6] M. A. Alhomim , B. M. Alharbi and R. A. McCann, “A Fractional Order Approach for Modeling Nonlinear Behavior in Boost DC-DC Converters with CPL,” 2020 IEEE Green Technologies Conference (GreenTech), Oklahoma City, OK, 2020, pp. 1-5.

[7] B. M. Alharbi, M. A. Alhomim and R. A. McCann, “ Robust Control for Cascade Boost Converter Based on H-infinity Controller” 2020 IEEE Kansas Power and Energy Conference (KPEC), Manhattan, KS ,USA, 2020, pp. 1-5.

[8] B. M. Alharbi, M. A. Alhomim and R. A. McCann, ” An Efficient High Voltage Gain Using Two-Stage Cascaded Interleaved Boost Converter for Solar PV System with MPPT Technique”, 2020 IEEE PES Innovative Smart Grid Technologies Conference (ISGT), Washington, DC, 2020, pp. 1-6.

[9] M. A. Alhomim , B. M. Alharbi, O. M. Aldosari, S. Batiyah, and R. A. McCann, ” Fractional-Order System Identification of a DC- DC Converter”, Ready to submit to a journal.

[10] B. M. Alharbi, M. A. Alhomim, O. M. Aldosari and R. A. McCann, “Cascade Interleaved Boost Converter Based MPPT and H-infinity for PV Application”, Submitted to Systems Science and Control Engineering